PRODUCTION AND CHARACTERIZATION OF HfO_2 HIGH-k DIELECTRIC LAYERS BY SPUTTERING TECHNIQUE

A Thesis Submitted to
The Graduate School of Engineering and Sciences of
Izmir Institute of Technology
in Partial Fulfillment of the Requirements for the Degree of

MASTER OF SCIENCE

in Physics

by
Ayten CANTAŞ

June 2010
İZMİR

We approve the thesis of **Ayten CANTAŞ**

_____

Dr. Gülnur AYGÜN ÖZYÜZER
Supervisor

_____

Prof. Raşit TURAN
Committee Member

_____

Assist. Prof. Yusuf SELAMET
Committee Member

30 June 2010

_____

Prof. Nejat BULUT
Head of the Physics Department

_____

Assoc. Prof. Talat YALÇIN
Dean of the Graduate School of
Engineering and Sciences

ACKNOWLEDGEMENTS

I would like to express my gratitude to all those who gave me the possibility to complete this thesis. Firstly, I would like to express my sincere gratitude to Dr. Gülnur Aygün Özyüzer who has been my supervisor since the beginning of my work. Her encouragement and support made this thesis possible. I also would like to thank Assoc. Prof. Dr. Lütfi Özyüzer for making me motivated during my research. Moreover, I would like to express my thanks to Prof. Dr. Raşit Turan who gave me the chance to use his research laboratories while I was at Middle East Techniqual University and also special thanks his research group especially to Mustafa Kulakçı.

I am also grateful to express my satisfactions with doctorate candidate Adem Enes Erol because of his support with knowledge of science and behaviour to me like a brother.

I would like to thank to TUBITAK for funding the project ‘‘TBAG-107T117’’ during my thesis. I also thank to the METU Central Laboratory for the X-Ray photoelectron spectroscopy (XPS) measurements.

Serkan Bağdaş who is engaged with me is another person I would like to thank. We have shared together bitter and sweet days during my undergraduate and master educations. He was firstly my best friend and then my love. His unforgottable helpfulness and encouragement increased my success during my education.

Last but not least, I wish to express my cordial appreciation to my family; my mother, Güler Cantaş, my father, Haydar Cantaş and my sister Fulden Cantaş for their precious contributions of moral support anytime and anywhere. I feel very lucky to have such a perfect family.

I am pleased to express my gratefulness to all my friends at the department for their sharing out their joyful times with me during my sleepless nights.

ABSTRACT

PRODUCTION AND CHARACTERIZATION OF HfO_2 HIGH-k DIELECTRIC LAYERS BY SPUTTERING TECHNIQUE

HfO_2 thin films have been deposited on Si by in-situ spectroscopic ellipsometric sputtering technique. The grown films have been examined by various diagnostic and analysis techniques (Spectroscopic Ellipsometer (SE), FTIR, XRD, XPS). The optimization of in-situ SE sputtering system has been processed according to the measurement results of the grown HfO_2 films. From the measurements simultaneously taken by using SE, film thickness, refractive index and real part of dielectric function have been examined as a function of deposition time. It was found that the thickness changes linearly with deposition time. The formation of undesired SiO_2 interfacial layer has been tried to be prevented and searched by using FTIR. MOS capacitors from the oxides having best qualities have been produced to obtain electrical properties of grown oxides. The process of production-characterization and development of oxidation conditions have been achieved and the following results have been obtained:

(a) Low O_2/Ar gas ratio and 30-40 watt power have been considered as the most convenient oxidation parameters.

(b) The formation of SiO_2 interface has not been prevented but formation of Hf_xSiO_y has been obtained.

(c) The refractive index value (n=2.1) of bulk HfO_2 at 632 nm has been obtained.

ÖZET

YÜKSEK DİELEKTRİK DEĞERLİKLİ HfO_2 FİLMLERİNİN SAÇTIRMA YÖNTEMİ İLE BÜYÜTÜLMESİ VE KARAKTERİZASYONU

Saçtırma (sputtering) tekniği aracılığıyla in-situ spektroskopik elipsometre ile kontrollü vakum ortamında Hf ve O elementleri bulundurularak Si pulu üzerine HfO_2 filmi büyütülmesi gerçekleştirilmiştir. Büyütülen oksit tabakaları çeşitli tanı ve analiz teknikleri (Elipsometre, FTIR, XRD, XPS) ile incelenmiştir. Oksitleme şartları, çeşitli ölçüm sistemlerinden elde edilen sonuçlara göre, oksitin HfO_2 moduna sahip olması durumu göz önünde bulundurularak incelenmiş ve saçtırma yöntemi ile oksit büyütme işleminin optimizasyonu yapılmıştır. Spektroskopik elipsometre ile büyütmeye eş zamanlı alınan ölçümler ile film kalınlığının, kırılma indisi ve kompleks dielektrik sabitinin gerçel kısmının film büyütme zamanına göre değişimi incelenmiştir. Film kalınlığının oksidasyon zamanı ile doğru orantılı olarak değiştiği sonucu elde edilmiştir. FTIR kullanılarak büyütülen filmde arayüz SiO_2 oluşumu araştırılmış ve istenmeyen bu oluşumun engellenmesi üzerine çalışmalar yapılmıştır. Yapısal ve optiksel açıdan en iyi özelliklere sahip örnekler kullanılarak MOS (Metal Oksit Yarıiletken) aygıtlar üretilerek bu aygıtların elektriksel özellikleri incelenmiştir. 'Üretim-karekterizasyon ve büyüme koşullarının iyileştirilmesi' döngüsü başarı ile kurulmuş ve şu sonuçlar elde edilmiştir: (a) En uygun oksitleme parametresi olarak düşük O_2/Ar gaz oranı ve uygulanan güç açısından 30-40 watt belirlenmiştir. (b) SiO_2 arayüz oluşumu tamamen engellenememiş, suboksit formda Hf_xSiO_y arayüzü elde edilmiştir. (c) Bulk halindeki HfO_2 632 nm de sahip olduğu 2.1 değerindeki kırılma indisi değerine ulaşılmıştır.

To my perfect Family

TABLE OF CONTENTS

LIST OF FIGURES

LIST OF TABLES

Table **Page**

CHAPTER 1

INTRODUCTION

1.1. Introduction

Since the leakage current is an important parameter for device performance (Robertson, et al. 2004), continuous scaling down of the microelectronic devices has led to an interest to use new oxides with a higher dielectric constant in dynamic random access memories (DRAMs).

In semiconductor technology, silicon dioxide is an important material because of its high quality as a gate insulator when grown on Si surface to fabricate metal-oxide-semiconductor transistors. On the other hand, SiO_2 films less than 2 nm thick yield serious leakage current due to direct tunneling of electrons and cause device reliability problems. One solution, as shown in fig. 1.1, is to use thicker oxides with higher dielectric constant to obtain the same equivalent capacitance (Robertson 2000). Therefore, new materials having higher dielectric constant (high-*k*) are under consideration as potential replacements for SiO_2. These oxides should have many required important properties in device applications; a high thermodynamic stability when grown on Si, good interfacial properties between the semiconductor and the oxide with low defect density and breakdown strength at high applied electric fields. Since the current flows in the semiconductor channel next to interface, these materials need to have low diffusion coefficient as well as having high enough band offsets to act as barriers for electron and hole trappings (Wilk, et al. 2001). Materials such as Al_2O_3, Y_2O_3, ZrO_2, HfO_2, TiO_2, La_2O_3 and Ta_2O_5 have been investigated for such applications, but very few of them have the required qualities (Nam, et al. 2002). New dielectric materials should have potential barriers good enough in order to prevent the emission of electrons or holes from leaking through their bands. Therefore, conduction band (CB) offset and forbidden band gap (E_g) value restrict the selection of high-*k* materials. The comparison of related properties for candidate materials is given in Table 1.1. High-*k* dielectric materials with dielectric constant from 10 to 80 such as Ta_2O_5 (Chaneliere, et al. 1998), $SrTiO_3$ (McKee, et al. 1998), Al_2O_3 (Manchanda, et al. 2001) are used for data

storage (DRAM) applications. Among them, Ta_2O_5, $SrTiO_3$, TiO_2 do not have good thermodynamic stability when grown on Si (Alers, et al. 1998, Taylor, et al. 1999, Atanassova 1999).

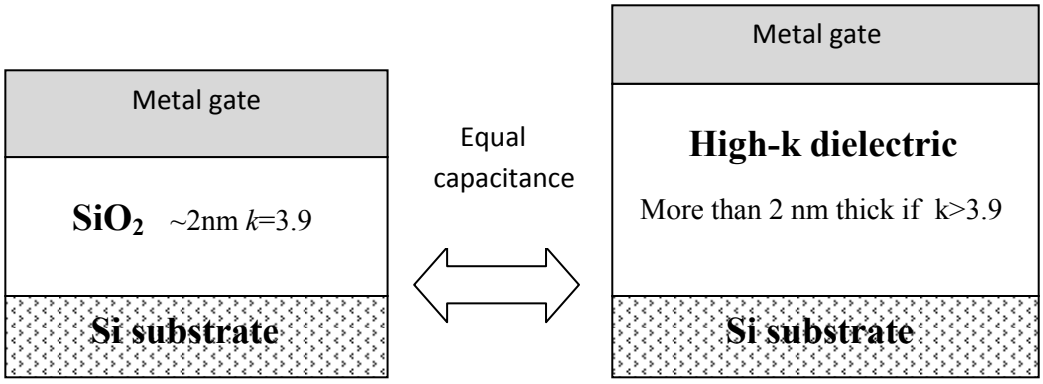

Figure 1.1. Comparison of gate dielectrics used in transistor gate stacks. Both structures result in the same gate stack capacitance.

Although Al_2O_3 has high forbidden band gap energy, an amorphous structure and thermodynamically stabilite up to high temperatures when grown on Si, its low dielectric constant between 8-10 eliminates it from being a permanent solution (Andre, et al. 2006). The formation of an undesired Si-Al-O interfacial layer for Al_2O_3 films on Si after O_2 anneal at T~700°C has been recently noted as well (Krug, et al. 2000).

As it can be seen from table 1.1**,** a limited number of materials possess all of these properties. Among them, HfO_2 attracted a huge attention for dielectric applications. Due to the fact that amorphous structures also tend to minimize electronically active defects, they are usually preferred for gate dielectrics. HfO_2 has also a low leakage current level, wide forbidden band gap energy (E_g~5.6 eV) (Aarik, et al. 2004) and thermal stability when it is contacted with Si. As being a high-*k* dielectric material, amorphous HfO_2 has an important position in the Metal Oxide Semiconductor (MOS) transistors. Amorphous HfO_2 is considered to be one of the most favorable materials to be replaced with SiO_2 as an insulating material for future MOS technology. The main reason of being so interesting is due to its high dielectric constant *k* (20-25) compared to that of SiO_2 (~3.9) (Gong, et al. 2009). Since HfO_2 is transparent material in the spectral range from infrared to the ultraviolet, it is one of the important high refractive index thin film materials (n = 2.1 at 632 nm wavelength for the bulk HfO_2).

It can also be used as an anti-reflecting coating due to its low absorbing property. These properties make HfO_2 films as a promising material in microelectronics and optoelectronic devices. However, these films' optical properties, dielectric constant and electrical properties are strongly dependent on their microstructure. Successful implementation of HfO_2-based insulating stacks requires a basic understanding of the HfO_2/Si interface and its impact on the electrical properties.

The properties of the interfacial layer (IL) between Si and HfO_2 are of importance because they have a direct effect on the electron transport in the Si surface channel. The composition and properties of the IL strongly depend on a number of parameters variable containing film deposition technique, silicon crystal orientation, pre-deposition process, growth temperature and a variable of after post deposition processes.

Table 1.1. Comparison of some important properties of high-*k* dielectric materials.

Material	Dielectric Constant	Energy Gap E_g (eV)	Conduction Band offset (CB) To Si (eV)	Crystal Structure
La_2O_3	30	4.3	2.3	Hexagonal, Cubic
SiO_2	3.9	8.9	3.2	Amorphous
Al_2O_3	9	8.7	2.8	Amorphous
Y_2O_3	15	5.6	2.3	Cubic
Ta_2O_5	26	4.5	1-1.5	Orthorhombic
TiO_2	80	3.5	1.2	Tetragonal
HfO_2	25	5.7	1.5	Monoclinic, Tetragonal, Cubic
ZrO_2	25	7.8	1.4	Monoclinic, Tetragonal, Cubic

There are various deposition techniques to fabricate these dielectric films with high dielectric constant. Some of these techniques are thermal oxidation (TO), metal-organic chemical vapor deposition (MOCVD), ion beam deposition (IBD), atomic layer deposition (ALD), pulsed laser deposition (PLD), laser oxidation (LO), remote plasma oxidation (RPO), rf and /dc magnetron sputtering technique (RF/-DC MS) (Giustino, et al. 2004).

In this study, RF magnetron sputtering was considered to grow oxidize hafnium oxide thin films. Because it's high deposition rate makes the sputtering a main technique in oxidation, most of the literature has been directed toward the sputtering technique. Sputtering is a fairly simple and trusted thin film deposition process, especially for the growth of amorphous films. The deposition of high-*k* dielectric materials is based on sputtering of a metal or metal oxide target by the bombardment with inert plasma. Particles from the sputtered target are collected on the substrate after interaction with the plasma inside the vacuum chamber. Sputtering technique has a controlled oxidation property so required physical properties and the thickness of the grown film can be studied. Detailed physics of magnetron sputtering technique will be given in section 4.

In summary, optical characterizations and thickness evaluation of films were done by an in-situ Spectroscopic Ellipsometer (SE). The structural characterization of the oxidized films was investigated by X-Ray Diffraction (XRD). The elemental composition and the chemical bonding were analyzed by means of X-Ray Photoelectron Spectroscopy (XPS) and Fourier Transform Infrared Spectroscopy (FTIR). The electrical properties of the layers have been obtained by high-frequency Capacitance-Voltage (C-V) and Conductance-Voltage (G-V) techniques.

This work has been mainly done in Izmir Institute of Technology (IZTECH) and some characterization techniques were used in Physics Department of Middle East Technical University (METU) as being a collaboration project between Izmir Institute of Technology (IZTECH) and Middle East Technical University (METU) Physics Departments, supported financially by TÜBİTAK with a project number of 107T117.

Thin film growth, in-situ SE, AFM and XRD measurements were done at IZTECH, while some of the works have been carried out during mutual visits to METU. XPS, electrical measurements, MOS and FTIR measurements were carried out at METU.

The theoretical background on electromagnetic waves (EM) and their interaction with matter are given in the chapter 2. The detailed explanation above magnetron sputtering technique is reported in the chapter 3 and MOS structures are given in the chapter 4. Chapter 5 includes experimental details, related to optical measurements, surface and interface analyses. Chapters 6, 7, 8 and 9 consist of results and discussions of analyses. The final chapter includes the conclusion of our research.

CHAPTER 2

SPECTROSCOPIC ELLIPSOMETRY

2.1. Introduction

The technique of ellipsometry was developed by Paul Drude in 1887 and he also derived the equations of ellipsometry, which are used even today. It has long been recognized as an important tool for the study of surfaces and thin films since the time of 1887 (Azzam, et al. 1977). After that, the equations for the propagation of electromagnetic waves were derived by Maxwell. He used this technique to study the dielectric function for a number of absorbing and transparent materials with and without over-layers (Drude, et al. 1890). Rothen *et al.* (1945) gave the term "ellipsometry" in order to distinguish this technique of measuring the change of the state of polarization of light upon reflection from conventional measurements of polarimetry. The early ellipsometers were operated manually and measurements with them were very time consuming. Muller and Farmer reported real-time monitoring ellipsometer in 1984. Thanks to this instrument the number of taken data was increased. From real-time data analysis of the real-time data set, the initial thin film growth process of the thin film can be characterized on the atomic scale. In order to perform accurate data analysis, understanding of the ellipsometry measurement in a detailed manner is necessary.

We currently have a spectroscopic ellipsometer SE which is attached to a magnetron sputtering system in located in the dielectric laboratory of The Izmir Institute of Technology, where we can measure in from 300 nm to 850 nm spectral range. Since SE is an optical technique, knowledge of optics and understanding behavior of light in a medium is inevitable.

2.2. Electromagnetic Waves in Dielectric Media

Light is a transverse electromagnetic wave caused by the oscillation of electric and magnetic fields with frequencies ranging from about 3×10^{11} to 3×10^{16} Hz.

Electromagnetic waves are characterized by a broad wavelength range of wavelengths and frequencies, each associated with a specific intensity (or amplitude) and quantity of energy. The distribution of energy among the various waves is called the spectrum of the radiation and various regions of the spectrum are named as radio waves, ultraviolet radiations, visible radiations etc.

Mathematically, light waves are described easily by using sinusoidal waves, such as y = sin x or y = cos x. When light enters into media, however, it shows rather complicated behavior due to refraction or absorption of light. The propagation of light in media can be expressed by the complex refractive index, i.e. or by two values known as the refractive index and extinction coefficient.

The light waves in a medium are described by Maxwell's equations. Electromagnetic field is described by the intensities of $\vec{E}$ and $\vec{H}$ of the electric and magnetic fields, respectively. They can be given in any medium as,

$$\vec{\nabla} \times \vec{H} = (\vec{J}_{ext} + \vec{J}_{cond}) + \frac{\partial \vec{D}}{\partial t} \tag{2.1.a}$$

$$\vec{\nabla} \times \vec{E} = -\frac{\partial \vec{B}}{\partial t} \tag{2.1.b}$$

$$\vec{\nabla} \cdot \vec{D} = \rho \tag{2.1.c}$$

$$\vec{\nabla} \cdot \vec{B} = 0 \tag{2.1.d}$$

where the parts a, b, c, d of this equation correspond, respectively, to Ampere's Law, Faraday's Law of Induction, Gauss' Law for Electricity, Gauss' Law for Magnetism.

$\vec{B}$ is the magnetic field vector, $\rho=\rho_{ext}+\rho_{ind}$ is the volume charge density, $\vec{H}$ is the magnetic field intensity vector and $\vec{D}$ is the electric displacement vector given by:

$$\vec{D} = \varepsilon \vec{E} = \varepsilon_0 \vec{E} + \vec{P} \tag{2.2}$$

$$\vec{H} = \frac{\vec{B}}{\mu} = \frac{\vec{B}}{\mu_0} - \vec{M} \tag{2.3}$$

ε and μ are the permittivity and permeability of medium, respectively, while ε_0 and μ_0 are the permittivity and permeability of free space, respectively. $\vec{J}$ is the current density vector includes the currents due to electron conduction ($\vec{J}_{cond}$) in metals and semiconductors as well as external currents ($\vec{J}_{ext}$).

Interaction of light with dielectric affects the atoms. When positive and negative charges are exposed to electric field, the negative charges receive electrical forces in the opposite direction to the electric field while positive charges receive it in the same direction to the electric field. The electric component of electromagnetic wave produces dipole moment due to the dielectric polarization of atoms.

Among several types of dielectric polarizations, the most important polarization for the characterization of semiconductor is electric polarization. In an atom, negative charges are bound strongly to positively charge atomic nucleus with springs. When the positions of electrons and nucleus are deflected oppositely by the electric field, electric polarization occurs. The polarization of atoms is described with in terms of time-dependant polarization vector $\vec{P}$ whose direction is from the negative charge to the positive charge.

$$\vec{P} = \varepsilon_0 \chi_{e,r} \vec{E} \tag{2.4}$$

The dimensionless functions $\chi_{e,r}$ is called the real (*r*) electric (*e*) susceptibility which depend on light frequency. As a result, electric induction $\vec{D}$ can be evaluated by a linear function of the intensity $\vec{E}$;

$$\vec{D} = \varepsilon_0 \vec{E} + \chi_{e,r} \varepsilon_0 \vec{E} = \varepsilon_0 \vec{E} \left(1 + \chi_{e,r}\right) = \hat{\varepsilon}_r \varepsilon_0 \vec{E} \tag{2.5}$$

where $\hat{\varepsilon}_r = 1 + \chi_{e,r}$ is the relative permittivity. Relative permittivity is a dimensionless complex number and defines as a dielectric constant of medium. The dielectric constant $\hat{\varepsilon}_r$ increases as the dielectric polarization and susceptibility increase.

2.2.1. Refractive Index

When light enters optically different media, the refraction of light occurs. The refraction of light is determined from the real part of the refractive index *n* which is defined by;

$$n = \frac{c}{v} \tag{2.6}$$

where *v* is the speed of light in a medium. Propagation of light is slower in a medium with higher refractive index, the propagation of light is slower.

The electromagnetic wave equation is a second-order partial differential equation that describes the propagation of electromagnetic waves through a medium or in a vacuum. So as to find the homogeneous form of the wave equation in terms of either the electric field $\vec{E}$ or the magnetic field $\vec{B}$, the curl of both sides of the Eq. (2.1b), ($\nabla \times (\vec{\nabla} \times \vec{E}) = \nabla \times (-\frac{\partial \vec{B}}{\partial t})$), is taken and with the help of Eq. (2.2), (2.3) and the relation $\vec{J} = \sigma \vec{E}$, the wave equation for the electric field is acquired .

$$\nabla^2 \vec{E} = \varepsilon\mu \frac{\partial^2 \vec{E}}{\partial t^2} - \sigma\mu \frac{\partial \vec{E}}{\partial t} = 0 \tag{2.7}$$

The wave equation for the magnetic field is obtained with the same way as follows;

$$\nabla^2 \vec{B} = \varepsilon\mu \frac{\partial^2 \vec{B}}{\partial t^2} - \sigma\mu \frac{\partial \vec{E}}{\partial t} = 0 \tag{2.8}$$

The solution of the homogeneous electromagnetic wave for the electric component is:

$$\vec{E}(\vec{r}, t) = \vec{E}_0 e^{i\omega t} \tag{2.9}$$

If the propagation direction is merely through the z axis, the wavelength for the electric field is written as;

$$\frac{\partial^2 E(z)}{\partial z^2} = -K^2 E(z) \tag{2.10}$$

here K is called the propagation number from the wavelength λ, its magnitude is $2\pi/\lambda$. It shows the number of waves present in the distance from 0 to 2π. K is also defined as;

$$K = \frac{\omega N}{c} = \frac{2\pi N}{\lambda} \tag{2.11}$$

N is described as complex refractive index of medium. Refractive index consists of real (n) and imaginary (k) parts.

$$N = n - ik \tag{2.12}$$

While real part of complex refractive index is characterized by refractive index n, imaginary part is characterized by extinction coefficient k.

2.2.2. Extinction and Absorption Coefficients

Different types of materials show different levels of absorption, causing the light to either to be blocked or allowed to be passed. Absorption is an important parameter because it plays a role in anti-reflecting coatings of thin films and in optoelectronic devices. When the absorption coefficient deals with light energy, the **Beer-Lambert Law** (eq. 2.13) defines the parameters of the transparency. The light intensity of electromagnetic waves is given by;

$$I = \left|E\right|^2 = \left|E\,to\right|^2 \exp(-\frac{4\pi k}{\lambda} x) \tag{2.13}$$

However, for the determination of transmittance, $I = n\left|E\right|^2$ is used (Hecht, 2002).

$$I(z) = I_0 e^{-\alpha z} \tag{2.14}$$

where $I_0 = \left|E_{to}\right|^2$ is the initial intensity and α is the absorption coefficient. The relation between α and k can be found as

$$\alpha = \frac{2k\omega}{c} \tag{2.15}$$

Extinction coefficient k is obtained from measurement. Absorption coefficient, α, which is used calculation of band gap can be determined directly. In a medium without absorption, the propagation number of light K can be written by inserting the Eq. (2.11) into the Eq. (2.10):

$$K = \frac{\omega N}{c} = \frac{2\pi n}{\lambda} \tag{2.16}$$

where λ is wavelength and n is refractive index of a medium. In regions where the material does not absorb, the real part of the refractive index tends to increase with frequency. Electromagnetic wave travelling in a transparent medium can be determined;

$$E = E_{t0}\left[\exp i(\omega t - Kx + \delta)\right] = E_{t0}\left[\exp i\left(\omega t - \frac{2\pi n}{\lambda}x + \delta\right)\right] \tag{2.17}$$

Here, E_0 is in a transparent medium while E_{t0} is amplitude of wave in a different medium. Figure (2.1.b) shows the propagation of wave in transparent medium. In transparent medium, wavelength of light becomes λ/n due to the reduction in velocity. Because of the light reflection at the interface, $E_{t0} \langle E_0$.

In the medium that shows strong absorption n can not only enough. For the determination of light absorption extinction coefficient k is introduced as well as n. Therefore, in the light absorbing medium N is used as a complex refractive index.

Both n and k is wavelength dependant and they are also real and positive. An electromagnetic wave traveling in a light-absorbing medium can be obtained in the following equation;

$$E = E_{t0}\exp\left[i\left(\omega t - \frac{2\pi N}{\lambda}x + \delta\right)\right] = E_{t0}\exp\left(-\frac{2\pi k}{\lambda}x\right)\exp\left[i\left(\omega t - \frac{2\pi n}{\lambda}x + \delta\right)\right] \qquad (2.18)$$

Equation 2.18 represents the electromagnetic wave as shown in the fig. 2.1.a. In the absorbing medium, wavelength of light is $\frac{\lambda}{n}$ so light absorption has no effects on the wavelengths in media. However, since light absorption occurs ($k > 0$), the amplitude namely intensity (I) of electromagnetic wave decreases along the x direction with $\exp\left(-\frac{2\pi kx}{\lambda}\right)$.

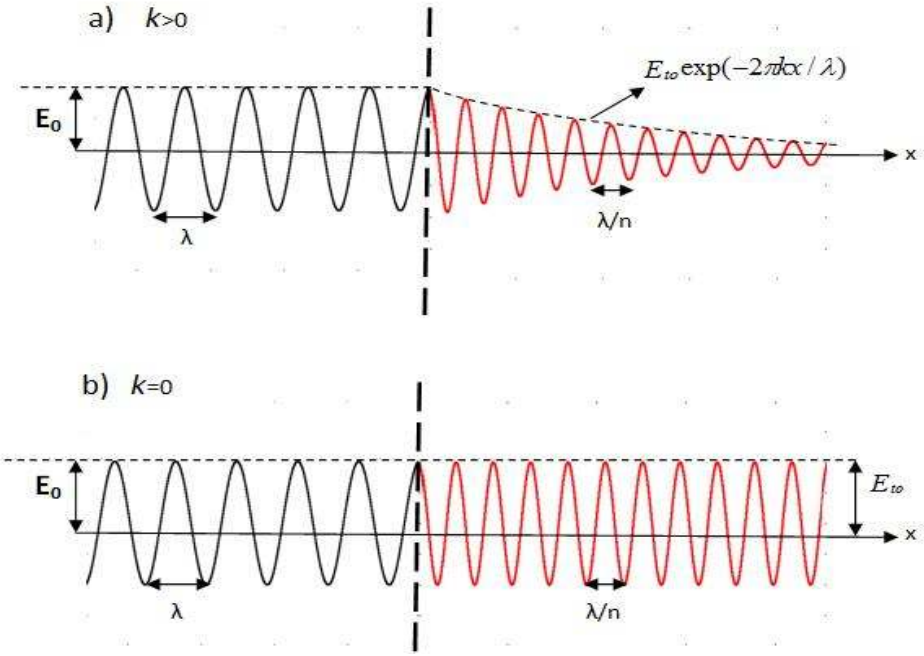

Figure 2.1. Propagation of electromagnetic wave in a) light absorbing medium (k>0) and b) transparent medium (k=0).

2.2.3. Dielectric Response of Material to Light

When electromagnetic wave impinges on matter, the electrons in the medium are forced to oscillate with the oscillation frequency of the electromagnetic wave. The oscillation of the electrons can be described in terms of a polarization of the matter at the incident electromagnetic wave frequency, and these oscillations modify the electric

field in the material. The dielectric polarization occurs as a result of separation of electric charges by external electric fields in a medium. A pair of electric charges generated by dielectric polarization is named electric dipole. The magnitude of the polarization generated within dipole moment is expressed by dielectric constant or permittivity. The relative permittivity or dielectric constant defined by the following equation is used;

$$\varepsilon = \frac{\varepsilon_p}{\varepsilon_0} \tag{2.19}$$

where ε_p is the permittivity of dielectric medium. As a result of the acceleration of electric dipole moments, electric field is generated from positive charge to negative charge. These electromagnetic radiations obey the Huygen's principle in which acting as the source of secondary electromagnetic waves combining with the incident field to form the total field.

The propagation speed of light decreases in a medium with high refractive index. This implies that the propagation speed becomes slower in dielectrics with high ε values. Therefore, there is a close relation between the dielectric constant and the refractive index. The complex refractive index $N = n - ik$ is defined as

$$N^2 = \varepsilon \tag{2.20}$$

ε is a complex number and the complex dielectric constant is defined by

$$\varepsilon = \varepsilon_1 - i\,\varepsilon_2 \tag{2.21}$$

With the combination of eq. 2.20 and 2.21, we get

$$\varepsilon_1 = n^2 - k^2 \tag{2.22}$$

$$\varepsilon_2 = 2nk \tag{2.23}$$

In a medium without absorption $\varepsilon_1 = n^2$ and $\varepsilon_2 = 0$. In this situation, ε_1 values become larger with increasing n. As a result, refractive index and extinction coefficient can be determined depending on complex dielectric constant as shown below.

$$n = \left\{ \left[\varepsilon_1 + \left({\varepsilon_1}^2 + {\varepsilon_2}^2 \right)^{0.5} \right] / 2 \right\}^{0.5} \tag{2.24}$$

$$k = \left\{ \left[-\varepsilon_1 + \left({\varepsilon_1}^2 + {\varepsilon_2}^2 \right)^{0.5} \right] / 2 \right\}^{0.5} \tag{2.25}$$

2.2.4. Transmission and Reflection Properties of Light

When light advances into a medium, some of the light is reflected and some of it transmitted. The reflection and transmission of light is determined by the complex index of refraction or complex dielectric constant of a medium. Reflection R is the change in direction of a wavefront at an interface between two different media so that the wavefront returns into the medium from which it was originated. Light transmission T is the percentage of incident light that passes through a media.

Considering an electromagnetic wave enter a medium of refractive index n_i with angle of incidence θ_i from the medium of refractive index n_t, it is reflected with θ_i and refracted with θ_t according to Snell's laws.

$$n_i \sin(\theta_i) = n_t \sin(\theta_t) \tag{2.26}$$

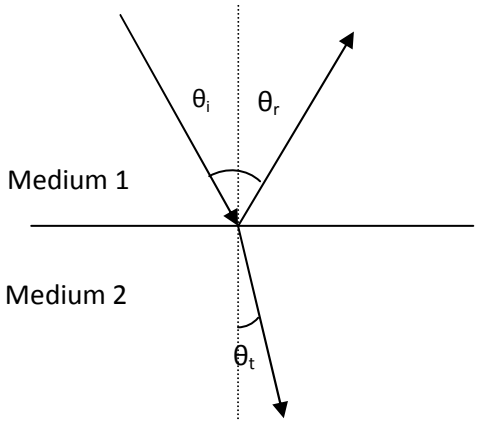

Figure 2.2. Refraction of light at the interface between two media of different refractive indices.

To determine the amplitudes of reflected and transmitted beams, Fresnel coefficient equations relating the amplitude of the incoming, reflected and transmitted beams are used.

$$r = \frac{E_{ref}}{E_{inc}} \quad \text{and} \quad t = \frac{E_{trans}}{E_{inc}} \tag{2.27}$$

2.3. Spectroscopic Ellipsometry

2.3.1. What is Ellipsometry?

Spectroscopic Ellipsometry (SE) is a versatile and powerful optical characterization technique for the investigation of the dielectric properties, i.e. complex refractive index and dielectric function and thickness of thin films (Buiu, et al. 2008). It has applications in many different fields, from semiconductor physics to microelectronics and biology, from basic research to industrial applications. Ellipsometry has many advantages which can be ordered as follows.

i. In a single measurement, at least two parameters are determined at each wavelength of a spectrum.
ii. Since ellipsometry measures intensity ratio instead of pure intensity, it is less affected by intensity unbalances of light.
iii. Non-destructive technique so, used for in-situ measurements.
iv. High thickness sensitivity.

However, there are two general restrictions on the ellipsometry measurements.

i. Surface roughness of samples has to be small.
ii. The measurements must be performed at oblique incidence.

Ellipsometry requires that the angle of incidence light should be well defined. The incidence angle of light used in ellipsometric measurement is set at the Brewster angle. The choice of the incidence angle, however, varies according to the optical constants of samples. For semiconductor characterization, the incidence angle is typically 70–80°. The incident light beam therefore needs to be collimated.

2.3.2. Principles of Ellipsometry Measurement

2.3.2.1. Experimental setup

Ellipsometry measures the change of polarization state upon reflection or transmission from a surface (Johs, et al. 1997, Duncan, et al. 1992). In order to do this analysis, the polarization state includes the following as shown in the Fig. 2.3,

a) Light source
b) Polarizer
c) Compensator (optional)
d) Analyzer
e) Detector

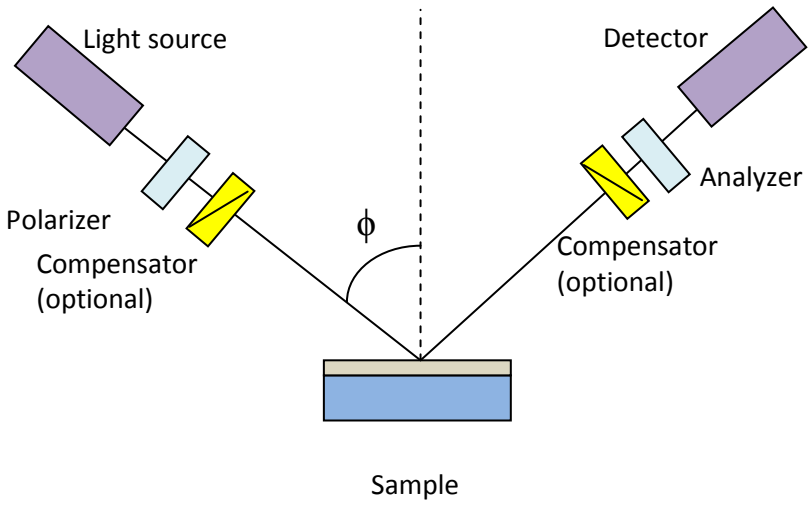

Figure 2.3. Schematic representation of ellipsometry.

Un-polarized light that is completely random orientation and phase produced by a light source is sent through a polarizer. The polarizer is oriented between the p- and s-planes so that both arrive at the sample surface. The resulting light is linearly polarized. After reflecting from the sample surface, linearly polarized light turns to elliptically polarized light where the ellipsometry gets its name (Fig. 2.4).

Elliptically polarized light travels through an analyzer. The detector converts light to electronic signal to determine the reflected polarization.

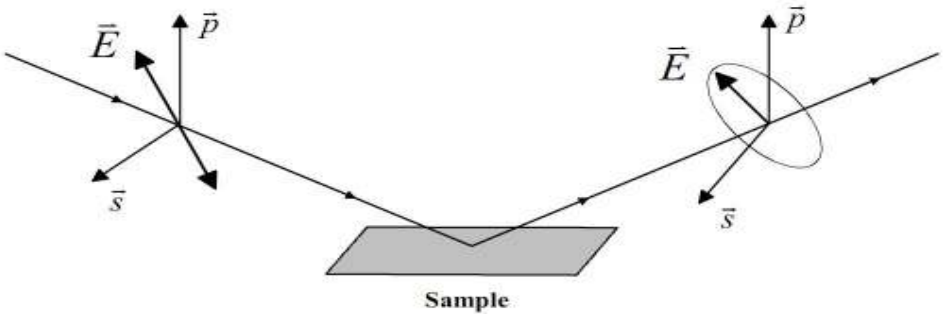

Figure 2.4. Basic principle of ellipsometry: Linearly polarized light is incident, elliptically polarized light is reflected.

2.3.2.2. Measurements and Data Analyses of Ellipsometry

Ellipsometry characterizes light after reflection or transmission from samples. Ellipsometric measurements are the amplitude ratio Ψ and phase difference Δ between light waves. The data from an SE measurement is not useful by itself, but data analyses requires an appropriate optical model. The selection of correct optical model and construction of layers are the important steps to extract the useful information, i.e. thickness and optical constants of sample. In the process of this modeling, the number of layers must be selected and the optical functions of each layer must be determined. A sample consists of a stack of materials within an ambient medium. Figure 2.5 shows a representative model consisting of air/ thin film/ substrate structure. N_0, N_1 and N_2 are complex refractive indices of air, thin film and substrate, respectively. Ψ and Δ are fitted by using a suitable model for the stack layer. After fitting, the change in polarization is obtained from the eq. 2.46. Finding the best fitting between the model and the experiment gives directly thickness *d* and optical constants, i.e. refractive index *n* and extinction coefficient *k*.

$$\rho = \frac{R_p}{R_s} = \tan(\psi)\exp(-i\Delta) \tag{2.28}$$

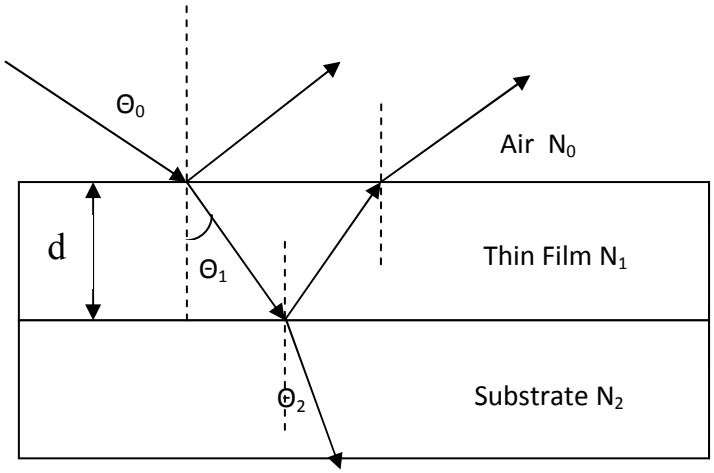

Figure 2.5. Optical model.

2.3.2.3. Selecting a Suitable Model

When measuring samples with ellipsometry, the interaction of light with sample causes a change in intensities or polarization of the measuring beam. This change is measured and contains the information on sample. The behavior of the sample when reflecting light is theoretically calculated using a theoretical description of the sample, i.e. the model, and compared with the measured behavior.

There are a few dielectric function models. These models can be given as Sellmeier, Cauchy, Drude, Lorentz, Tauc–Lorentz, harmonic oscillator approximation (HOA) model (Tompkins, et al. 2004). In this study, Cauchy modelling was used to describe HfO_2 films as well as SiO_2 interfacial layer which are transparent in the visible range.

2.3.2.4. Cauchy Modelling

Cauchy's equation is a relationship between the refractive index and wavelength of light for a particular transparent material. It is named for the mathematician Augustin Louis Cauchy, who defined it in 1836. The Cauchy model is used in a transparent region where $\varepsilon_2 \sim 0$ (Fujiwara, 2007).

The Cauchy Relations are;

$$n(\lambda) = n_0 + C_0 \frac{n_1}{\lambda^2} + C_1 \frac{n_2}{\lambda^4} + \ldots \tag{2.47}$$

$$k(\lambda) = k_0 + C_0 \frac{k_1}{\lambda^2} + C_1 \frac{k_2}{\lambda^4} + \ldots \tag{2.48}$$

where n is the refractice index, k is the extinction coefficient, λ is the wavelength. The coefficients C_0 and C_1 equal to 10^2 and 10^7, respectively, that can be determined for a material by fitting the equation to measured refractive indices at known wavelengths.

CHAPTER 3

MAGNETRON SPUTTERING TECHNIQUE

3.1. Thin Film Technology

Thin film deposition techniques are either purely physical or purely chemical methods. However, some techniques are based on glow discharges and reactively sputtering techniques combine both physical and chemical reactions. Recently, there have been many developed film deposition process. Sputtering deposition is one of the common processes for fabrication layers in the thickness range of a few nanometers to about micrometers.

This technique can be divided into four categories namely, DC, RF, reactive and magnetron. The magnetron sputtering is the dominant method of physically depositing films by plasma methods. In this work, RF magnetron sputtering technique was used to grow HfO_2 thin films.

3.2. Sputtering Technique

Sputtering is a widely used technique for the erosion of surfaces and the deposition of films. Sputtering is practiced by means of plasma which generates particles energetically charged. When a solid target surface is bombarded with these energetic charged particles, i.e. accelerated ions, target atoms are scattered backward due to the collisions between energetic particles. This situation is named as sputtering. It is widely used for film deposition on semiconductor surface wafers. Sputtering process has many advantages which can be ordered as follows;

1. Deposition rates do not differ from one material to another,
2. Deposition rates are high for some materials,
3. Thickness control is very simple by setting a timer,
4. The lifetime of sputtering target is as long as hundreds of runs.

3.2.1. Sputtering Yield

Any suitably energetic atomic particles such as atoms, ions, electrons, photons, and neutrons as well as molecular ions and molecules impinging on a surface can cause sputtering. The sputter yield, *Y*, is the ratio of the number of emitted particles per incident particles (Stuart, 1982):

$$Y = \frac{Number\ of\ emitted\ particles}{Number\ of\ incident\ particles} \tag{3.1}$$

The sputtering yield is identical for the different incident particles with the same energy because physics of sputtering is based on momentum transfer and kinetic energy transfer from incident particle to the surface atoms. Therefore, energy and the angle of the incident particle, relative masses of target and bombarding species, surface morphology and purity of the target affect the sputter yield. However, sputtering yield is independent of the particle's charge (Seshan, 2002). Sputter yield shows variations with the angle of incident ions. It increases with the incident angle between 60-80 and decreases for larger angles.

3.3. Sputtering Systems

3.3.1. Direct Current (DC) Sputtering

A DC power supply is used to create plasma in the system. DC sputtering is the simplest kind of plasma device and consists of an anode and cathode inside a vacuum chamber. With sufficient voltage across the electrodes and the appropriate gas pressure, the gas will breakdown into a plasma discharge. As a result of the collision between energetic electrons accelerated by electric field and argon gas molecules (Ar), positive ions are generated. After bombardment of positive ions to the cathode surface, secondary electrons are generated from the cathode surface. These secondary electrons are accelerated back and collide with gas atoms in order to increase the ionization of the gas molecules and increase the discharge.

Direct current sputtering (DC) has limitation of low deposition rate and difficulty of depositing insulators. Since surface of the target can be charged rapidly due to the electrons from DC supply, only conductive targets can be sputtered by using DC sputtering.

3.3.2. Radio Frequency (RF) Sputtering

RF sputtering has the same atomistic processes which occur in the dc discharge. However, the difference between them is that the plasma is created by the RF supply at high frequency. The most common frequency is 13.56 MHz. Rf source operates with a different way than the dc source. Since anode and cathode are electrically reversed, this eliminates charge built up on an insulating surface by providing an equal number of ions. This allows insulators or conductors to be sputtered by RF sputtering. RF sputtering offers advantages over DC. For instance, lower voltages and lower gas pressure can be used. Higher deposition rates can be obtained.

3.3.3. Reactive Sputtering

Chemical reactions of atoms emitted from target fly from the target to sample surface to form their compound film. In existence of a reactive gas, i.e. oxygen gas, emitted target atoms can quickly react with them on the film surface to form an oxide. This event is known as reactive sputtering. Reactive sputtering is generally used for the deposition of oxide and nitride thin films.

3.3.4. Magnetron Sputtering

The magnetron sputtering is the design of high deposition rate sputtering technique. The magnetron is a magnetically assisted discharge. There is an electric field perpendicular to the target surface and there are magnets to create lines of magnetic flux which are parallel to the surface of the target (see Figure 3.1.).

Motion of a charged particles in the presence of magnetic and electric field is described by Lorent'z formula given in Eq. 3.2. According to this formula, secondary electrons emitted from target surface follow a helical trajectory around the magnetic field lines with an induced drift. In magnetron sputtering, induced current which flows parallel to the target surface is called 'the E×B drift current'. This property enhances the ion bombardment with containing electrons in the discharge and sputtering rates with improving the collision probability of electrons with gas molecules.

$$m\frac{d\vec{v}}{dt} = q\left(\vec{E} + \vec{v} \times \vec{B}\right) \tag{3.2}$$

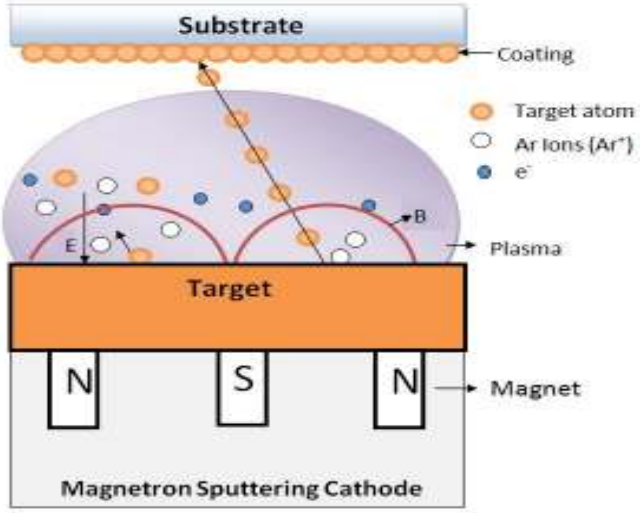

Figure 3.1. The schematic representation of rf magnetron sputtering process.

Advantage of magnetron sputtering over diode sputtering is that secondary electrons are prevented from being the bombardment of substrate, so that, no real substrate heating observed. Depending of the electrical properties of the target material, magnetron sputtering can be used either dc mode or RF mode.

CHAPTER 4

METAL-OXIDE-SEMICONDUCTOR STRUCTURES

4.1. Introduction

Metal-Oxide-Semiconductor (MOS) capacitors are the heart of every digital circuit such as single memory chip, dynamic random-access memory (DRAM), switched capacitor circuits, analog-to-digital converters and filters, optical sensors and solar cells (Tyagi 1991). The progress in MOS technology results in an increment of the numbers of MOS transistors integrated in any microelectronic devices. The increase in number of transistors is essentially due to the reduction of transistor size. This exponential growth of integration density with time is known as Moore's law. A schematic view of a MOS capacitor is shown in the Fig. 4.1.

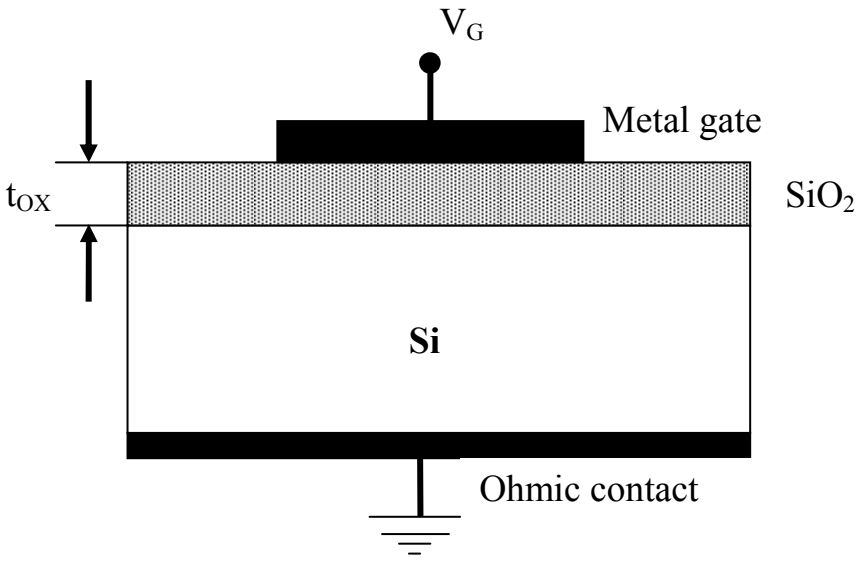

Figure 4.1. Cross-sectional view of a MOS capacitor.

MOS capacitor contains a silicon substrate on which a thin SiO_2 layer is deposited. A thin metal (usually Al) which is named with as *gate electrode* is deposited

on the top of the SiO_2 layer. A second metal layer forms an ohmic contact to the back of the silicon substrate.

4.2. Ideal MOS Capacitor

In ideal MOS capacitor, when a metal is making intimate contact with a semiconductor, so that charge will flow from the semiconductor to the metal the thermal equilibrium is established and the Fermi levels on both sides line up. Figure 4.2 shows the energy band diagram of an ideal MOS structure made on a p-type and n-type semiconductor under thermal equilibrium.

The energy difference between the vacuum level and the Fermi level is described as a work function. This quantity is denoted by $q\phi_m$ for the metal and $q\phi_{sc}$ for the semiconductor. $q\phi_{sc}$ equals to $q\chi+qV_p$ where $q\chi$ is the electron affinity and qV_p is the energy difference between E_c and Fermi level. The potential difference between the work functions, $q\phi_m - q(\chi + V_p)$, is called the contact potential. The energy difference between metal Fermi level and oxide conduction band, $q\phi_B$, is named with *metal-to-oxide barrier energy (height)*. The importance of this energy barrier is that it prevents carriers from flowing freely from the metal to silicon or vice versa. For an ideal MOS structure following descriptions are valid.

i. The metal and semiconductor have the same work function.
ii. The oxide is a perfect insulator without any charges.
iii. The energy band diagram for the semiconductor is valid up to the surface.
iv. No charges exist either on the oxide-semiconductor interface or in the bulk except those induced by the voltage at the gate.

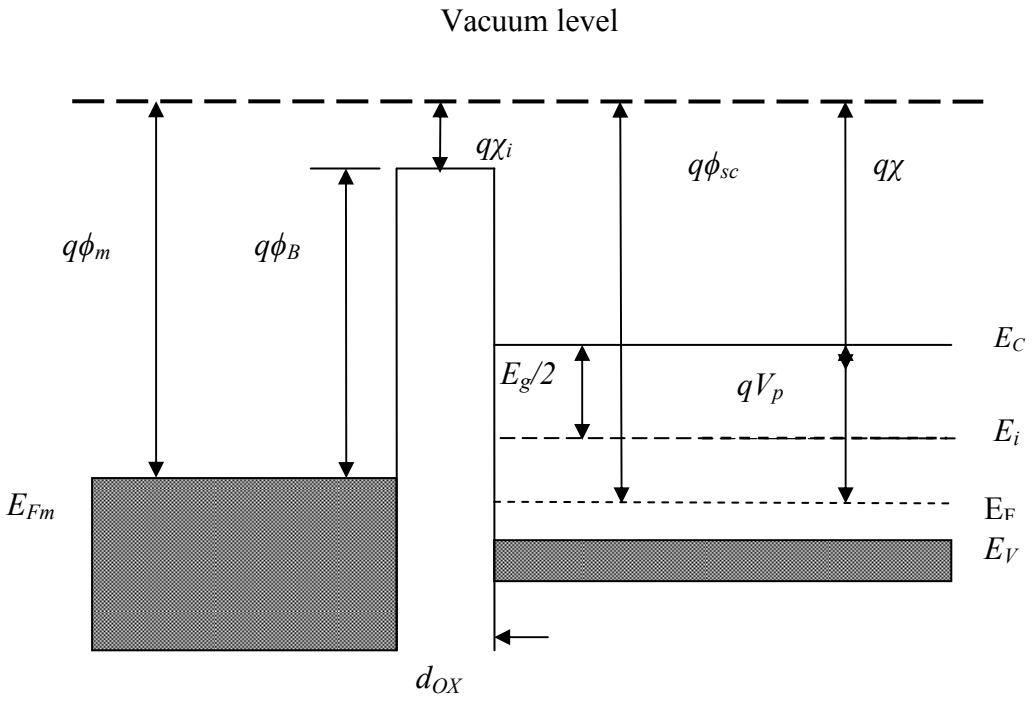

Figure 4.2. Energy band diagram of an ideal MOS capacitor on a) p-type semiconductor b) n-type semiconductor under thermal equilibrium (V=0) (Source: Sze 1981).

4.2.1. MOS Capacitor under Different Bias Conditions

When the metal gate is biased at various gate voltages V_G, three different situations can in principle arises: *i)* Below the flatband voltage, V_{FB}, *ii)* between the flatband voltage and the threshold voltage, V_{th}, *iii)* larger than the threshold voltage. These bias regimes are called the accumulation, depletion and inversion mode of operation (Zeghbroeck 2004). They depend on the type of the substrate and bias direction. To understand the role of applied bias modes and the relationships between band-bending, charge, and electric field of an MOS capacitor, discussion is carried out, here, MOS capacitors including p type Si substrate. The analysis of MOS capacitors with an n type Si substrate is similar but differences are related with only doping type and Fermi level (Zeghbroeck 2004). Meanwhile, some definitions related to voltages need to be given at this point before the discussion of different biasing conditions is given.

Flat Band Voltage: In an ideal MOS capacitor, the voltage separating the accumulation and depletion regime is referred to as the ***flatband voltage***. It is given as the difference of metal and semiconductor work function as follows;

$$V_{FB} = \phi_m - \phi_{sc} \tag{4.1}$$

Flat band voltage is also obtained from conduction peak voltage of 1MHz or 100 kHz measurements.

Threshold Voltage: The ***threshold voltage*** is usually defined as the gate voltage where an inversion layer forms at the interface between the insulating oxide layer and the substrate of the transistor.

4.2.1.1. Accumulation

Accumulation is a bias condition which occurs when a voltage whose value is less than flat band voltage as shown in figure 4.3.(a) is applied to the gate.

In accumulation mode, majority carriers accumulate in semiconductor surface region. Majority carrier concentration at the SiO_2 – Si interface is greater than the majority carrier concentration in the neutral bulk.

4.2.1.2. Depletion

Depletion layer is an insulating region within a conductive material where the mobile charge carriers have diffused away, or have been forced away by an electric field (fig. 4.3.(b)). It is also called depletion layer. The depletion layer width increases with increasing gate voltage.

4.2.1.3. Inversion

Inversion is a bias condition as shown in figure 4.3(c). Minority carrier concentration at the SiO_2 – Si interface is greater than the majority carrier concentration in the neutral bulk. Figure 4.3 shows accumulation, depletion and inversion conditions of n-MOS (p-type substrate).

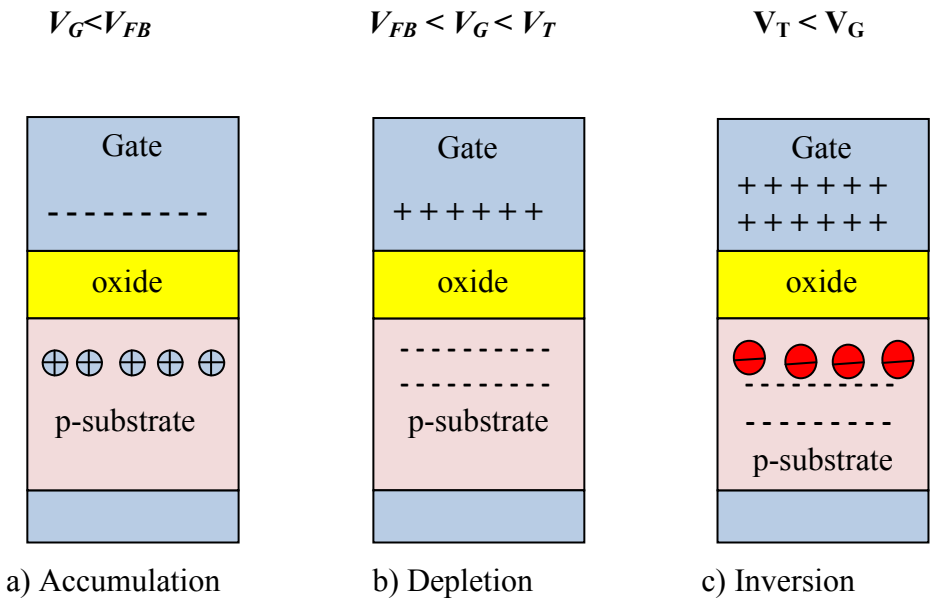

Figure 4.3. Charges in an *n*-type Metal-Oxide-Semiconductor structure (*p*-type substrate) under accumulation, depletion and inversion conditions.

4.2.2. Silicon Surface Space Charge Region

The relations between the potential at semiconductor surface, surface space charge and the electric field are shown in this section. These relations play important role in electrical characteristics of an ideal MOS structures. Figure 4.4 shows an energy band diagram of MOS capacitor before thermal equilibrium. It consists of a p type Si substrate on which a thin SiO_2 layer is deposited. A thin Al metal is deposited on the top of the SiO_2 layer as a gate electrode. The back side of the Si substrate has an ohmic contact as shown figure 4.1.

When two different permissible energy systems are brought into contact as shown in figure 4.4, then the Fermi level plays an important role in the equilibrium conditions. In the event of the same Fermi level on both sides, thermal equilibrium is obtained. If Fermi level in each system is not equal just before the contact, then on contact electrons will flow from the system with higher initial E_F to the system lower initial E_F.

This electron flowing continues until equlibrium obtained, i.e. Fermi levels of two systems are equal (figure 4.5). There must also be an energy balance between the materials. In summary; the thermal equilibrium should satisfy the following requirements: *i)* Fermi levels of semiconductor and metal must be equal, *ii)* There must be an energy balance from one material to the other. As a result of equilibrium, semiconductor has a surface potential $\Psi=\Psi_s$ which is called semiconductor surface band bending. Ψ is defined as an intrinsic Fermi level difference between neutral bulk of the semiconductor and SiO_2/Si interface. This potential is zero in the bulk of the semiconductor. Using the band bending, the hole and electron density distribution at the silicon surface under an applied bias can be calculated as a function of Ψ from following equations (Nicollian, et al. 2003).

$$n_p = n_{po}\exp\left(\frac{E_F - E_i}{kT}\right) = n_{po}\exp\left(\frac{q\psi}{kT}\right) \tag{4.2}$$

$$p_p = p_{po}\exp\left(-\frac{E_i - E_F}{kT}\right) = p_{po}\exp\left(-\frac{q\psi}{kT}\right) \tag{4.3}$$

where Ψ is positive when the band is bent downward.

n_{po} and p_{po} are equilibrium densities of electrons and holes, respectively, in the bulk of the semiconductor

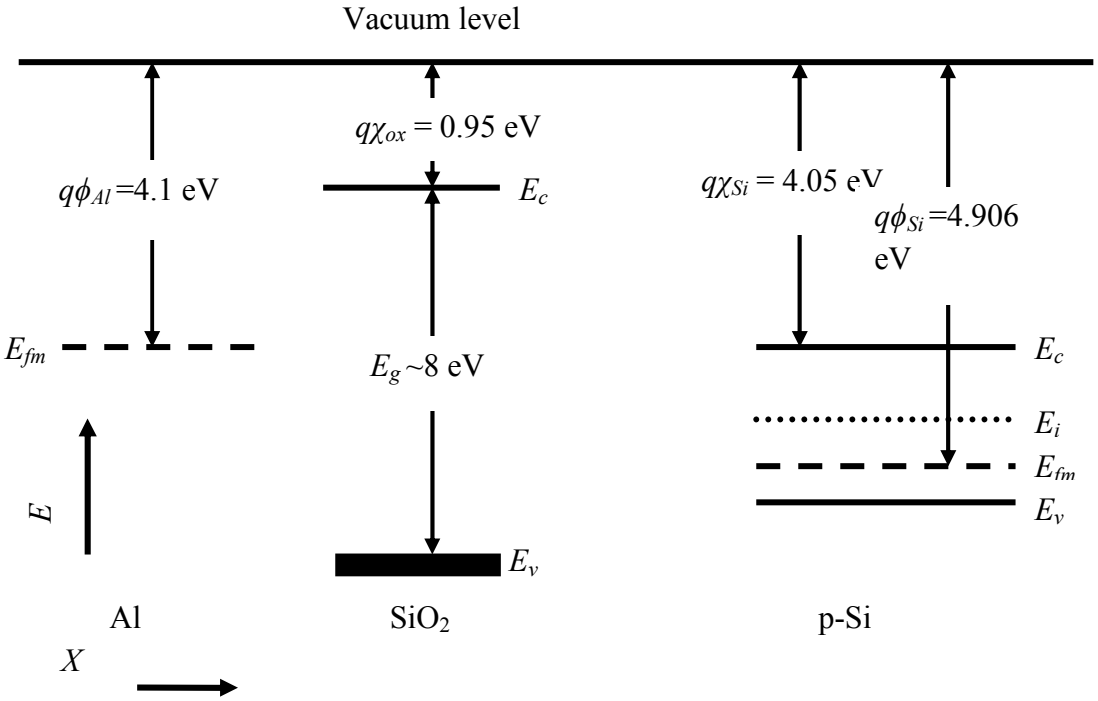

Figure 4.4. Energy band diagram of MOS capacitor before thermal equilibrium. (Source: Aygun 2005).

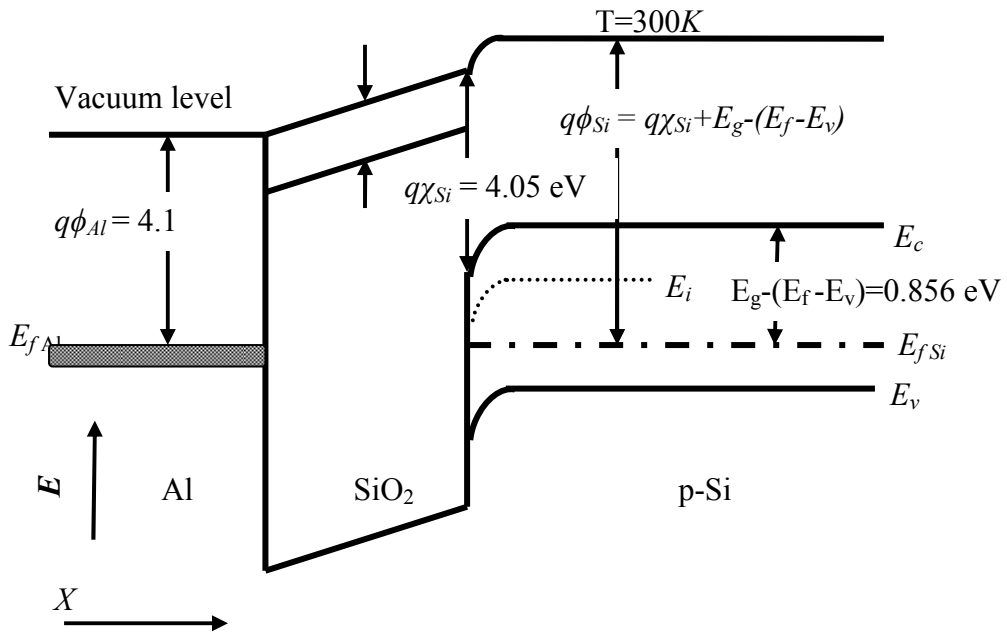

Figure 4.5. Energy band diagram of MOS capacitor after thermal equilibrium. (Source: Aygun 2005).

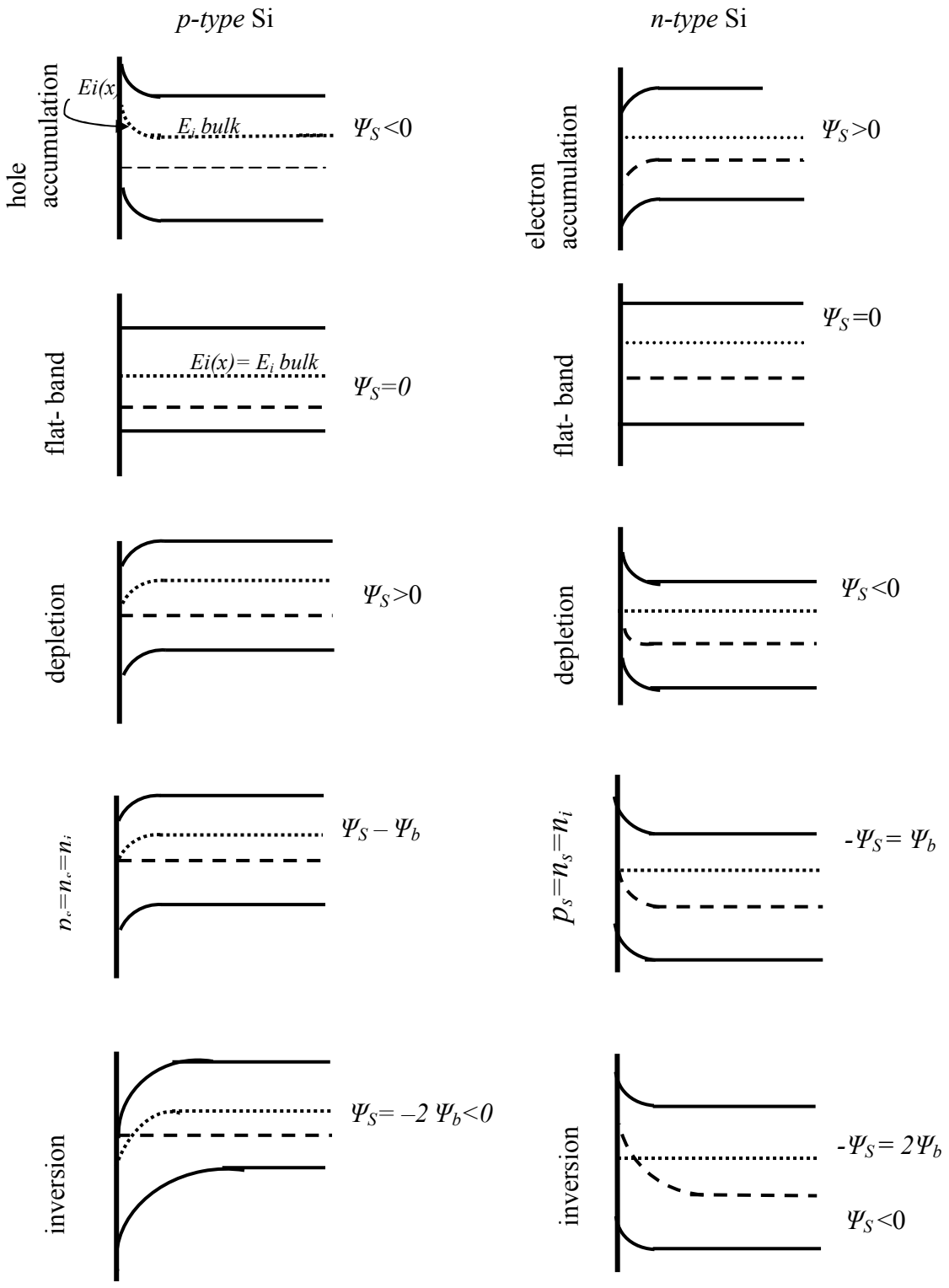

Figure 4.6. Ψ_s values for different physical conditions for p-type and n-type semiconductors (Source: Nicollian 2003).

4.3. C-V Characteristics of the MOS Capacitor

4.3.1. The Ideal MOS System

The MOS structure in the Figure 4.1 acts as equivalent of a serial combination of the silicon and the oxide capacitance per unit area and the oxide capacitance per unit area. The static capacitance is defined as $C_{stat}=Q_T/V_G$ where Q_T is the total charge density on the capacitor and V_G is the bias applied to it. Since charges on an MOS capacitor vary nonlinearly with voltage, the differential capacitance is defined as;

$$C_{dif} = \left| \frac{d Q_{Si}}{d V_G} \right| \tag{4.6}$$

Finally, the total capacitance per unit area of the MOS capacitor C_{dif},

$$\frac{1}{C_{dif}} = \frac{1}{C_{ox}} + \frac{1}{C_{Si}} \tag{4.7}$$

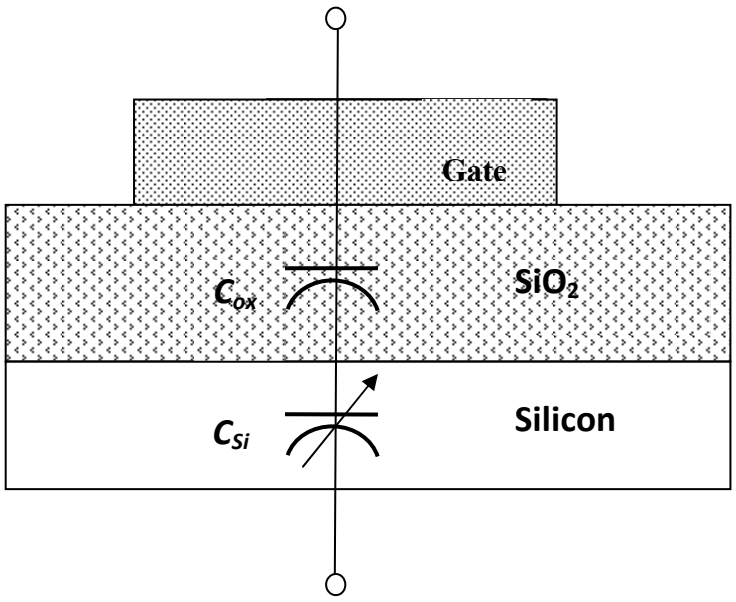

Figure 4.7. Cross section of an MOS capacitor showing a simple equivalent circuit. (Source: Nicollian 2003).

4.3.1.1. Frequency Effect

When ac voltage across the MOS capacitor changes rapidly, the electron concentration in the inversion layer cannot change instantaneously. The C-V characteristics will then be a function of the frequency of the ac signal.

Figure 4.8 shows frequency dependence of C-V curve of ideal MOS structure. The negative voltage side of curve begins with the high capacitance of the semiconductor which implying the accumulation of holes. While the negative voltage is reduced, a depletion region acting as a dielectric layer is shaped near the semiconductor surface with a decrement of capacitance.

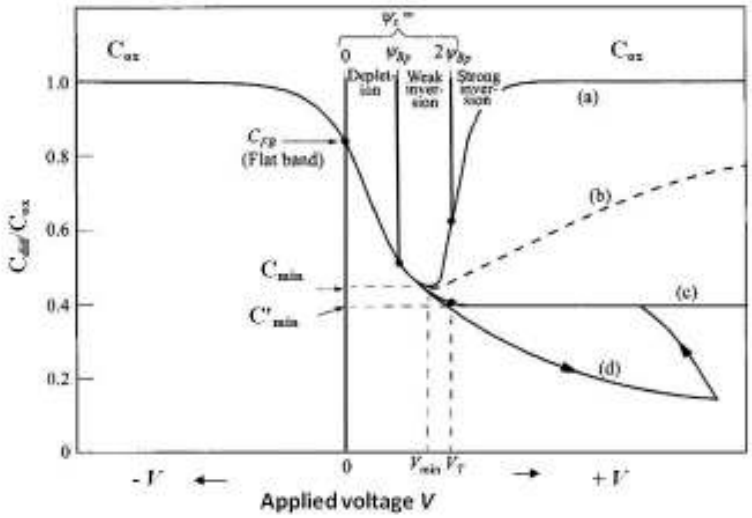

Figure 4.8. MOS capacitance-voltage curve with p-type semiconductor for a) Low frequency, b) Intermediate frequency, c) High frequency, d) High frequency with deep depletion (Source: Sze 1981).

When the magnitude of capacitance goes to minimum, then it is influenced between weak and strong inversion depending on electron concentration at the surface. When the inversion layer narrows, electrons must fill the states in conduction band at the silicon surface to higher bands.

Similarly, when the inversion layer widens, electrons must fill the states in conduction band at the silicon surface to lower bands than the equilibrium level. This increment of inversion layer only happens at low frequencies.

The increase of capacitance on the right side is not observed at high frequency measurements of MOS C-V curve.

4.3.2. Non-Ideal MOS System

The SiO_2/Si interface in a non-ideal MOS capacitor is not understood exactly. It is thought that the transition from Si to SiO_2 results in the formation of incompletely oxidized of SiO_x here $x \leq 2$. In non-ideal MOS structure, there are an interface traps and oxide charges which affect the ideal MOS characteristics. The four general types of charges associated with the interface are shown in Figure 4.9. These charges can be given in four general categories as follows;

i. Fixed oxide charges Q_f.
ii. The mobile oxide charge Q_m.
iii. Interface trapped charge or fast states Q_{it}.
iv. The oxide trapped charge Q_{ot}.

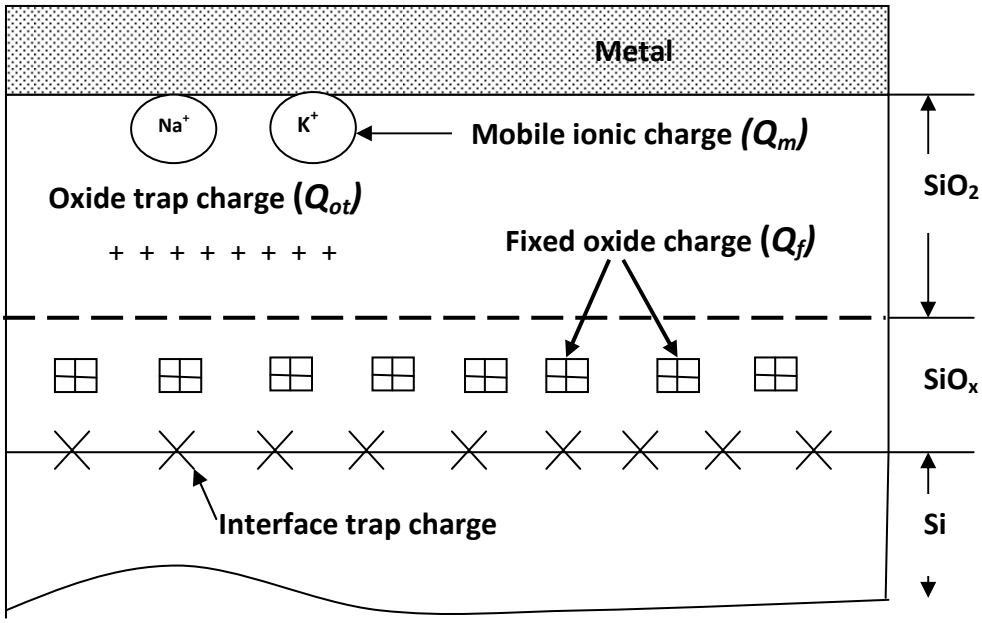

Figure 4.9. Charges associated with thermally oxidized silicon
(Source: Deal 1980).

4.3.2.1. Fixed Oxide Charges (Q_f)

Fixed oxide charge is generally a positive charge and located at or near the interface. The origin of this charge is related to the incomplete chemical bonding of the atoms near the dielectric/semiconductor interface. The charge Q_f is not in electrical communication with the underlying silicon so it is stationary under an applied electric field. Its density is not affected by the oxide thickness and the kind of impurities inside the silicon.

Fixed oxide charge causes the voltage shift of the C-V curve. For n and p-type Si the positive Q_f casuses the voltage shift through the negative, the negative Q_f causes the voltage shift through the positive gate voltage. The voltage shift is determined with respect to ideal C-V curve where Q_f is zero. Figure 4.10 shows the voltage shift of high frequency C-V curve for n and p type silicon when Q_f is positive and negative.

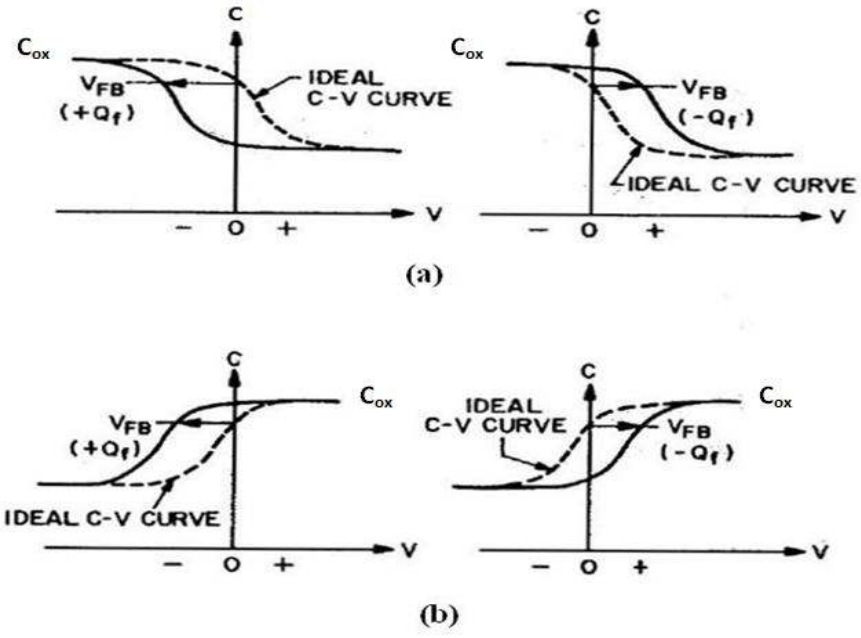

Figure 4.10. C-V curve voltage shift due to positive and negative fixed oxide charge for (a) p type silicon, (b) n type silicon (Source: Sze 1981).

The magnitude of voltage shift is given by;

$$V_{FB} = \phi_{MS} - \frac{Q_f}{C_{ox}} \tag{4.8}$$

where V_{FB} is the flat band voltage, C_{ox} is accumulation capacitance and ϕ_{MS} is the difference of work function. The work function difference between Al gate and p-type Si, Φ_{MS}, is -0.7 eV and between Al gate and n type Si, Φ_{MS}, is -0.3 eV.

4.3.2.2. The Mobile Oxide Charge (Q_m)

The mobile oxide charge Q_m is due to the presence of alkali ions like Na^+, K^+, and Li^+. Heavy metal ions may also contribute to this charge. When a voltage is applied to gate, this charge can move through the oxide causing a change in the flat band voltage.

4.3.2.3. Interface Trapped Charge or Fast States (Q_{it})

Interface trap charges are located at the Si-SiO_2 interface with energy states in the silicon-forbidden band gap. This interface trapped charge has also been called *surface states*, *fast states*, or *interface states*. The interface trapped charge Q_{it} can be produced due to the excess silicon, excess oxygen and impurities. Q_{it} can be positive when interface gives up an electron and negative when interface accepts an electron. Unlike fixed charges or trapped charges, they are in electrical communication with the underlying silicon.

Interface traps can be charged or discharged, depending on the surface potential. When a voltage is applied to gate metal, interface trap levels move up or down while the valance level remains fixed.

A change of charge in the interface trap occurs when it crosses the Fermi level. This change of charge contributes the MOS capacitance and change the ideal MOS curve as shown in Figure 4.11.

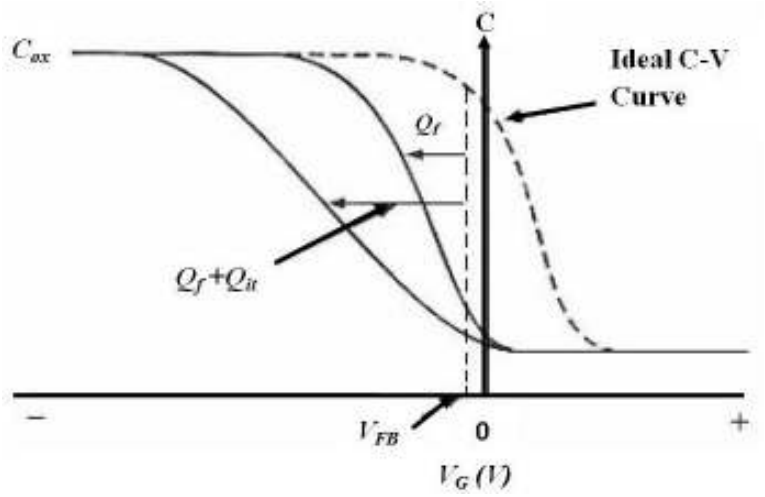

Figure 4.11. High-frequencies capacitance versus gate voltages of MOS capacitor with a p-type substrate showing effects of interface trapped charge and fixed oxide charge (Source: Aygun 2005).

4.3.2.4. The Oxide Trapped Charge (Q_{ot})

Oxide trap charge can be either positive or negative depending on trapped electrons or holes trapped in the bulk of the oxide. The trapped charges may result from ionizing radiation such as X-ray radiation or hot-electron injection and they are distributed inside the oxide layer. Unlike fixed oxide charges, oxide trapped charges are sometimes avoided by low temperature annealing treatments, although neutral traps remain.

4.4. Current Mechanisms in MOS Capacitors

Low leakage current in thin film dielectric layer is becoming a significant parameter for the quality of MOS transistors. Therefore, the identification and modeling of different leakage components is very important for estimation and reduction of leakage current. In metal-semiconductor contacts, there is a great variety of the thin film current transport mechanisms. These are;

1. Fowler-Nordheim Tunneling
2. Direct Tunneling
3. Band-to-Band Tunneling

4. Trap Assisted Tunneling
5. Poole-Frenkel Tunneling
6. Space-charge limited current
7. Hopping Conduction (Ohmic Conduction)
8. Schottky-like Emission (Modified Poole-Frenkel Current)
9. Surface-State Tunneling
10. Diffusion Current
11. Recombination-Generation Current

The tunneling probability of an electron depends on the thickness of the barrier, the barrier height, and the structure of the barrier. Therefore, the tunneling probabilities of a single electron are different for each tunneling mechanism, resulting in different tunneling currents. In this study, the Poole-Frenkel Tunneling was used for our I-V measurements.

4.4.1. Poole-Frenkel Tunneling

Although, the conductance of the insulator is thought to be zero in an ideal MOS structure, an electrical insulator can conduct electricity when the electric field or temperature is high. Electrons can move slowly through an insulator by the following method. The electrons are generally trapped in localized states where the conduction band of insulator.

Occasionally, random thermal fluctuations will give that electron enough energy to get out of its localized state, and move to the conduction band. However, the structural defects cause additional energy states close to the band-edge called traps. These traps restrict the current flow because of a capture and emission process. The current is a simple drift current described by

$$J_{PF} = nq\mu E \tag{4.9}$$

where n is the carrier density and μ mobility. The carrier density depends exponentially on the depth of the trap which is corrected for the electric field.

$$n = n_0 \exp\left[-\frac{q}{kT}\left(\phi_{PF} - \sqrt{\frac{qE}{\pi \varepsilon_i}} \right) \right] \tag{4.10}$$

Taking everything into account, the current density expression for the Poole–Frenkel effect is:

$$J_{PF} = q\, n_0\, \mu \exp\left[-\frac{q}{kT}\left(\phi_{PF} - \sqrt{\frac{qE}{\pi \varepsilon_i}} \right) \right] \tag{4.11}$$

J is the current density, E is the applied electric field, q is the elementary charge, φ_{PF} is the barrier height (in zero applied electric field) that an electron must cross to move from one atom to another in the crystal, ε is the dynamic permittivity, k_B is Boltzmann's constant, T is the temperature.

CHAPTER 5

EXPERIMENTAL PROCEDURE

5.1. Purpose

The main purpose of this study is to grow thin HfO_2 films on Si substrate under suitable vacuum conditions below 10^{-6} Torr by magnetron sputtering technique and investigate its optical properties by an in-situ spectroscopic ellipsometer (SE) mounted on the magnetron sputtering system. The grown films were examined to obtain their structural and interfacial properties by various diagnostic and analyses techniques including Fourier Transform Infrared Spectroscopy (FTIR), X-Ray diffraction (XRD), X-ray Photoelectron Spectroscopy (XPS). Having good enough qualities defined in terms of optical and structural techniques, some HfO_2 grown films were used to construct metal-oxide-semiconductor (MOS) capacitors in order to analyze their electrical properties.

The growth of HfO_2 films was realized in terms of different oxidation parameters to be able to define the best oxidation conditions including RF power range, various gas ratios, substrate cleaning procedure and Si substrate' types. In this chapter, details of experimental procedures including substrate preparation, thin film growth stages and all characterization apparatus will be described.

5.2. Experimental Procedure for Hafnium Oxide Thin Film on Si

There are a number of different fabrication processes of HfO_2 high-*k* films. Some of these techniques are thermal oxidation (Hayashi 2003), various types of chemical vapor deposition (Teren, et al. 2005), ion beam deposition (Mori, et al. 2003), atomic layer deposition (Sayan, et al. 2001), pulsed laser deposition (Ikeda, et al. 2002), laser oxidation (Aygun, et al. 2008), remote plasma oxidation (Kang, et al. 2005), (RF and DC) magnetron sputtering technique (Khomenkova, et al. 2010) and sol-gel process (Neumayer, et al. 2001).

Since each method has some certain advantages as well as disadvantages, it is not yet clear which one is the best choice for device applications. Among them, we have used RF magnetron sputtering technique to grow thin HfO_2 films. The procedures for reactively sputtered grown of HfO_2 thin films on Si substrate are given as below;

1. n-type and p-type Si substrates with having resistivities, respectively, of 1-5 and 7-17 Ω -cm were used.
2. Two substrate cleaning procedures were used to obtain their difference and importance.
    (i) Some substrates were cleaned with 1% diluted HF for approximately 30 sec and then rinsed with highly pure de-ionized water. After that, they were dried with a 99% pure nitrogen gas. Then, they were set into to the vacuum chamber.
    (ii) Substrates were cleaned respectively in acetone, alcohol and de-ionized water with an ultrasonic vibration cleaner for 10 minutes at each step. Then, they were rinsed in de-ionized water, just before drying with 99% pure nitrogen gas, prior to loading them into the vacuum chamber.
3. Target to substrate distance was fixed at 7.4 cm for each deposition. Substrates were neither rotated nor heated.
4. Vacuum chamber was evacuated at around 10^{-6} Torr by a Turbo Molecular Pump (TMP).
5. After reaching to the required pressure, a constant amount of 30 sccm Ar gas was sent into the chamber as long as the deposition process finishes.
6. RF power was applied over the Ar gas to obtain a homogeneous plasma.
7. Hf metal target was pre-sputtered for 60 sec before the film growth process started.
8. Oxygen gas, additional to Ar gas, was introduced into the vacuum chamber to be able to realize the oxidation of Hf sputtered particles (99.99 % purity) and grow thin oxide film.
9. During the oxidation process takes place for 3 min, optical measurements were taken simultaneously with a defined time steps by an SE with a fixed angle of 70º at the wavelength of 632 nm.
10. Film thicknesses were varied from 5 to 20 nm.
11. Following the oxidation process' completion, SE data were fitted by means of a suitable modeling for the film stack. Fitting process has been realized to obtain

the optical constants; i.e. refractive index, n, and real part of dielectric constant, ε_1, and film thickness, d.

12. The grown films were analyzed by non-destructive techniques like AFM, XRD, FTIR.
13. Electrical characterization of the films was realized constructing MOS capacitors after evaporating Al gate electrodes on oxide films.

RF magnetron sputtering technique was used to grow HfO_2 thin films. When RF power is applied between the target and substrate, electric field is created from substrate to target. Ar gas is ionized due to the collisions between the electrons coming from the power supply and argon atoms and plasma is generated. Magnetic field is created by magnets located under the target. Electrons are trapped on the surface of target by magnetic field to increase the collisions and to keep the plasma going continuous (Figure 3.1.). Ionized argon atoms move through the target by means of electric field. They give their energy to target atoms in order them to cause to move to the substrate' surface.

The deposition of HfO_2 film directly on Si surface often causes inevitable formation of silica or silicate interfacial layers which limit the capacitance of gate oxide stack. Hf diffusion into a Si substrate results in the formation of Hf-silicate or oxygen diffusion into interfacial area leads to the formation of SiO_x interfacial layer (Park, et al. 2002, Siervo, et al. 2006). In order to decrease the IL thickness, it is preferred to take a thin Hf metal layer serving as a buffer layer between oxide and Si substrate (He, et al. 2004, Nam, et al. 2002). This Hf buffer layer can prevent oxygen diffusion to Si. Therefore, in this work ultrathin HfO_2 films were prepared on Hf/Si substrate by RF, i.e. radio-frequency, magnetron sputtering technique.

5.3. Construction of MOS Structures

Al was evaporated on HfO_2/Si oxide films in order to be able to construct MOS structures for the electrical characterization of oxide stack. The steps followed for the MOS construction can be seen in figure 5.1. Metal contact on high-k thin film was obtained using the evaporation system at evaporation pressure around 10^{-3} Torr.

Metal contact was obtained by evaporation of Al at 70-80 °C degree onto the oxide layer. Al gate areas change from 2.92×10^{-6} m^2 to 5.70×10^{-7} m^2 by means of used metal mask.

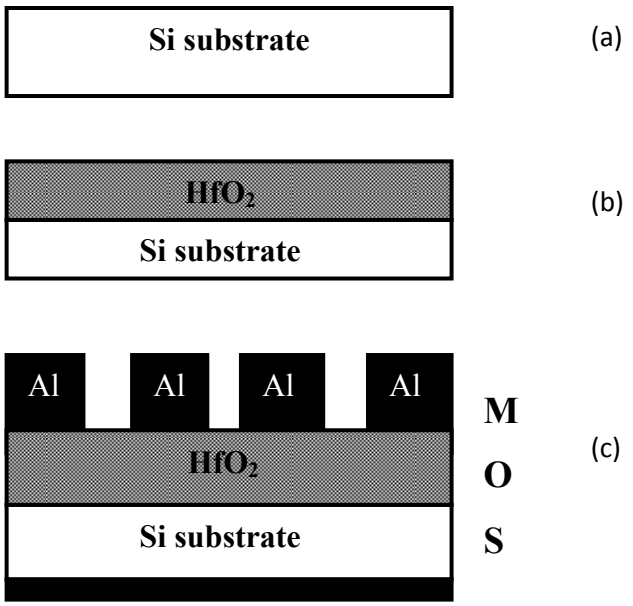

Figure 5.1. Fabrication steps of an MOS capacitor: a) Si substrate, b) HfO_2 film grown on Si, c) Metal deposition on HfO_2 oxide film.

5.4. Measurement Systems

5.4.1. Spectroscopic Ellipsometer

Spectroscopic Ellipsometer (SE) is a non-destructive optical measurement technique. It is based on the change of polarization state when polarized light is reflected off from the sample (Azzam 1977, Schubert 2004). In general, the reflected light is elliptically polarized and this gives its name to the technique (Figure 5.2.). Ellipsometer measures two variables Ψ and Δ with respect to wavelength λ. The phase delay, Δ, and the amplitude ratio, $\tan(\Psi)$ are related to the Fresnel coefficients;

$$\tan(\Psi) = \left| \frac{r_p}{r_s} \right| \qquad \text{and} \qquad \Delta = \delta_p - \delta_s \tag{5.1}$$

where r_p and r_s are the complex Fresnel reflection coefficients, respectively, for p and s states and δ_p, δ_s, are the phase changes for these two states. The phase and amplitude difference of incident and reflected light is related to the optical properties of the film.

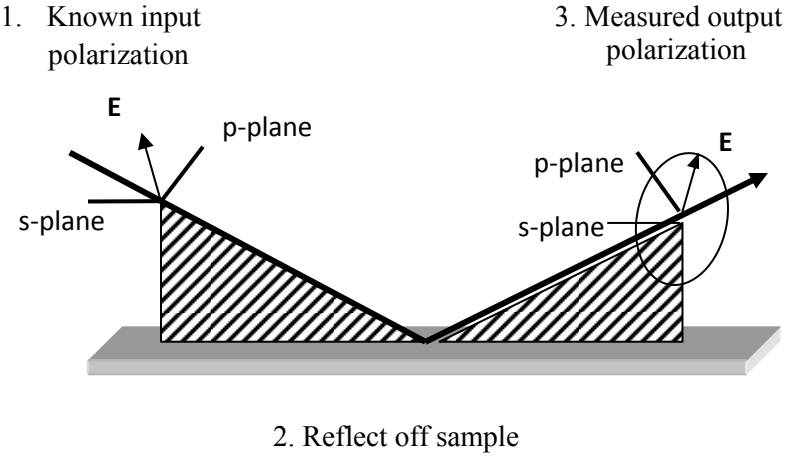

Figure 5.2. Typical ellipsometry configuration, where linearly polarized light is reflected off from the sample surface and the change in polarization state is measured to determine the sample's response.

A model is constructed to describe the film system. Measured data are 'fitted' by means of a model of layers and, as a result, the unknown properties of film system are calculated. Figure 5.3 shows the used model for fitting process of ellipsometrically measured data in this work. Thin film thicknesses and optical constants, i.e. refractive index n, and extinction coefficient k can be defined by SE measurements.

SENTECH SE 801 type SE system was mounted onto the magnetron sputtering system located at the dielectric laboratory of the Physics Department of Izmir Institute of Technology. This system was used for the measurements of optical constants and thickness of grown thin films during the course of this work (Figure 5.4. and 5.5.).

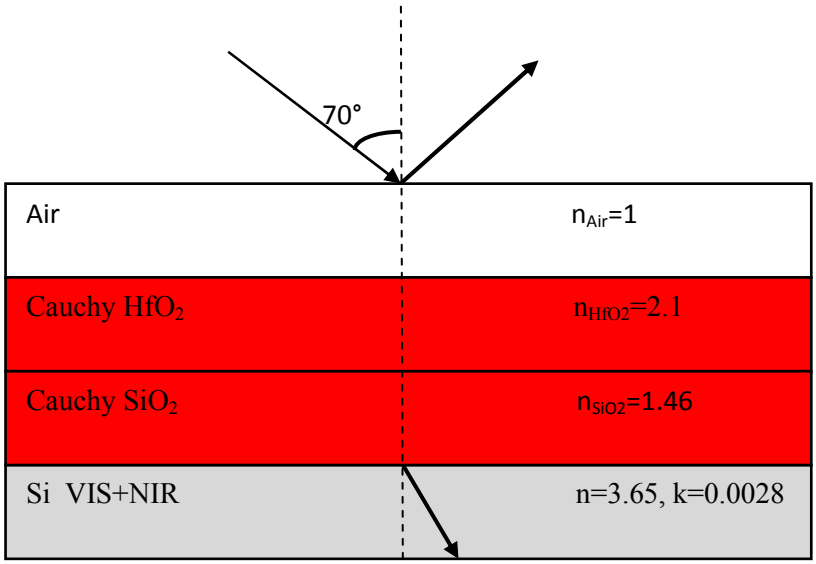

Figure 5.3. Ellipsometric modelling.

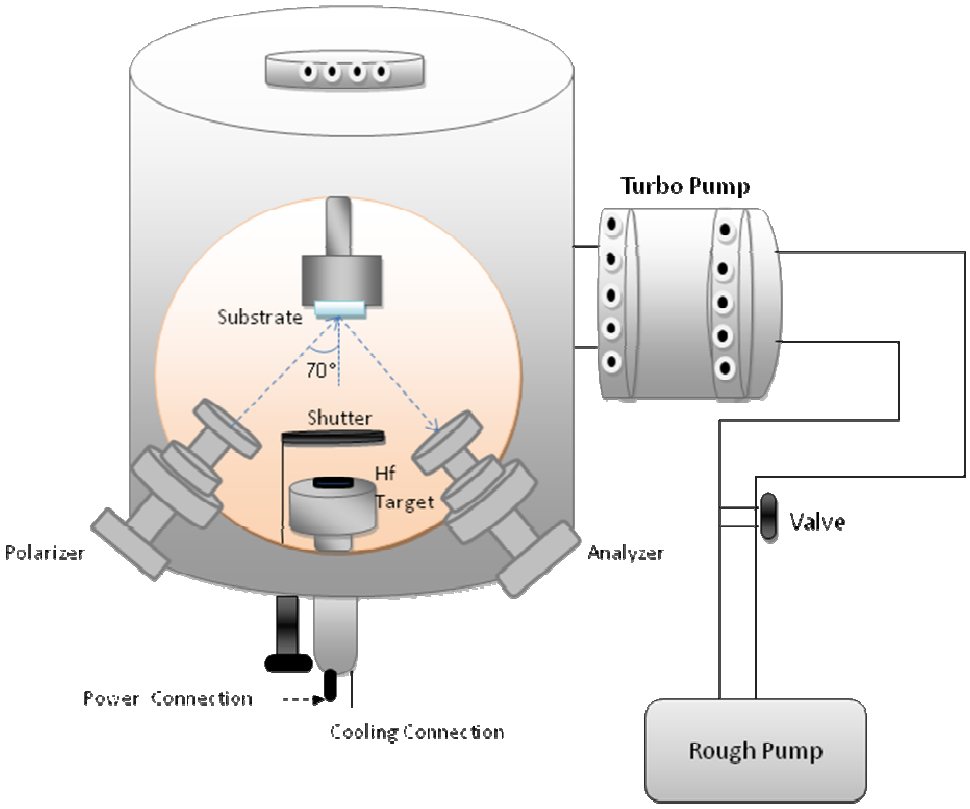

Figure 5.4. Schematic view of growth chamber with an in-situ SE system.

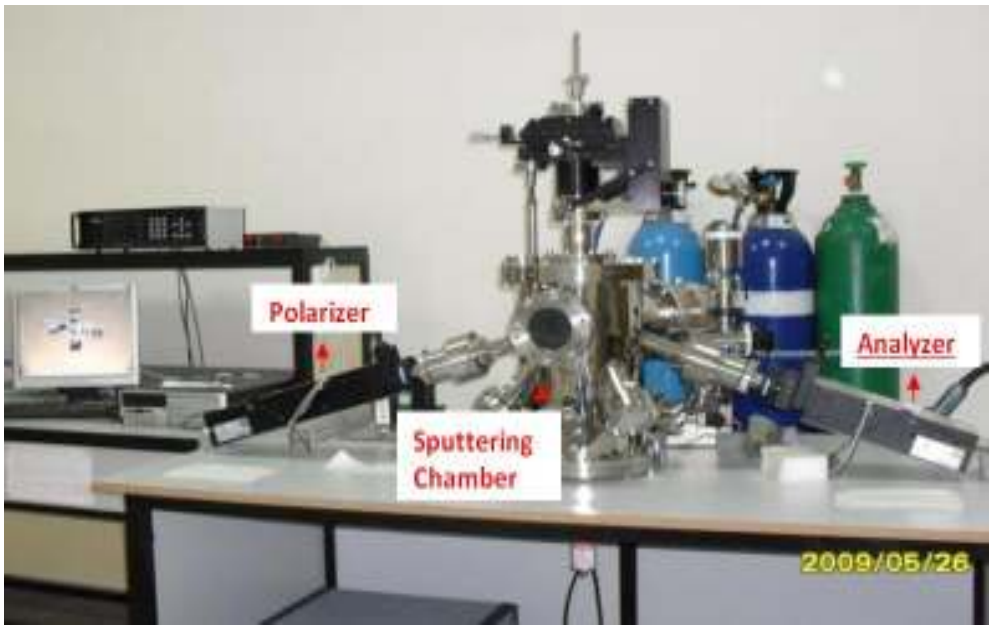

Figure 5.5. Picture of the magnetron sputtering system with SE.

5.4.2. X-Ray Diffraction

X-rays are em waves having wavelengths branging about 0.02 to 100 Å (1 Å = 10^{-10} m). Due to the fact that wavelength of X-rays is comparable to the size of atoms, they are ideally suited for exploring the structural arrangement of atoms and molecules in a wide range of materials, i.e. they can penetrate into material depending on the density of matter. X-rays primarily interact with electrons inside atoms. When X-ray photons collide with electrons, some photons from the incident beam will be deflected away from the direction where they originally travel. Diffracted waves from different atoms interfere with each other and produce intensity distribution. If the atoms are periodically ordered, the diffracted waves will consist of sharp interference peaks with the same symmetry inferring the symmetrical distribution of atoms. The constructive X-ray diffraction condition is defined by Bragg's law;

$$2d \sin\theta = n\lambda \tag{5.6}$$

where the integer n is the order of the diffracted beam, λ is the incident X-Ray beam' s wavelength, d is the distance between adjacent crystal planes and θ is the angle of incidence as well as that of reflected beam (see Figure 5.6.).

The distances between the planes of the atoms, i.e. *d,* can be obtained vice versa by means of Bragg's Law. Therefore, X-Ray diffraction gives about the information of solids' structures, i.e. amorphous or crystalline**.** Depending on the intensity, position and width of the diffracted peaks, type as well as the quality of crystalline structure of the film can be determined.

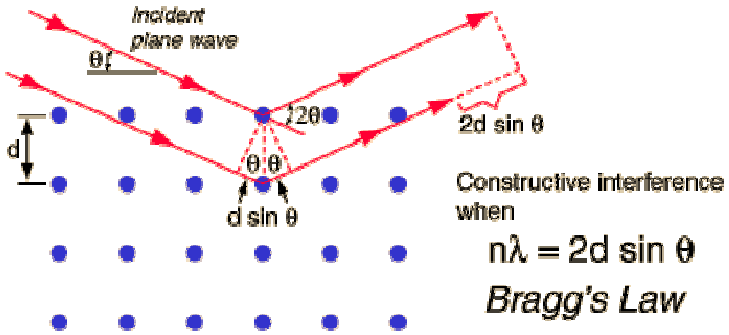

Figure 5.6**.** X-ray Diffraction pattern.

The crystallinity of grown films was examined by taking XRD patterns. They were carried out at grazing incidence mode by using a Panalitical X'Pert Pro MRD (Materials Research Diffractometer) located at Physics Department of IZTECH. Thin Film XRD system equipped with *CuK*α radiation of average wavelength of 1.54059 Å with grazing incidence angle 0.5°. The XRD patterns and peak matching processes of the observed peak positions at specific 2θ values were carried out using a computer database system.

5.4.3. Fourier Transform Infrared Spectroscopy (FTIR)

Fourier Transform Infrared Spectroscopy (FTIR) is a measurement technique in which the infrared photons are absorbed and, as a result, the molecular bonds vibrate. The resulting FTIR spectrum represents the molecular absorption or transmission of the film with respect to wavenumber.

FTIR spectral interpretation is highly important for indentifying unknown materials. Basic principle of FTIR technique is based on molecular vibrations. The bonds' vibration of molecules occurs at variable frequencies depending on type of bonds and elements.

If a bond is exposed to infrared radiation, this infrared energy is absorbed at specific wavenumbers as a consequence of quantum mechanical behavior. Consequently, the bond's vibrations will increase. Since the characteristic band spectrum is a fingerprint of any sample, the main structure of compounds can be identified and characterized by the spectral locations of their IR absorptions.

BRUKER Equinox 55 FTIR spectroscopy located in the Physics Department of the Middle East Technical University was used to determine the chemical composition and the bonding structure of films.

5.4.4. X-Ray Photoelectron Spectroscopy (XPS)

X-ray photoelectron spectroscopy (XPS) is a technique for measuring the elemental composition, chemical and electronic state of containing elements within a film material. XPS spectra are obtained by irradiating a material with an X-ray source and simultaneously measuring the number of escaping electrons and their kinetic energies (KE) from the material being analyzed. MgK_α (1253.6 eV) and AlK_α (1486.6 eV) are frequently used as X-ray sources. They interact with the atoms of the material in a limited surface region by means of photoelectric effect. The emitted electrons from the material have kinetic energies given by:

$$KE = h\upsilon - BE - \phi_S \tag{5.7}$$

where hυ , BE, and ϕ_s are, respectively, photon energy, binding energy of the atomic orbital from which the electron emitted, and spectrometer's work function. The obtained spectrum is the plot of a number of emitted electrons per energy interval versus their kinetic energies. Each element has an individual elemental spectrum, and the spectral peaks from a mixture are approximately the sum of the elemental peaks from the characteristic components. Therefore, the intensity of peaks is related to concentration of the element within the searched region.

Thus, the technique provides a *quantitative analysis of the surface composition.* XPS data were obtained with ESCA located in Central Laboratory of METU.

5.4.5. MOS Capacitance Measurements

One important aim of this thesis is to investigate the electrical behavior of grown high-*k* dielectrical thin films, MOS structures were constructed to be able electrically characterize these films. High frequency (HF), i.e. 1 kHz, 10 kHz, 100 kHz and 1 MHz, Capacitance Voltage (C-V). C-V and Conductance Voltage (G-V) and measurements were performed under dark conditions from MOS capacitors at room temperature. Applied voltage was changed from accumulation to inversion and then, from inversion to accumulation with a 0.1 V increments at each step. HP 4192A LF Impedance Analyzer was used for HF C-V and G-V measurements. This equipment controlled by a Labview program is located in the Physics Department of the Middle East Technical University.

5.4.5.1. Series Resistance Correction

Serious resistance (R_s) is an important error term. Capacitance values are measured as lower than their normal values without R_s compensation. Its existence causes small-signal energy loss in MOS capacitor.

Series resistance can be given as a result of five main sources. These are (i) the contact resistance between the metal contact and the silicon, (ii) the resistance of the top and rear metal contacts, (iii) contamination of the film, (iv) contamination between back contact and Si, (v) a non-uniform doping distribution in the Si substrate.

Series resistance due to the first four sources can be taken account to have R_s as low as possible. However, it is not always possible to produce perfect films. There are several ways to decrease its effect. Some of these are (i) using right sample fabrication technique, (ii) taking measurements at lower frequencies, (iii) measuring the serious resistance and then applying correction to measured admittances. That is why, series resistance correction should be applied to the measured C-V and G-V data. Both capacitance and conductance measurements are affected by series resistance because series resistance depends on the applied voltage and frequency.

The effect of series resistance increases with the increment of frequency and is greatest in strong accumulation. In order to apply series resistance correction, equivalent circuit of MOS capacitor given in figure 5.7 should be taken into consideration.

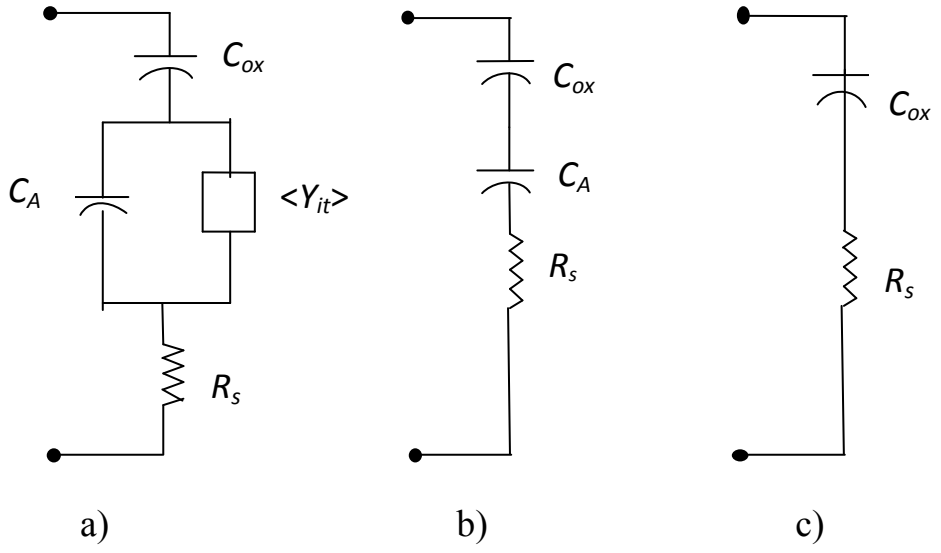

Figure 5.7. Simplified equivalent circuit of a MOS device to show the effect of series resistance in strong accumulation.

In these circuits, C_{ox} is the oxide capacitance while C_A is the capacitance of the accumulation state. The serious resistance is represented by R_s. $\langle Yit \rangle$ is the average interface trap admittance. In figure 5.7. (a), accumulation state capacitance C_A is parallel with $\langle Yit \rangle$. Since C_A is large enough, i.e. $\omega C_A \gg \langle Yit \rangle$, therefore $\langle Yit \rangle$ is shunted. In this situation, figure 5.7. (a) turns to figure 5.7. (b). Since $C_A \gg C_{ox}$, figure 5.7. (b) can be formed into figure 5.7. (c).

In strong accumulation admittance Y_{ma} across A-A in figure 5.7. (c) in terms of the capacitance C_{ma} (measured capacitance in accumulation) and parallel conductance G_{ma} (measured conductance in accumulation) is;

$$Y_{ma} = G_{ma} + j\omega C_{ma} \tag{5.8}$$

Impedance is

$$Z_{ma} = \frac{1}{Y_{ma}} \tag{5.9}$$

Series resistance is the real part of the impedance:

$$R_s = \frac{G_{ma}}{G_{ma}^{\ 2} + \omega^2 C_{ma}^{\ 2}} \tag{5.10}$$

The capacitance C_{ma} can be found from the relation in the following,

$$C_{ma} = \frac{C_{ox}}{1 + \omega^2 R_s^{\ 2} C_{ox}^{\ 2}} \tag{5.11}$$

By substituting R_s into the eq. (5.11), C_{ox} can be derived as shown in the eq. (5.12).

$$C_{ox} = C_{ma}\left[1 + \left(\frac{G_{ma}}{\omega C_{ma}}\right)^2\right] \tag{5.12}$$

Frequency dependent corrected capacitance C_c and corrected equivalent parallel conductance G_c are

$$C_c = \frac{\left(G_m^{\ 2} + \omega^2 C_m^{\ 2}\right) C_m}{a^2 + \omega^2 C_m^{\ 2}} \tag{5.13}$$

$$G_c = \frac{\left(G_m^{\ 2} + \omega^2 C_m^{\ 2}\right) a}{a^2 + \omega^2 C_m^{\ 2}} \tag{5.14}$$

where

$$a = G_m - \left(G_m^{\ 2} + \omega^2 C_m^{\ 2}\right) R_s \tag{5.15}$$

A labview program written by Dr. G. Aygun was used to calculate the series resistance of a MOS device. C-V and G-V measurements were taken using HP 4192A Impedance Analyzer and transported to the connected computer as data file by means of a serial port.

CHAPTER 6

INFLUENCE OF OXYGEN QUANTITY ON PROPERTIES OF REACTIVELY SPUTTERED GROWN HAFNIUM OXIDE THIN FILM

6.1. Introduction

Since oxidation parameters are important on the quality of the grown film, different parameters, i.e., O_2/Ar, sputtering power, substrate cleaning process were used to increase the quality of HfO_2 thin films. The aim of this section is to grow thin HfO_2 oxide film with a high refractive index as well as preventing the formation of SiO_2 interfacial layer on Si substrate. Here, we mainly focused on the importance of oxygen variation, i.e the effect of O_2 quantity in O_2/Ar gas ratio on reactively rf sputtered grown thin HfO_2 film properties.

6.2. Experimental Details

HfO_2 thin film was grown on *p*-type (100) Si wafers at 30 W rf power for 3 min sputtering time duration. Flow rate of Ar was held constant at 30 sccm while the oxygen quantity was varied from 3 to 15 sccm in order to get a gas mixture having O_2 to Ar gas ratio from 0.1 to 0.5. Base pressure of the sputtering chamber was below 10^{-6} Torr while working pressure during the sputtering was 67 mTorr.

Thin film deposition was constituted from the two layer growth stages. Firstly, Hf metal layer was deposited on Si substrate for 60 sec in Ar ambiant in order to be able to avoid the formation of any unrequired interfacial suboxide layer (He, et al. 2004, Aygun, et al. 2009). Secondly, O_2 gas was sent into the growth chamber as a reactive gas additional to Ar sputtering gas. Detail explanation of magnetron sputtering technique and oxidation parameters is given in chapter 4 and 5, respectively.

In-situ SE was used to obtain thickness and optical properties of grown film as a function of time (see Figure 5.8). The crystalline structure of the film was examined by

GIXRD pattern of 2θ scan. FTIR was used to obtain information on both the chemical composition and the structure of the film. The measurements were taken between 400-1200 cm^{-1} spectral range.

6.3. Results and Discussion

6.3.1. Spectroscopic Ellipsometer (SE)

SE has been used to investigate the structure and optical constants of thin films. SE characterization requires a convenient modelling for the thin film stacks. When an appropriate model is constructed, the thickness as well as optical constant of thin film can be simultaneously obtained by using ellipsometric parameters Ψ and Δ.

Thickness, refractive index and dielectric constant of HfO_2 films are constructed using Cauchy dispersion model in IR and UV regions. Cauchy modeling is suitable for optically transparent materials in the used region of 300 - 850 nm (Khoshman, et al. 2006). The Cauchy model's dispersion relations are given by eqs. (2.47) and (2.48). Real and imaginary parts of dielectric constants are given by the following equations;

$$\varepsilon_1 = n^2 - k^2 \qquad \text{and} \qquad \varepsilon_2 = 2nk \tag{6.1}$$

where n is the refractive index, k is the extinction coefficient, ε_1 and ε_2 are dielectric constants which describe transparent and extinction part, respectively.

Since both layers are optically transparent to the light used in the spectral range of interest, i.e. $\lambda > 350$ nm, extinction coefficients were obtained as zero. Table 6.1 demonstrates the fitting parameters and results for all layers. In this chapter, we mainly focused on the effect of oxygen quantity on the formation of interface as well as structural and chemical characteristics of HfO_2 films.

Table 6.1. Experimental and fitting results using Cauchy model for obtaining optical parameters for HfO_2 and SiO_2.

O_2/Ar	**λ (nm)**	**d_{HfO2} (nm)**	**n_{HfO2}**	**d_{SiO2} (nm)**	**n_{SiO2}**
0.1	632	9.98	2.09	0	1.452
0.2	632	6.99	1.98	0	1.452
0.3	632	6.84	1.90	0.2	1.452
0.4	632	7.04	1.83	0.5	1.452
0.5	632	5.74	1.82	0.5	1.452

Figure 6.1 shows the thickness of HfO_2 layer with respect to O_2 to Ar gas ratio. It is apparent from this figure that the thickness of grown film is found to be decreasing as an increment in the oxygen quantity of O_2 to Ar gas ratio. When O_2 to Ar ratio is smaller than 0.2, thickness of grown film exponentially increases. The oxide growth rate seems to be constant when the O_2 ratio is between 0.2 and 0.4. However, the growth rate is extremely affected and shrank when the O_2 to Ar ratio is larger than 0.4. The possible reasons of huge growth rate changes of Hf-oxide film with respect to oxygen to argon gas ratio inside of the sputtering chamber may be given in a few assumptions. Due to the fact that the increased amount of oxygen gas in the vacuum chamber; (i) the scattering centers of sputtered Hf atoms are increased and, therefore, the scattered atoms are prevented from being reached to the substrate, (ii) the effective cross sectional area for the reaction to be occurred on the substrate is decreased, (iii) the oxygen diffusion to the interfacial region increased and, therefore, an undesired interfacial layer formation is occured. The supportive results can also be seen from the literature that, not only the oxygen diffusion rate grows but also the growth rate of HfO_2 film decreases at high levels of oxygen concentrations (Buiu, et al. 2006). Therefore, the increased amount of oxygen ratio affects the evolution of hafnium-oxide film thickness in a reversibly manner, together with resulting in a low film density. As a result, it is clear that the oxidation process at low oxygen contents especially around 0.1 for O_2 to Ar gas ratio is more effective than those obtained at higher oxygen contents.

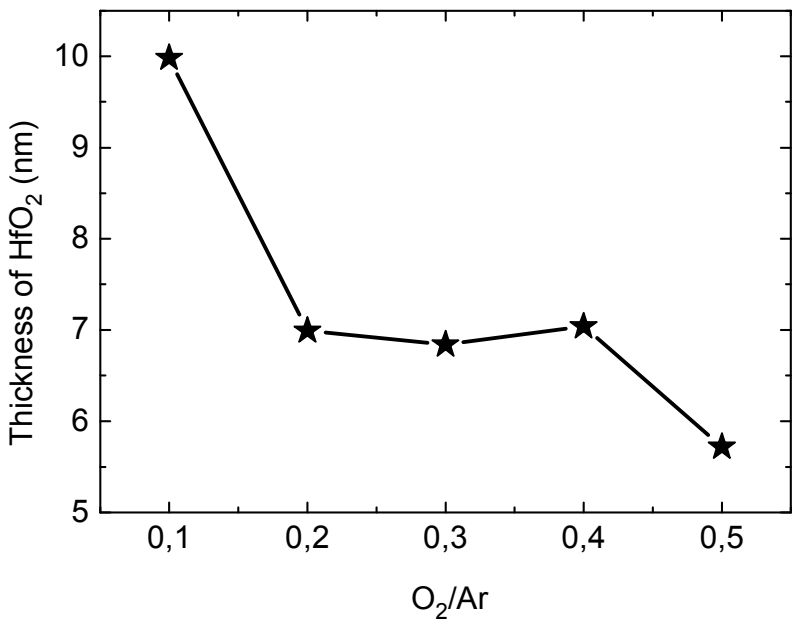

Figure 6.1. Thickness dependence of HfO_2 films with respect to O_2/Ar gas ratio.

Figure 6.2 shows real part of refractive index, *n*, as a function of oxygen quantity. It is revealed that the refractive index of sputtered films decreases with respect to increment of oxygen quantity. It is obvious that its value is approximately equal to the bulk value of HfO_2 (n=2.1 at 632 nm) for the lowest amount of oxygen gas used in our experiments. This could be the result of the film density because the index of refraction value highly depends on this parameter (Pereira, et al. 2004).

However, further work to improve the quality of grown layer, i.e. in-situ or ex-situ annealing, is necessary to keep a light on this issue. Additionally, the magnitude of refractive index shows how good the transparency level of the grown film is (Pereira, et al. 2004). This is really in a very good agreement with the real part of dielectric constant (see Figure 6.3).

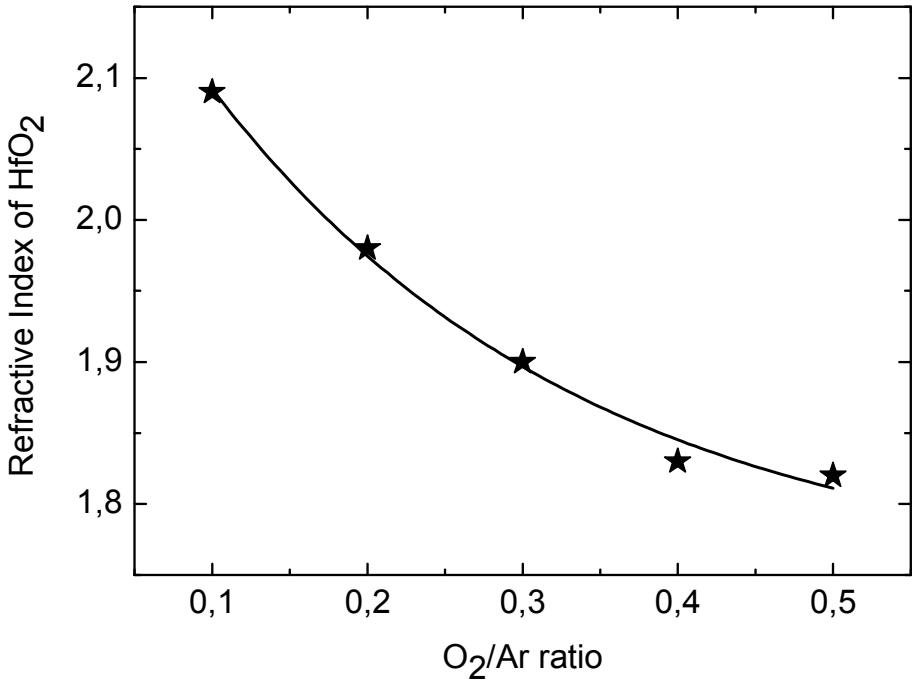

Figure 6.2. Change in refractive index with respect to oxygen to argon gas ratio increment. Note that 2.1 is the refractive index of bulk HfO_2 at 632 nm wavelength.

Complex dielectric constant of any material is given as $\tilde{\varepsilon} = \varepsilon_1 + i\varepsilon_2$. Real and complex part of dielectric constant, i.e., ε_1 and ε_2 defines, respectively, the transparency and absorbance of the material in interested. Since HfO_2 is transparent to the wavelength range of SE measurements, Cauchy dispersion is a suitable model to be used (Sharlandjiev, et al. 2008, Martinez, et al. 2007). Similar to refractive index dependence on gas ratio, real part of dielectric constant decreases as a function of O_2 to Ar gas ratio for the grown hafnium oxide thin film. The dielectric constant values are decreasing with an exponential form as the amount of O_2/Ar ratio is increased. The highest dielectric constant is obtained for 0.1 value of O_2 to Ar gas ratio. The imaginary part of the complex refractive index, ε_2, was determined as zero indicating that no optical loss due to band gap absorption in the HfO_2 film. The values of the refractive index and real part of dielectric function tended to decrease with the decrease in film thickness (Hori, et al. 1991).

Figure 6.4 shows wavelength distribution of transmission and reflection of HfO_2 films depending on oxygen quantity. Very small changes in transmittance and reflection values were detected with respect to gas ratio increments.

However, it can be said that the lowest used oxygen ratio has increased transmission and lowered reflection spectrum values for the grown films.

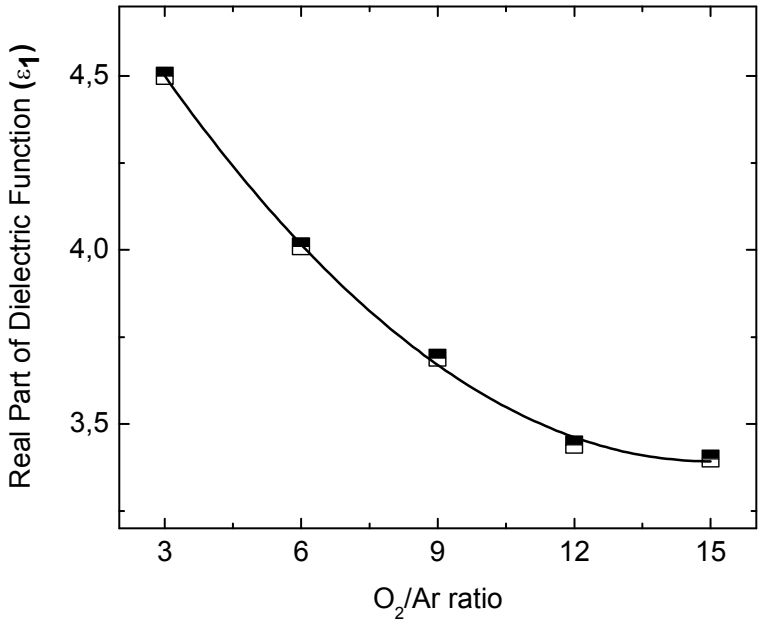

Figure 6.3. Real part of dielectric constant as a function of oxygen to Ar gas ratio at the wavelength of 632 nm for a thin hafnium oxide film.

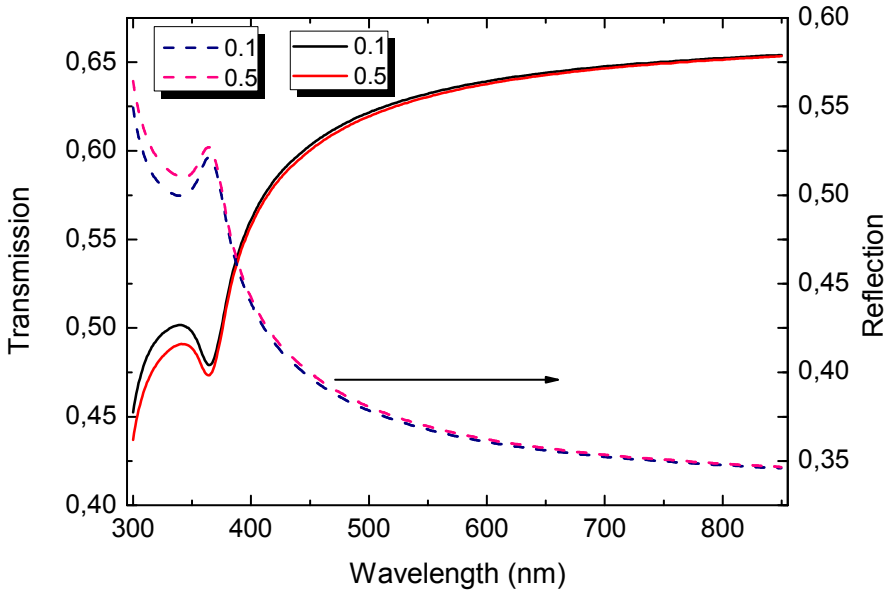

Figure 6.4. Transmission and reflection plots of HfO_2 films depending on gas ratio.

In addition to oxygen quantity, effects of power on refractive index and thickness of films grown with 0.25 oxygen to argon gas ratio were analysed. Figure 6.5 shows the power dependence of grown films' thicknesses. It exponentially increases with respect to applied power.

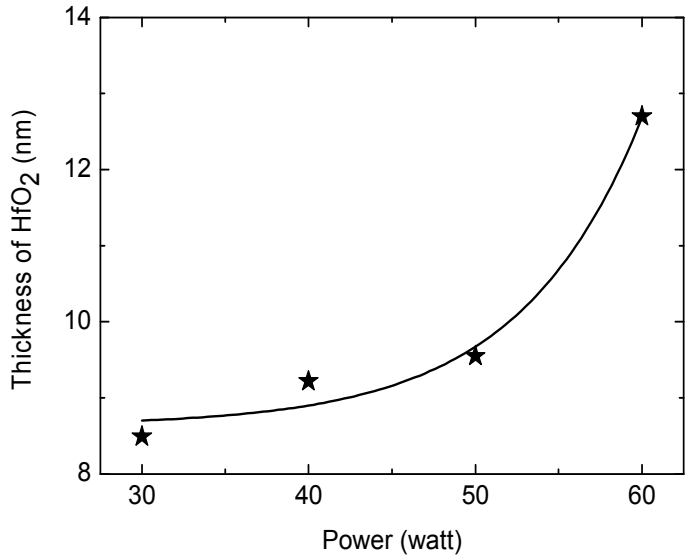

Figure 6.5. Power dependence of grown films' thickness with 0.25 oxygen to argon gas ratio.

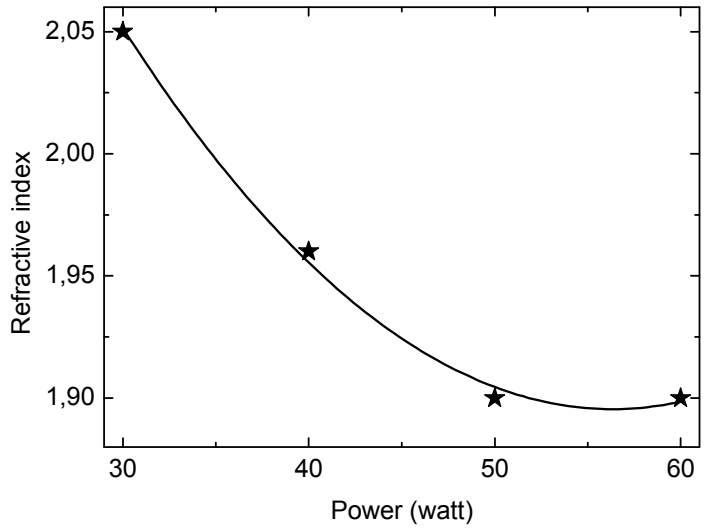

Figure 6.6. The change in refractive index with applied power.

Since high applied power can break off more Hf particles, this results in an increment of film thickness. However, increasing applied power causes higher powered Hf atoms to hit to sample surface and accordingly to disorder the atoms.

Consequently, it is seen in figure 6.6 that there is a reduction on refractive index and density of the film because of the damage on film due to the increased power (Duenas, et al. 2007).

6.3.2. XRD Structural Properties

The grown films were characterized by X-Ray diffraction (XRD) (Figure 6.7) to detect the structure and phase composition depending on the oxygen quantity in the O_2/Ar gas ratio. XRD measurements of HfO_2 thin films grown on Si substrate collected in grazing incidence mode with 0.03º increment between 10º and 65º degree. The film with lower oxygen content shows a very weak crystallized structure.

Two peaks are from the monoclinic phase and the third is from orthorhombic phase (Sharlandjiev, et al. 2008). No other crystalline phases, i.e.tetragonal, hegzagonal and cubic have been observed. The film including 3 sccm oxygen has the lowest intensity peak which is disappearing in higher oxygen content for $2\theta \sim 32º$ attributed to (111) monoclinic phase of HfO_2 (Martinez, et al. 2007, Neumayer, et al. 2001).

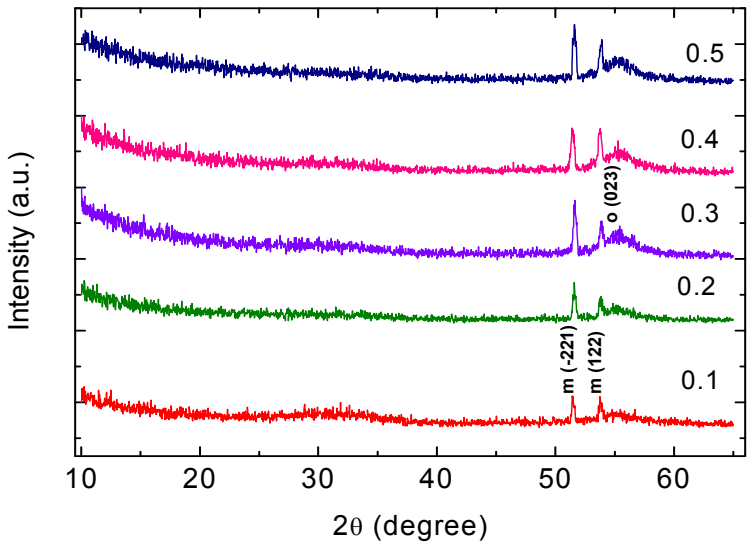

Figure 6.7. XRD patterns for HfO_2 films deposited different amount of O_2 to Ar gas ratio.

The intensity of the peaks at 2θ ~ 51.5º and 55º attributed to (-221) and (122) monoclinic phase of HfO_2, respectively and 2θ ~ 53.8º attributed to (023) orthorhombic phase of HfO_2 increases as the oxygen gets higher (Feng, et al. 2009).

It is worth noting that there is consistency in the observation that both the crystal structure and the optical constants depend on the oxygen quantity.

6.3.3. FTIR Characterization

The bond structure of HfO_2 films were investigated depending on the oxygen content in the film by FTIR in the 400-1200 cm^{-1} range at absorbance mode. In order to observe the absorbance of only grown films, the infrared absorption spectra of bare-Si substrate was taken as background spectra and subtracted from the total spectrum. Figure 6.8 shows different structures depending on oxygen quantitiy.

The noticable difference is seen in the formation of Si-O stretching vibration mode peak and Hf silicate peak is observed between 1080 to 1136 cm^{-1}. The film grown with 0.1 gas ratio has no SiO_2 interface peaks but only Hf-O peaks. The formation of Si-O stretching vibration mode peak and Hf silicate peak was obtained in the film grown with 0.2 gas ratio and its intensity increased with higher gas ratios. Since it is possible to determine thickness of interface from intensity of vibration peak, it is clear that a thin SiO_x layer ($x<2$) is present on the top of silicon, resulted from the increment of oxygen amount. Since HfO_2 shows poor barrier characteristics to oxygen diffusion, its quantity determines the formation of oxygen rich interface (Pereira, et al. 2005). Ellipsometry is helpful to detect the interfacial region. According to SE calculations, interfacial unrequired thickness increases with oxygen increments as well.

The vibration peak positioned at 610 cm^{-1} related with absorption of a Si phonon was observed for the film grown with 0.3 gas ratio (Martinez, et al. 2007). In all films, the existence of various peaks related to Hf-O bonds was observed in the lower wavenumber region (400-600 cm^{-1}).

The peaks observed at around 410 (Aygun, et al. 2009), 500 (Neumayer, et al. 2001) and 550 cm^{-1} (Chen, et al. 2007) are in agreement with the results for monoclinic HfO_2 (Martinez, et al. 2007). This result is supported with XRD for the same films above.

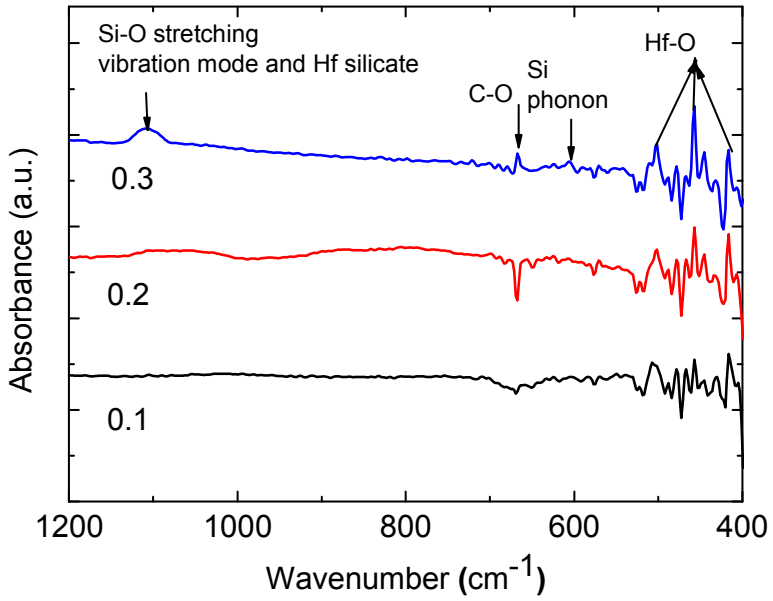

Figure 6.8. Effect of the oxygen quantitiy on FTIR spectra, showing the peaks related to Hf-O bonds and indicating also the presence of Si-O bonds.

6.4. Conclusion

HfO_2 films were fabricated on *p*-type Si (100) substrates by magnetron sputtering method having thin Hf metal layer prior to film growth. During this study, oxygen quantity was changed while the total quantity of argon gas was kept constant in order to investigate the effect of oxygen amount in the gas ratio on the crystallinity, optical constants and structural properties of grown films.

Cauchy dispersion relation was used for modeling the materials, in which the refractive index n and dielectric constant ε_1 decrease with respect to O_2 quantity increment. It has been observed that the optical constants are significantly affected by oxygen content. The XRD results show that appropriate choice of deposition parameters enables to grow polycrystalline HfO_2 films with different orientations and sizes of grains. The formation of the interfacial SiO_x starts to grow at 0.2 gas ratio and getting increasing through higher gas ratio. As a result, crystallinity, thickness and the optical properties' of the grown films strongly depend on deposition parameters. Based on these results, we attribute to use low amount of oxygen due to diffusion of oxygen through the grain boundaries of the HfO_2 film.

CHAPTER 7

DEPTH PROFILE STUDY OF THIN HfO_2 LAYER

7.1. Introduction

Device size in the microelectronic technology continuous to scaling down. As dielectric insulator SiO_2 has been reached its physical thickness limits, a huge leakage current propagates along grain boundaries which affect the capacitance of devices (Buiu, et al. 2006). Our aim is to improve the device performance by using a thicker insulator material with a higher dielectric constant than that of SiO_2 (Wang, et al. 2008). To achieve this, we focus on HfO_2 high-*k* dielectric material to be replaced with SiO_2 as a gate oxide.

In this chapter, the in-situ depth profiles of HfO_2 layers in terms of optical, structural, chemical, and electrical properties were studied for future applications in microelectronics.

7.2. Experimental Details

Hafnium oxide thin films have been deposited on n-type Si substrates by reactive rf magnetron sputtering in a mixed oxygen/argon atmosphere. Sputtering deposition was realized at room temperature with 40 Watt RF sputtering power and 0.1 O_2 to Ar gas ratio. It is well known that an unintentional interfacial layer formation between the high-*k* dielectrics and Si substrate is unavoidable.

In order to prevent this undesired interfacial layer formation between thin HfO_2 grown film and Si substrate, a thin Hf metal barrier layer was deposited on Si substrate prior to oxidization (Aarik, et al. 2004). More details about the oxidation system and process are given in chapter 3 and 5.

After deposition of HfO_2, the film was studied optically by using SE. The X-ray diffraction with Cu K_α radiation on grazing incidence mode with an incidence angle of

0.5º was applied to study the phase composition of the film. The chemical composition of film was studied by using FTIR. Then, the MOS capacitors were constructed (see chapter 4.3) in order to obtain the electrical characteristics, i.e. Capacitance-Voltage (C-V), Conductance-Voltage (GV). For the capacitance and conductance measurements, high frequency regime (1, 10, 100, 1000 kHz) was used. Series resistance correction (see chapter 5.4.6.1) was performed for 1000, 100, 10 and 1 kHz C-V and GV data.

7.3. Results and Discussions

7.3.1. In-Situ Spectroscopic Ellipsometric Analysis

The grown thin film was characterized optically by in-situ SE measurements in the wavelength range of 300 to 850 nm. The measurements were done for each 20 s during the film growth processing takes place. Thickness evolution of grown thin hafnium-oxide film is shown in Figure 7.1, where inset figure shows the refractive index of final film as a function of wavelength.

It is clearly seen that film thickness increases after opening the shutter, since active oxidation starts when the substrate faces with reactively sputtered Hf target in O_2 and Ar environment, and come to a final stabilized value in a very short time after the shutter is closed.

It is obvious that thickness of HfO_2 is directly proportional to deposition time (Toledano-Luque, et al. 2007), and it was measured as 13 nm at the end of growth process. This result indicates that growth process has constant deposition rate. As a result of SE measurement not any interfacial SiO_2 layer was encountered. This might be the result of Hf metal barrier layer. The growing of SiO_x interfacial layer is avoidable by the limitation of oxygen diffusion through the Si substrate. Therefore, the growth of HfO_2 film was observed increasingly.

Inset picture of Fig. 7.1 shows the refractive index versus wavelength in the range of 300 to 850 nm obtained from fitting results of (Ψ, Δ) for HfO_2 thin film. It is clear that refractive index value was obtained around 2.0 for thin film at 632 nm which is extremely close to that of bulk HfO_2 value.

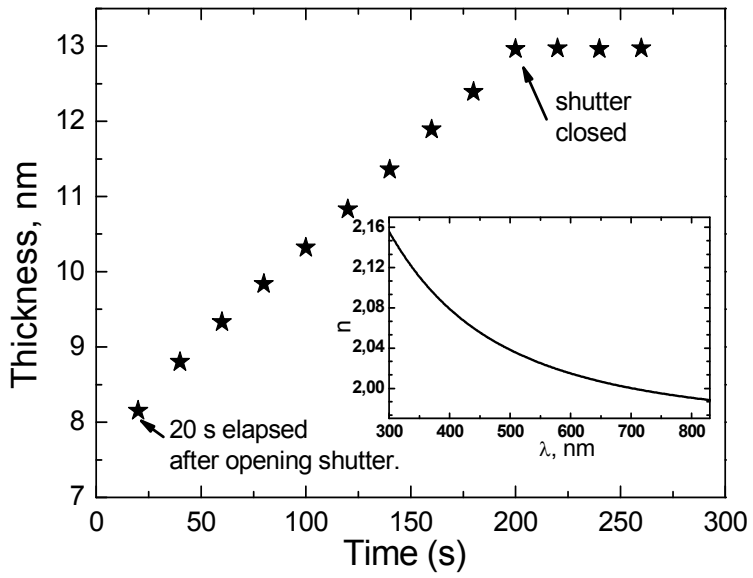

Figure 7.1. Spectroscopic ellipsometric values Ψ and Δ measured with respect to wavelength.

7.3.2. Structural Properties by Thin Film XRD

An XRD spectrum is shown in figure 7.2 that the film has amorphous structure of HfO_2 having a huge bump starting around 15^o continues till around 40^o. Due to the fact that Si substrate consumes the oxygen of HfO_2 film, hafnium silicate formation, i.e. $HfSi_xO_y$, was detected in the interfacial region of grown oxide film (Feng, et al. 2009). Intensive peak detected around 62.1^o was from the underlying Si substrate (Aygun, et al. 2009).

It is clear that the grown film is in the amorphous structure containing HfO_2 in addition to possible small amount of $HfSi_xO_y$. No peak belonging to SiO_2 was observed. It might be as a result of limitation of oxygen diffusion through the substrate because of Hf barrier layer and room temperature processing.

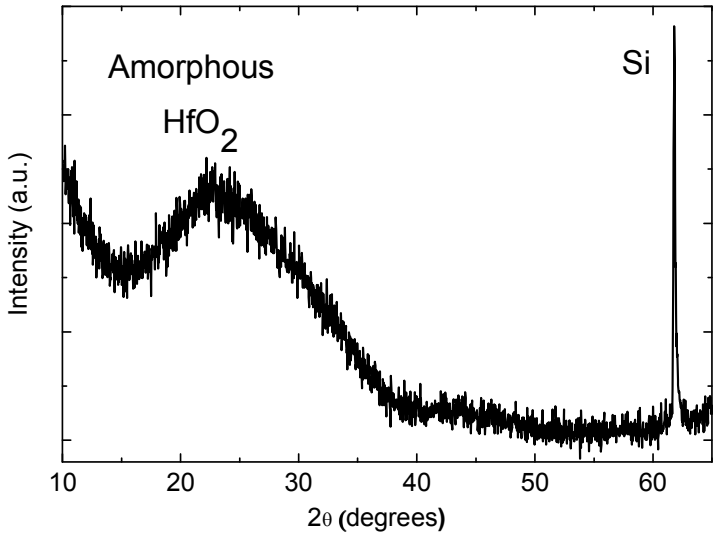

Figure 7.2. XRD analyze of the film.

7.3.3. Chemical Characterization in terms of FTIR Measurement

Figure 7.3 shows the chemical composition of grown film measured by FTIR in the range of 400 to 1200 cm^{-1}. Vibration band observed in the range of 1150 to 1050 wavenumber region corresponds to a close region of Si-O phonon vibrations (Aygun, et al. 2009). However, this peak is located ~1108 cm^{-1} and reflects the result of asymmetric stretch of SiO_4 (Neumayer, et al. 2001). Since having too low intensity around 1080 cm^{-1} of a very tiny shoulder, Si-O-Hf bonds are expected to be in a very low amount in the interfacial region of oxide film. The appearance of this peak depends on the formation of $HfSi_xO_y$ interface. Since the peak intensity reflects the vibration power as well as thickness of film, it can be inferred that there exists a very thin $HfSi_xO_y$ interface. The low intensity broad band shoulder located around 1090 cm^{-1} is assigned to $Si–O^-$ where O^- is a non-bridging oxygen ion bonded to a proton (Neumayer, et al. 2001).

It is obvious that there exists neither a detectable peak around 1075 cm^{-1} corresponding to SiO_2 interfacial layer, nor even in lower close wavenumber regions, i.e. lower than 1075 cm^{-1}, corresponding to SiO_x suboxide bondings. Therefore, it could be concluded that there is neither a detectable SiO_2 nor SiO_x measured in the oxide film.

Crystallinity of grown HfO_2 film can also be determined from the positions and shapes of these vibrations peaks. Generally, pure HfO_2 vibration bands are observed in the range of 800-600 cm^{-1} (Frank, et al. 2004). Hf-O bond vibrations, marked as well in the figure, are detected in the low wavenumber region between 400 and 600 cm^{-1}, (Neumayer, et al. 2001). The strong peak located around 608 cm^{-1} is reflecting the existence of HfO_2. The peaks around 515 and 720 cm^{-1} correspond also to HfO_2 bond structure. Khomenkova *et al.* (2010) declared that Hf-O peak positions shift to the higher wavenumber sides (>800 cm^{-1}) for the crystalline HfO_2 films. Since there is not a visible peak in the region higher than 800 cm^{-1}, it also supports that HfO_2 film has an amorphous structure supporting the XRD measurement results.

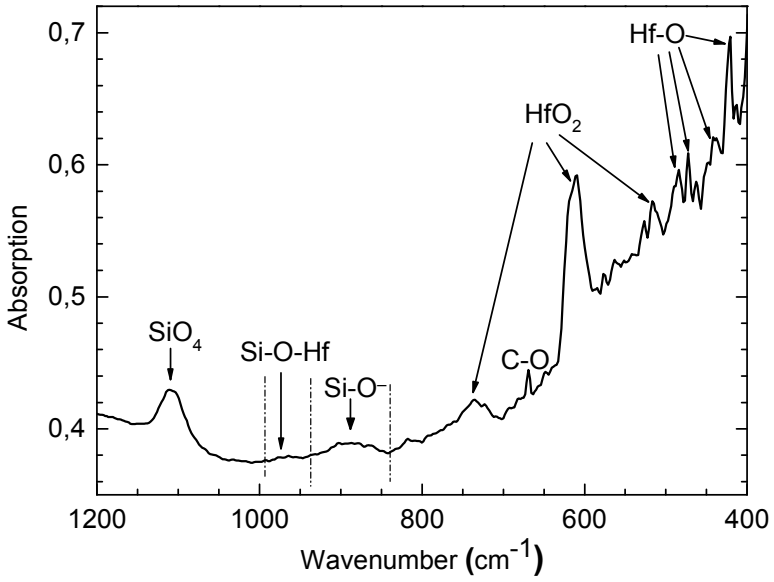

Figure 7.3. Absorption spectra of grown film were taken by FTIR. The Hf-O vibration bands corresponding to amorphous HfO_2.

On the other hand, peaks' positions shift to the lower wavenumber sides for the amorphous structure of HfO_2 film (Martinez, et al. 2007). Since the measurement was realized in air, C-O related peak is observed around 670 cm^{-1}.

7.3.4. Electrical Characterization

Figure 7.4 shows the Capacitance-Voltage (C-V) and Conductance-Voltage (G-V) results of MOS structures constructed from oxide film having $5.7x10^{-7}$ m^2 Al gate area. C–V curves were taken at high frequencies of 1, 10, 100 and 1000 kHz from MOS capacitors and series resistance correction were applied to capacitance and conduction data for all frequencies. Using these experimental data, calculations have been carried out to obtain the flat band voltage, V_{FB}. The flat-band voltage, V_{FB}, was obtained as 0.398 V from the position of G-V peak at 1 MHz frequency.

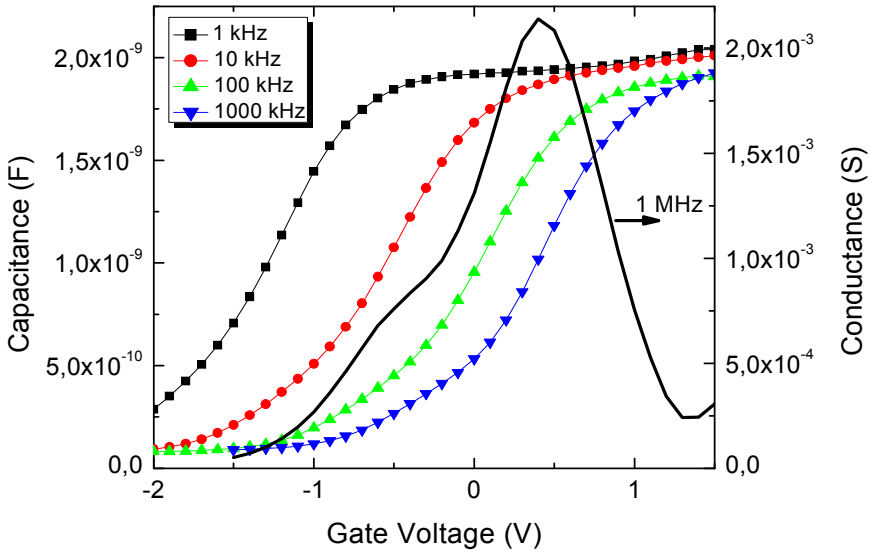

Figure 7.4. Capacitance-Voltage at high frequency regime of 1, 10, 100, 1000 kHz and Conductance-Voltage peak centering at the flat-band voltage data for 1000 kHz regime.

The dielectric permittivity calculated from the measured capacitance in accumulation at 1 MHz, after series resistance correction applied, was 4.84. It is equal to 5.26 for the 1 kHz. Although this value does not close to bulk value, being higher than that of ideal SiO_2 as a proof that there exists an oxide layer with higher dielectric constant than that of SiO_2, $\varepsilon_{SiO2} = 3.9$. The low dielectric constant of the film can be related to the formation of hafnium silicate interfacial layer obtained, as well, from FTIR spectrum.

It has been found that the formation of hafnium silicate IL, which is undesirable for gate oxide application for low leakage current, leads to a decrease of *k* value.

7.4. Conclusion

Reactive rf sputtering system combined with an in-situ SE was used to grow and characterize a high-*k* HfO_2 film on *n*-type (100) Si substrate. It is well known that there exist an unavoidable interfacial layer between HfO_2 and Si substrate.

In order to avoid forming of this interfacial layer, a thin Hf barrier layer was formed on Si substrate prior to forming oxide film. During, as well as after growth, SE measurements have been repeated at certain time intervals in order to optically characterize and obtain the depth profile of grown film. The film thickness was obtained as 13 nm with a refractive index ~2.0 at the wavelength of 632.8 nm. Analyses of SE measurement data showed that the film has no suboxide form of Si, namely SiO_x.

Following optical characterization by SE measurements, the grown film was characterized structurally by XRD. It was detected that the grown film has an amorphous structure. The chemical bonding structure was detected by FTIR measurement. The characteristic peaks of HfO_2 bonding were detected but not a SiO_x interfacial layer was detected. There existed a small peak corresponding to SiO_4 bonding structure. The amount of $HfSi_xO_y$ is also in the very small range. XPS depth profiling analysation is planned to be made in order to obtain a deeper investigation of film structure with chemical analyses methods. TEM picture from the interfacial cross section of film is planned to be taken to obtain a better visual aspect related to interfacial film formation, physical thicknesses of layers and amount of suboxide and/or Hf-silicate formations.

MOS structure was constructed to obtain a general idea about its electrical structure just by initial measurements of C-V and G-V at high frequencies. Capacitance values, as expected, had an increment through low frequencies in accumulation mode. It is well known that the characteristics of interfacial region have a very dominant effect on dielectric characteristics of the oxide film. Therefore, further study is necessary to shed on light on the formation of interfacial region between Si substrate and HfO_2 film.

CHAPTER 8

XPS DEPTH PROFILING STUDY OF HfO_2 THIN FILM GROWN BY RF MAGNETRON SPUTTERING TECHNIQUE

8.1. Introduction

Properties of thin oxide films on silicon vary widely in terms of their morphology and interface. For future electronic devices, gate oxides should also form high quality interfaces with silicon with low interfacial defects and roughness. The interface between HfO_2/Si is unwanted because it effects the device quality in the MOS structure. However, viable interfaces between HfO_2 and Si is SiO_x ($x<2$). In this view, the effect of an Hf metal barrier on the formation of interfacial area has been investigated by physical and structural characterizations of oxide film.

8.2. Experimental Details

The HfO_2 thin film was grown with 30 W RF sputtering power and 0.1 O_2 to Ar gas ratio on *n*-type silicon at room temperature. Prior to 3 min reactive HfO_2 film growth, a thin Hf metal was deposited for 60 s onto Si substrate. More details about the process of the magnetron sputtering and oxidation can be found in chapter 3 and 5. The thickness and optical properties of grown film were examined by an in-situ SE in the wavelength range of 300-850 nm. The crystal structure of film was investigated by XRD on grazing incidence mode. The composition and chemical states and its interface with Si were analyzed by FTIR and XPS.

8.3. Results and Discussions

8.3.1. In-situ Spectroscopic Ellipsometer Analysis

SE with 70° incidence angle of light was used to obtain thickness, d, and optical constants, i.e. refractive index, n, and real part of dielectric constant, ε_1, of HfO_2 film as a function of sputter time. Thickness and optical constants of film can be determined in terms of a regression analysis. This technique uses the best fit choice of measured and calculated ellipsometric data (Ψ, Δ). The manufacturer's software named as SpectraRay provides a regression analysis option. We found MSE value as 1.19. Therefore, we observed that the matching between the measured and the modeled data is as good as we would like to have. The resulting measured and calculated ellipsometric values (Ψ, Δ) are shown in figure 8.1.

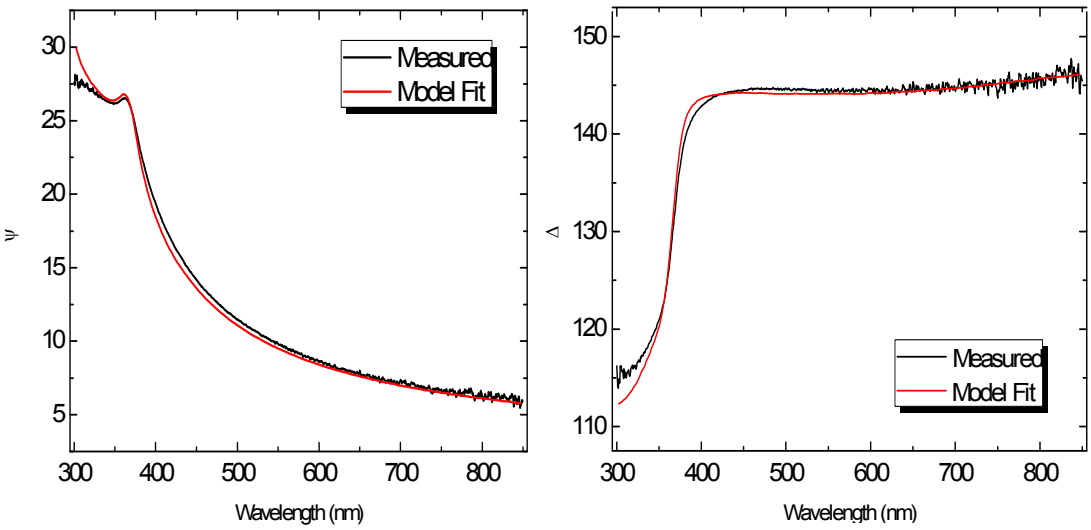

Figure 8.1. Ellipsometric values measured and fitted on a thin layer of HfO_2.

Figure 8.2 shows thickness and refractive index evolution with respect to time of grown film. Thickness of film increases linearly during the deposition and comes to a stabilized situation after closing the shutter, i.e. stop growing the film. Film growth rate is 2 nm/min. The final thickness of film is nearly 6 nm.

Simultaneously taken measurements let us search the interfacial formation. Any formation of SiO_x interface was detected by SE.

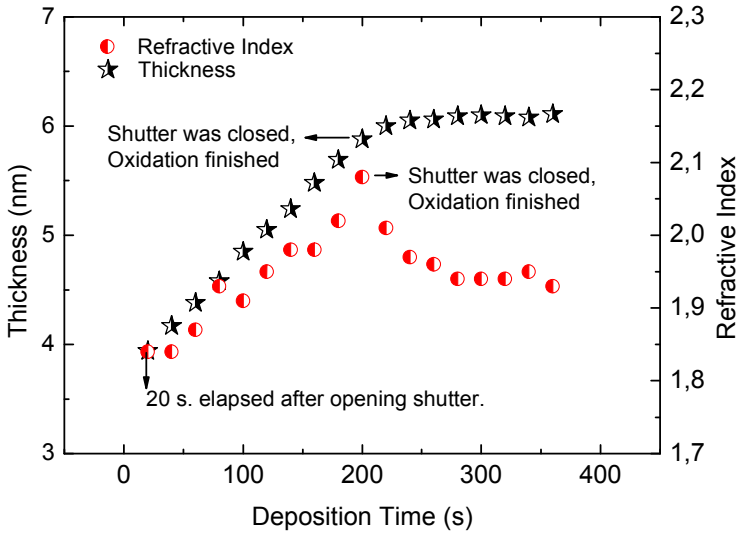

Figure 8.2. SE analyses of thickness and refractive index as a function of deposition time at 632 nm wavelength.

Similarly, refractive index evolution of grown films showed increment at first, then after reaching a maximum value of 2.07, starts decreasing until it reaches a stabilized level of ~1.93. As we know, the refractive index of a material is closely related to its packing density. Therefore, it is thought that some chemical reactions inside the film results the formation of porous structures, therefore lowering the density of grown film.

Dielectric constant of any material is complex and given as $\tilde{\varepsilon} = \varepsilon_1 + i\varepsilon_2$, where ε_1 defines the transparent and ε_2 the absorbed part. Since HfO_2 is transparent to the wavelength range we use (300-850 nm), absorbance of film was not counted. Figure 8.3 shows the variation of real part of the dielectric constant as a function of wavelength. During the deposition, ε_1 value showed increase at first.

Then after reaching a maximum value over time, it started decreasing. Due to the fact that some chemical reactions on the heated film with high energy sputtered particles, similarly, ε_1 value did not come to a stable level right after the deposition. Therefore, transparency of film increased as the film thickness increased during deposition.

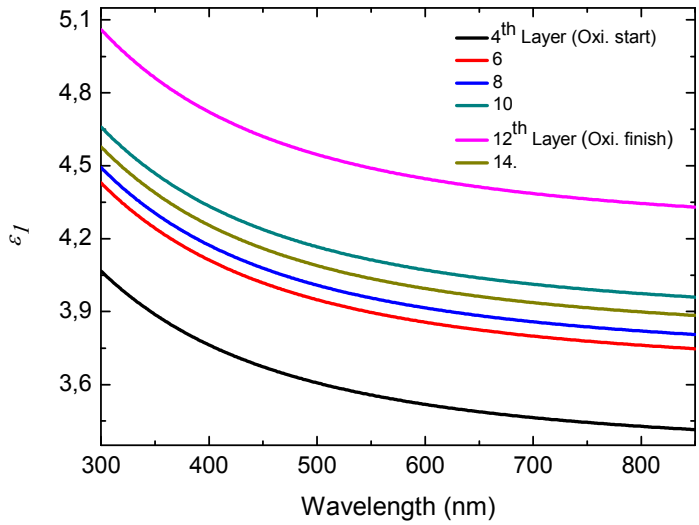

Figure 8.3. Real part of dielectric constant as a function of wavelength for a thin hafnium oxide film.

8.3.2. Structural Properties by Thin Film XRD

The HfO_2 film was characterized by XRD on grazing incidence mode with the aim to study the structure of grown film. Using the peak coming from Si substrate was eliminated with grazing incidence angle measurement. As can be seen from figure 8.4., 6 nm thick film has 2θ value of 51.5º attributed to (-221) monoclinic phase of HfO_2 (Feng, et al. 2009).

The grain size (crystallite size) of the film was obtained by using Debye-Scherer formula with X'pert High Score software (Patterson, et al. 1939, Wang, et al. 2005):

$$\tau = \frac{K\lambda}{B\cos(\theta)} \tag{8.1}$$

where K is a constant equal to 0.9, λ is the wavelength of CuK_α (1.54 A°), B is defined as full width at half maximum intensity (FWHM) in radians, θ is the Bragg diffraction angle and τ is the mean size of the crystalline domains (size of the grain).

Similarly, the lattice strain ε of the film was calculated by using Debye-Scherer calculator in X'pert High Score software with the formula:

$$\varepsilon = \frac{B}{4\tan(\theta)} \tag{8.2}$$

The grain size and lattice strain of diffraction peak oriented (-221) was obtained 24.5 nm and % 0.328, respectively.

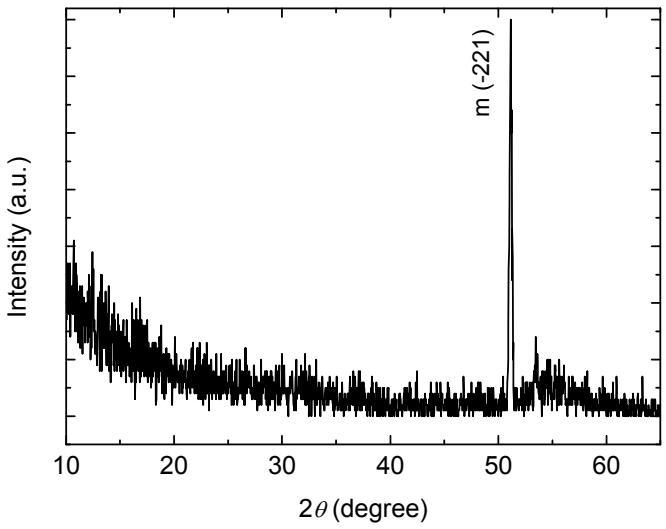

Figure 8.4. GIXRD data for HfO_2 film.

8.3.3. FTIR Spectra of RF Sputtered HfO_2 Film

Chemical composition of grown film was obtained by FTIR. Measurements were taken between 400 and 1200 cm^{-1} wavenumber region. In the high wavenumber region there is only one strong and broad absorption peak which lasts from 970 to 1150 cm^{-1} (see figure 8.5.). This peak consists of two contributions coming from Si-O phonon mode and hafnium silicate. Natural oxide position of SiO_2 is seen at 1075 cm^{-1}. However, this peak is located ~1105 cm^{-1}. The shift of SiO_2 peak position through higher wavenumber region can be explained with the existence of asymmetric stretching vibration of SiO_4 (Toledano-Luque, et al. 2007).

Si-O-Hf bonds are expected to be in very low amount at around 1080 cm^{-1} in the interface region of oxide. We interpret this band to the formation of $Hf_xSi_yO_z$ near the Si/HfO_2 interface.

The other observed Si phonon peak centers 610 cm $^{-1}$ with very low intensity. The appearance of Si-O phonon peak is caused by the formation of an SiO_x interfacial layer (Houssa, et al. 2006).

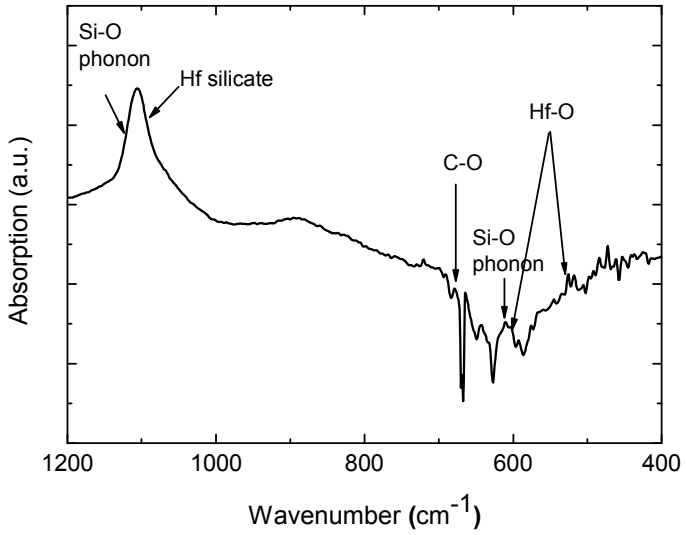

Figure 8.5. Absorption spectra of HfO_2 film obtained from FTIR.

Between 400-600 cm^{-1} many peaks which refer to Hf-O bonds were observed. They stay at around 512 and 600 cm^{-1}. D. A. Neumayer *et al.* (2001) reported that the observation of these peaks is a result of monoclinic phase of HfO_2. This result is in agreement with XRD. C-O bond was obtained nearly at 670 cm^{-1} with a very low intensity which corresponds to a clean film surface.

8.3.4 XPS Spectra of HfO_2 Film

Depth profile XPS not only provides chemical composition of film but also gives the formation of chemical bonding. The compounding elements and their quantities can be determined from the chemical bonding information. Figure 8.6 shows the surface scanning spectra of photoelectron peaks. The results indicate that the film consisted of HfO_2.

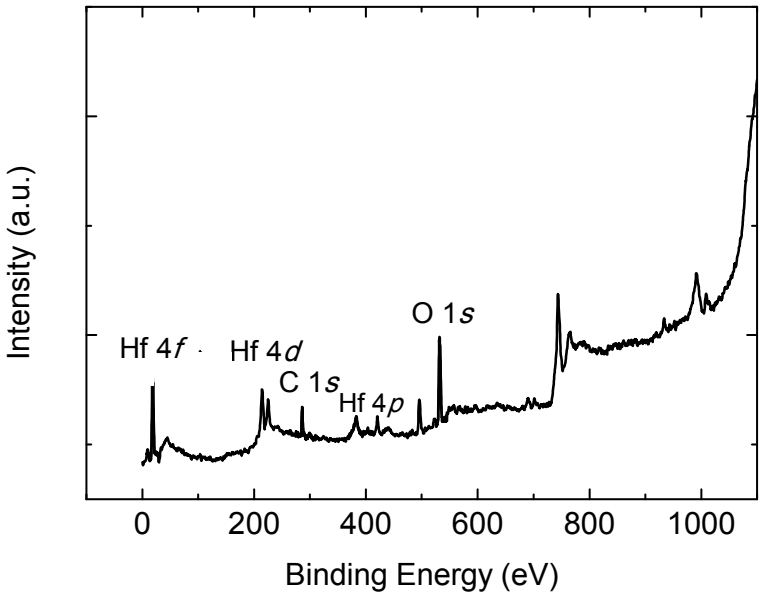

Figure 8.6. Wide-scan XPS spectrum of HfO_2 film.

8.3.4.1. Carbon *1s* signal

The surface spectrum shows a peak of C *1s* at 286 eV with negligible intensity indicating the presence of C-C bond (see Figure 8.7). This low intensity demonstrates that the surface of film is clean enough after short air exposure.

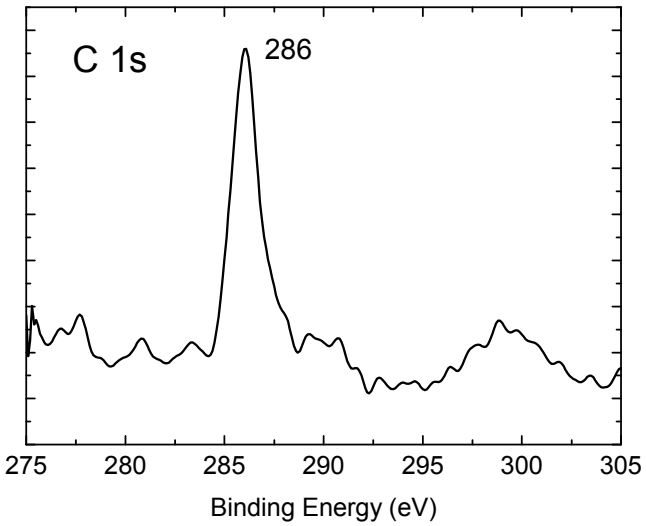

Figure 8.7. Narrow-scan XPS spectrum of C 1s film.

8.3.4.2. Si Depth Profile of The Film

Analyses of Si *2p* emission signals of the photoelectron spectrum allow us to separate it into two parts as given in figure 8.8 (a). The Si *2p* spectra includes five contributions which are coming mainly from (i) elemental Si (Si^0), (ii) higher oxidation states Si_2O (Si^{+1}), (iii) SiO (Si^{+2}), (iv) Si_2O_3 (Si^{+3}) and (v) the native oxide SiO_2 (Si^{+4}) (Aygun, et al. 2004, Maunoury, et al. 2007). Figure 8.8 (a) shows all XPS Si *2p* spectra of HfO_2 film. The left peaks start near 99.1 eV indicates as Si-Si bonding from the substrate whose intensity increases through the substrate as shown in Fig. 8.8 (b).

Although the elemental Si *2p* signal is observed at 99.3 eV (Aygun, et al. 2009, Yakovkina, et al. 2005), we obtained the main peak centered at 99.7 eV which can be explained by formation of substoichiometric oxide state (Si^{1+}) (Maunoury, et al. 2007). Yakovkina *et al*. (2005) noted that this binding energy is close to that of silicon in hafnium silicide ($99.5 < E_b < 100$ eV). For the first part of Si 2*p* signal, the chemical shift through the higher binding enery sides for deeper layers was also observed.

An additional peak of the Si *2p* emission spectra is found at higher binding energy sides corresponding to different oxidation states of the silicon. In figure 8.8 (c) peak position for the 2nd layer was found at 103.85 eV which belongs to fully oxidized state of Si (Si^{+4}). For depeer layers chemical shift through lower binding energy sides was observed. Maunoury *et al*. (2007) reported that chemical shift between Si^{+3} and elemental Si (Si^0) is equal to 2.9 eV. Some other research groups found this value between 2.48 and 2.65 eV (Green, et al. 2001). The chemical shift of elemental Si was obtained between 3.5 and 2.95 eV for depeer layers of the oxide. This can be explained as the oxide containing Hf-O-Si bonds which might reflect the formation of Hf silicate ($HfSi_xO_y$) (Tan. et al. 2005, Sokolov, et al. 2009). This result was supported by FTIR measurement.

As a result, figure 8.8 (a) shows that Si-Si bonds incease until substrate is reached while Hf-O-Si bonds of hafnium silicate exist starting from surface layer until 8th etching cycle and then disappear. After 8th layer, no interfacial formation was determined.

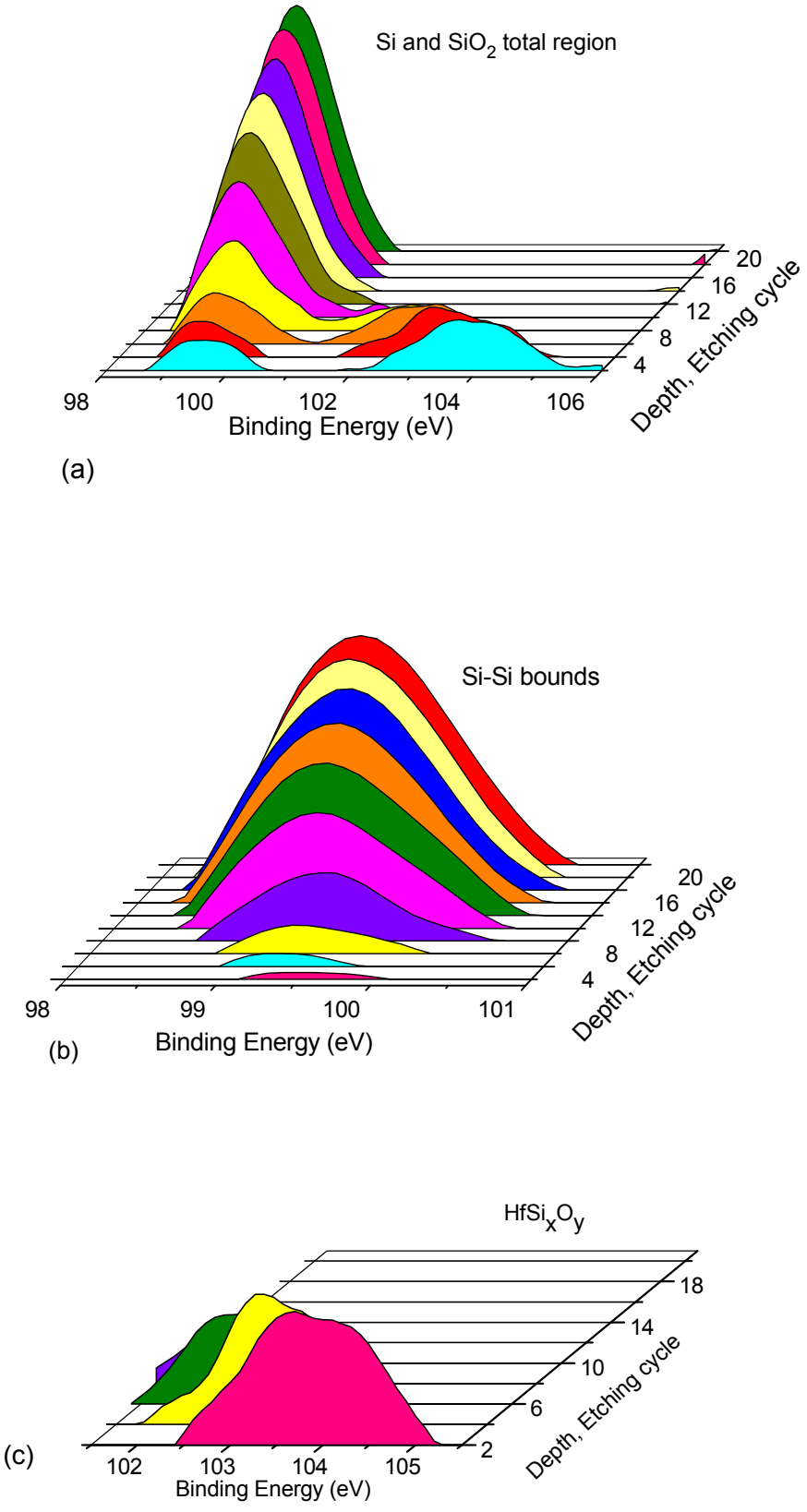

Figure 8.8. Si *2p* depth photoelectron spectra.

8.3.4.3. O *1s* spectrum

The depth profile of O *1s* spectrum is given in figure 8.9. The surface layer peak is between 530 and 536 eV. The highest intensity of O *1s* spectra was observed at the surface. The main peak was centered at about 531.5 eV for the surface layer indicates the O bounds in hafnium silicate (Aygun, et al. 2009).

The peaks were shifted to 532.6 eV for deeper layers corresponding to the presence of SiO_2 (Rangarajan, et al. 2002, Aygun, et al. 2009). The intensity of oxygen signal reduces through the 14^{th} layer and then disappears. After this etching level, the film corresponds to the substrate and, therefore, does not contain oxygen compound.

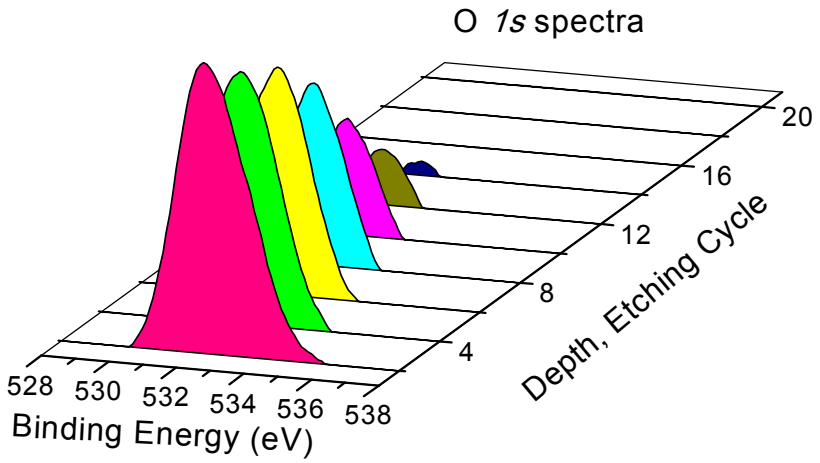

Figure 8.9. O *1s* spectra at different depth.

8.3.4.4. Hf *4f* Peak

Hf *4f* spectra appears from the contribution of (i) Hf metal (Hf^0), (ii) suboxide form of HfO_2 ($Hf^{x+}O^y$) and (iii) fully oxidized form of HfO_2 ($Hf^{4+}O_2$) (Suzer, et al. 2002). Hf *4f* spectra of surface layer is given in the figure 8.10. The Hf *4f* region contains only one sharp spin-orbit doublet. The depth profile of Hf *4f* spectrum is given in Fig. 8.11. All Hf *4f* region consists of $4f_{7/2}$ and $4f_{5/2}$ components at different binding energies of Hf-O bonds. The binding energy of Hf $4f_{7/2}$ was reported by other research groups of Wilk *et al*. (2001) and Cosnier *et al*. (2001) as 17.3 and 17.4 eV, respectively.

In our study, the Hf *4f* doublet has a spin orbit splitting of 1.5 eV at 17.9 and 19.4 eV for Hf $4f_{7/2}$ and $4f_{5/2}$, respectively. The metallic Hf has binding energy of 14.3 eV, so this indicated that elemental Hf did not originally exist (Gruzalski, et al. 1990). These peaks shift to higher binding energy sides for Hf $4f_{7/2}$ and $4f_{5/2}$ can be attributed to fully oxidized hafnium Hf^{4+} which is evidence the presence of hafnium-silicate at the interfacial area (Suzer, et al. 2002, Yakovkina 2005, Lee, et al. 2004, Kukli, et al. 2005).

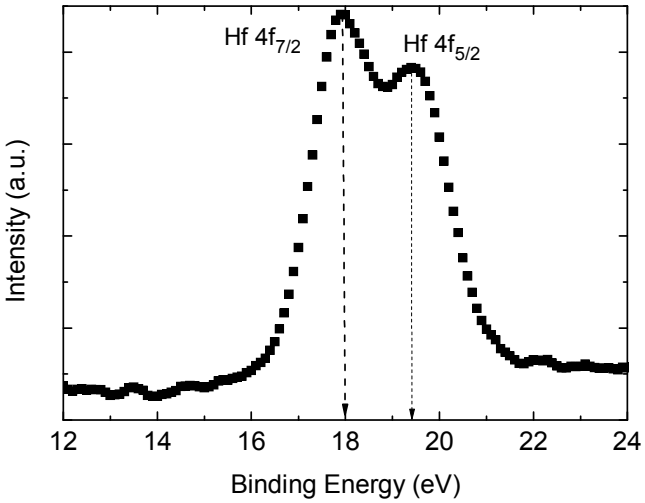

Figure 8.10. XPS Hf *4f* spectra of surface layer.

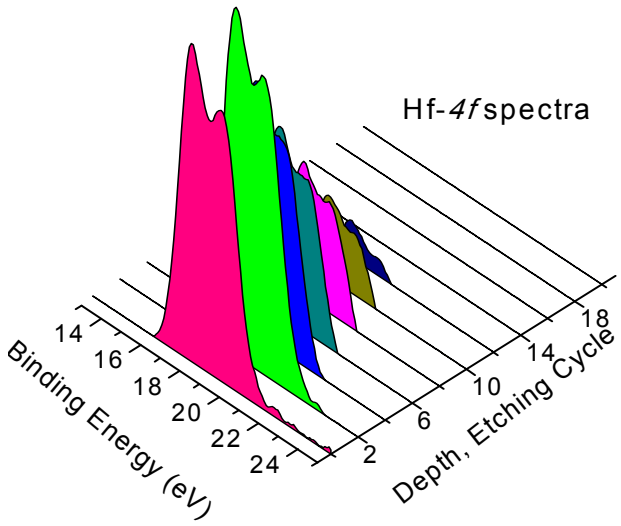

Figure 8.11. Hf *4f* spectra at different depth.

This result showed that when Hf metal is deposited on Si, a few atomic layers of $Hf_xSi_yO_z$ are formed at the interface. As expected, the intensity of Hf *4f* peaks shows reduction through the deeper layers. It disappears after 12^{th} layer since interface is reached.

8.4. Conclusion

Ultrathin HfO_2 film was prepared on *n*-type Si substrate by magnetron sputtering technique. A series diagnostic technique such as SE, FTIR, XRD and XPS were used to characterize the optical, structural and interfacial properties of grown film.

Optical results showed that HfO_2 film grown linearly with deposition time. Refractive index of HfO_2 film was obtained as 1.93 which is close to bulk form of oxide film. From the optical measurement, SiO_2 interface was encountered with ignorable thickness of 0.5 nm. GI-XRD spectra indicated that the film has polycrystalline structure with monoclinic phase of HfO_2. The FTIR spectrum indicated the formation of thick hafnium silicate interfacial region of this 6nm thick hafnium oxide film.

Effect of Hf metal on the formation of an undesired interfacial area was clearly explained with the XPS depth profiling spectra. It was found that Hf metal barrier limited diffusion of oxygen atoms through the Si substrate, and therefore, preventing to formation of SiO_x interface but not eliminated totally due to its poor barrier characteristic.

The existence of hafnium silicate ($Hf_xSi_yO_z$) layer was detected before very thin SiO_x interfacial layer. The Si-Si peaks were observed just before reaching Si substrate can be explained with that highly reactive sputtered Hf atoms consume some of the oxygen atoms from the underlying SiO_2 to form hafnium oxide by leaving Si-Si bounds behind (Aygun, et al. 2009, Yamamoto, et al. 2003). The presence of SiO_2 and $Hf_xSi_yO_z$ interface layers was also supported by FTIR analysis.

CHAPTER 9

ELECTRICAL CHARACTERIZATIONS OF HfO_2 FILMS

9.1. Introduction

Since the size of the microelectronic devices is scaling down, thickness of common gate dielectric material, named SiO_2, has been limited due to leakage current. Therefore, alternative high-*k* gate dielectric materials need to be searched for improving device performance. HfO_2 has an important position in the Metal Oxide Semiconductor (MOS) Transistors as a high–κ dielectric material. In this section, the electrical properties of sputter grown thin HfO_2 films were searched for future electronic devices.

9.2. Experimental

HfO_2 films grown by magnetron sputtering technique were fabricated as metal oxide semiconductor (MOS) transistors in order to obtain the electrical characteristics, i.e. Capacitance-Voltage (C-V), Conductance-Voltage (GV) and Current-Voltage (I-V). Detailed information of thin film growth and then MOS fabrication processes are given in chapter 3 and chapter 4, respectively. For the capacitance and conductance measurements, high frequency regime (1, 10, 100, 1000 kHz) was used. Series resistance correction (see section 5.4.6.1) was performed for all C-V and GV data. Different types of oxide charges (see section 4.3.2) and hysteresis effect were extracted from the C-V and G-V data. Leakage current density of capacitor as a function of applied voltage was studied.

9.3. Results and Discussions

9.3.1. Electrical Characterization

In this part of our study, electrical and dielectrical properties, i.e. capacitance-voltage (C-V), conductance-voltage (G-V) and current-voltage (I-V) of different samples are presented. C – V curves were taken at high frequencies of 1, 10, 100 and 1000 kHz for MOS capacitors having 5.7 x 10^{-7} m^2 Al gate area. Series resistance correction was applied to all capacitance and conduction data. Using these experimental data, calculations have been carried out to obtain the flat band voltage, V_{FB}, fixed oxide charges, Q_f, slow states, Q_s, and interfacial defect states, Q_{fast}.

Figure 9.1 shows C – V curves with accumulation, depletion and inversion regions and one G – V curve showing the conduction peak of MOS capacitors after the series resistance correction is applied.

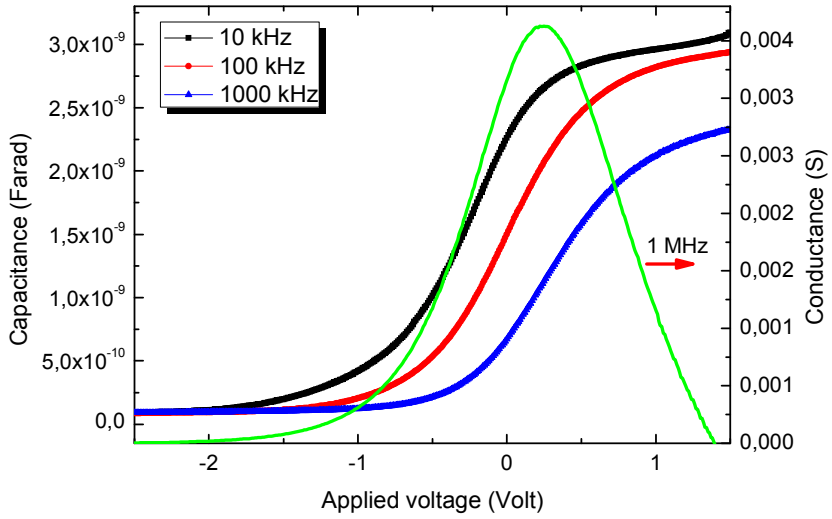

Figure 9.1. Capacitance with respect to applied voltages for 10, 100, 1000 kHz and conductance versus applied voltage for 1MHz.

It is clear that C-V curve shifts through the right side for higher frequency. Fixed oxide charges (Q_f) are the reason of this C-V curve shift. The amount of fixed oxide charges can be related to the value of V_{FB} by the following equation;

$$V_{FB} = \Phi_{MS} - \frac{Q_f}{C_{acc}} \tag{9.1}$$

where C_{acc} is the measured capacitance in accumulation and Φ_{MS} is the work function difference between Al gate and Si substrate. Fixed oxide charges, Q_f are calculated from the accumulation capacitance value, C_{acc}, and flat band voltage, V_{FB}, the voltage value corresponding to conduction peak. Table 9.1 gives oxidation parameters and oxide charges at each frequency for MOS samples.

Table 9.1. Growth and electrical parameters of HfO_2 films.

	Applied Power (Watt)	30	30	30	50	60
	O_2/Ar gas ratio	0.1	0.15	0.2	0.2	0.1
V_{fb} (V)	1MHz	-0.043	-1.63	-1.41	-2.18	-1.21
Q_f (10^{11} cm^{-2})	1 MHz	-6.48	17.71	13.75	27.11	14.12
	100 kHz	-8.22	37.10	35.88	38.12	14.94
	10 kHz	-8.55	44.19	42.48	43.45	15.98
	1 kHz		45.81	45.91	44.89	16.00
Q_s (10^{11} cm^{-2})	1 MHz	2.69	2.30	3.185	1.60	1.03
Q_{fast} (10^{11} cm^{-2})	10-1000 kHz	-39.85	-3.65	-8.39	-7.06	-75.93

When the flat band voltage is negative, then the expected presence of fixed oxide charges is positive and vice versa. The work function difference between n-type Si and Al is -0.3 eV. Flat band voltage was obtained from G-V peak for 1 MHz frequency as -0.043 V. As seen from the table, Q_f is negative.

The possible reason of these charges is an incomplete chemical bonding of the atoms near the dielectric/semiconductor interface.

One of these reasons could be the oxygen vacancies type electrically active defects in HfO_2. The films growth with 30 W applied power, but varying O_2/Ar gas ratio, i.e. 0.15, 0.2 and 0.25, had different amount of fixed oxide charge depending on oxygen quantities during growth (see Table 9.1).

9.3.2. Hysteresis Effect and Slow States

Oxide film exhibits C-V hysteresis at the frequency of 1 MHz, when the gate voltage is swept from accumulation to inversion and then from inversion to accumulation. Figure 9.2 shows the hysteresis effect of sample growth with 60 W applied power and 0.1 gas ratio. The potential difference between two measurements at around flat band voltage indicates the existence of slow states, Q_{slow}, which recharge during each back bias cycle and locate very close to the interface with Si/oxide. Slow charge density was found from the equation (9.2) as 1.03×10^{11} cm^{-2}.

$$Q_{slow} = \frac{V_{1st} - V_{2nd}}{Area \times q} \times C_{acc} \tag{9.2}$$

Thickness of this sample was determined as 14.85 nm by SE. Effective dielectric constant was calculated as 7.33 at 1 kHz frequency. The quantity of interfacial defect charges, Q_{fast}, is calculated from the difference of C-V curves near flat band voltage of 10 kHz and 1 MHz. It can be seen from Table 9.1 that density of fast charges was calculated from equation (9.3) as -3.65×10^{11} cm^{-2}.

$$Q_{fast} = \frac{V_{10\,kHz} - V_{1000\,kHz}}{Area \times q} \times C_{acc} \tag{9.3}$$

The oxide thickness value for this sample is 14.85 nm measured by the ellipsometry and the ε_{eff} value is 9.01 at the frequency of 1 kHz.

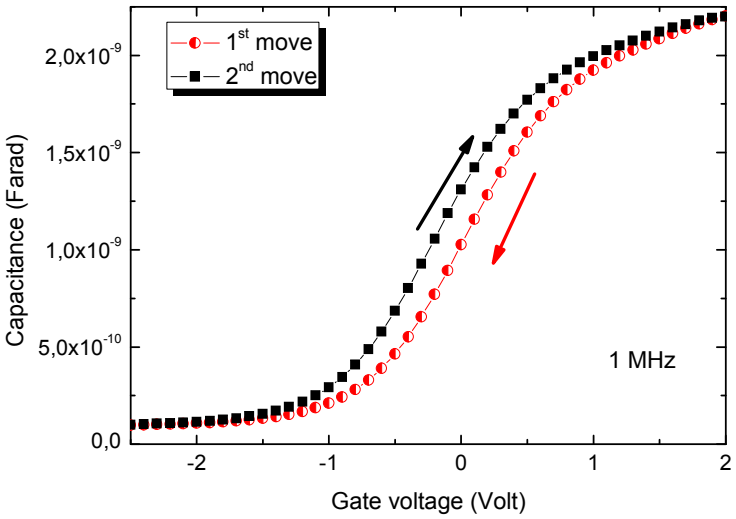

Figure 9.2. Capacitance with respect to applied voltage of the film growth with 60 W applied power and 0.1 gas ratio at 1 MHz frequency from accumulation to inversion (1st move) and from inversion to accumulation (2nd move).

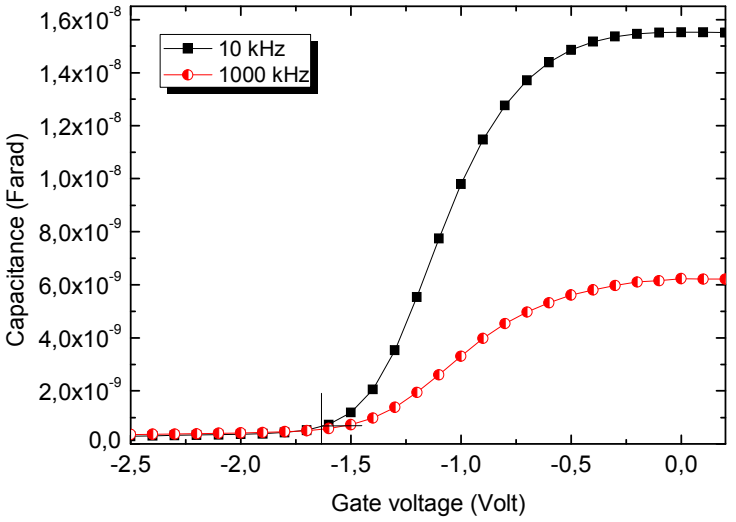

Figure 9.3. Capacitance with respect to applied voltage at 1 MHz and 10 kHz frequencies from accumulation to inversion mode.

9.3.4. I – V Characteristics of the Capacitors

It is supposed that there is almost not a detectable charge transmission, i.e. leakage current, on ideal insulators. However, in reality, when the applied electric field on MOS structure is increased or/and the temperature of MOS structure is increased,

then the charge carriers can penetrate from the forbidden barrier height resulting in a tunneling leakage current.

There are many types of leakage current mechanisms (see section 4.4) depending on MOS capacitor properties, applied physical conditions and working regimes. The leakage current density through the oxide as a function of applied voltage gives information about the quality of grown dielectric layer. For this reason, measurement of applied gate voltage to leakage current is useful to determine the electrical characteristics of MOS structures. Figure 9.4 shows current density versus applied gate voltage of graph of sample growth with 30 W applied power and 0.1 gas ratio. In the forward bias conditions (negative applied voltage values for which electrons are injected from Al gate), the leakage current starts from very low values ~10^{-8} A/cm^2 for very small applied voltages and it goes up to 10^{-6} A/cm^2 for around -2 V. Magnitude of external electric field applied to dielectric structure was calculated from dividing gate voltage by thickness of dielectric material.

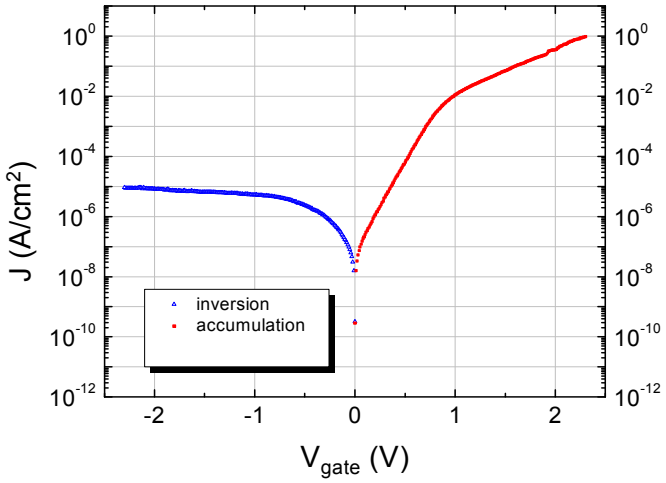

Figure 9.4. Leakage current versus applied voltage.

Figure 9.5 shows current density to applied electric field on dielectric film. Possible current mechanisms were determined, in reality, using I-V relation.

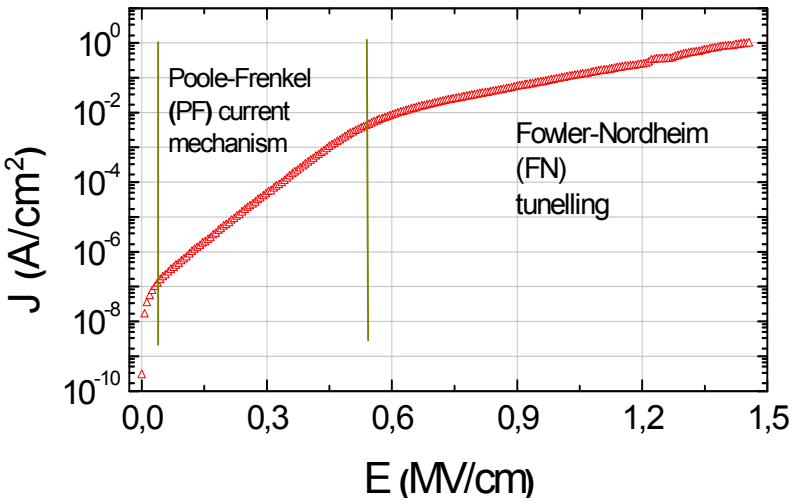

Figure 9.5. Current density versus applied electric field graph and possible current mechanism regions.

9.4. Conclusion

MOS capacitors were constructed from thin sputtered grown HfO_2 films to draw out their electrical properties. Dielectric and electrical parameters were extracted from the capacitance and conductance measurements at high frequencies in the range of 1 to 1000 kHz regime of MOS capacitors having 5.7 x 10^{-7} m^2 Al gate areas. The ε_{eff} values obtained from C-V curve were found the highest value for the lowest frequency since the accumulation capacitance value increases as frequency decreases.

Fixed oxide charges, Q_f, from the flatband voltage, from the flatband voltage, slow states, Q_s, from hysteresis effect at 1 MHz C–V curve, fast interface states, Q_{fast}, between 10 kHz and 1 MHz C–V curves were obtained.

The results show that the film properties need to be improved further. The reason of low dielectric constant is the formation of SiO_x and/or $HfSi_xO_y$ interfacial formation between HfO_2/Si. To improve the device performance, i.e. reducing leakage current and increasing the dielectric constant, the undesired interface formation is better to be eliminated from the oxide and Si substrate. In order to further decrement of this undesired region, our experiments will be repeated for detailed studies.

.

CHAPTER 10

CONCLUSION

The main material of microelectronics for more than a few decades has based on the Si technology because of its excellent mechanical, chemical and electrical properties. This is mainly because of the native oxide of Si, namely SiO_2, having perfect interface with Si. However, constant shrinking of the device geometries of today's technology of microelectronics forces the thickness of SiO_2 to its physical limits. Therefore, nowadays, the fabrication of alternative dielectrics with high dielectric constant (high–κ materials) is one of the main search topics of the microelectronics.

There are various methods to oxidize the semiconductor surfaces (see chapter 5.2). Among them, RF magnetron sputtering technique has attracted special attention due to its ability to grow amorphous thin film and its high growth rate. On the other hand, one of the great advantages of RF magnetron sputtering technique is that it has a well controlled method which is very important in terms of physical properties as well as thickness of the grown film.

In this thesis, our main aim was to grow hafnium oxide thin film on Si under suitable vacuum conditions controlling during growth process by an in-situ spectroscopic ellipsometric sputtering technique and was to characterize these grown films with respect to their structural, optical and electrical properties.

Chapter 2 starts with the explanation of the basic working principles of a spectroscopic ellipsometer. In order to understand physics of SE, knowledge of optics and behavior of light in a medium was given additionally.

In chapter 3, magnetron sputtering technique was introduced. The theory of the metal sputtering and reactively oxidation of it by magnetron sputtering technique was also given in this chapter.

In chapter 4, fabrication of Metal Oxide Semiconductor (MOS) structures was explained and energy band diagram of metal/oxide/semiconductor contacts were given. Ideal MOS capacitors and their C-V measurements were basically introduced.

Chapter 5 consists of three subtitles; sample preparation, MOS fabrication, characterization of HfO_2 thin films grown on Si substrate. In the sample preparation part, the film deposition parameters we used were given.

In fabrication part, steps of MOS device construction were given. In characterization part, technical properties of SE, XRD, FTIR, XPS and electrical characterization methods were introduced.

In the first part of our research (see chapter 6), parameters and the ideal growth conditions were investigated to grow HfO_2 thin films. To optimize parameters, some significant parameters were studied deeply, such as different oxygen quantity and applied sputter power. We tried to obtain growth parameters in order to eliminate the formation of SiO_x interface and as well as high refractive index film. Moreover, effects of oxygen quantity on thickness of grown film interfacial thickness and their film's refractive index value were performed for five different Oxygen/Argon gas ratios. The results showed that thickness of grown films decreased with higher used gas ratios. Similarly, refractive index of grown films showed decrement with an increment of O_2/Ar gas ratio. The film grown with 0.1 gas ratio has refractive index value of 2.05 which is close bulk HfO_2 refractive index (n= 2.1) at 632 nm wavelength. It was also encountered that thickness of SiO_2 interface was increased with the high amount of oxygen due to the possible increment of oxygen diffusion through oxide film.

Effects of applied sputter power have been also examined. Films grown with different applied power showed different thicknesses and refractive index values. The thickest film was obtained for the highest power whereas the highest refractive index value of film was obtained for the lowest applied power. As a result, in terms of the refractive index value and undesired interfacial layer formation, low oxygen quantity i.e. O_2/Ar gas ratio being between 0.1 and 0.2, and low applied power of around 30-40 W are obtained as the best oxidation parameters.

In chapter 7, the interface formation between HfO_2/Si interface was tried to be get under controll. To achieve this, a thin Hf metal layer was deposited on Si substrate prior to oxide film deposition. Optical, structural, chemical, and electrical properties of HfO_2 layers were studied for future applications of microelectronics. SE, FTIR, XRD and electrical measurements for dielectric constant value of the oxide layer were studied.

From SE measurements it was found that oxide film was growing linearly with deposition time and no SiO_2 interface was encountered. However, it was detected from FTIR analyses that the grown film has an SiO_4 and hafnium silicate interface. The interface effect on electrical characteristics of film was also realized with the result of low dielectric constant.

The conclusion that Hf metal barrier limits the oxygen diffusion through oxide but not eliminated totally due to HfO_2' poor barrier characteristics is found.

In chapter 8, the interface formation in the presence of Hf metal barrier was searched in a detailed manner with XPS and SE depth profile analyses. In-situ optical measurements showed that HfO_2 film grows linearly with deposition time but very thin about 0.5 nm of SiO_2 interface was obtained. It was shown that XPS depth profile technique is a good but not enough technique for determination of interface. It declared the existence of hafnium silicate ($Hf_xSi_yO_z$) layer before very thin SiO_2 interface layer. It was detected that the film is nonperfect and nonstoichiometric containing suboxides of Si in different amounts throughout the depth. It was concluded that deposition time of Hf metal on Si should be increased for improving microstructure of both oxide and near interface region.

In chapter 9, dielectric and electrical parameters were extracted from the capacitance and conductance of MOS capacitors. From these measurements, the fixed oxide charges, Q_f, slow states, Q_s, from hysteresis effect at 1 MHz C–V curve, fast interface states, Q_{fast}, between 10 kHz and 1 MHz C–V curves were obtained. Leakage current density of grown oxide was also determined.

The results show that the oxidation of Hf films by magnetron sputtering technique is a promising growth technique of amorphous HfO_2 films. Nevertheless, further research is necessary to improve the grown oxide qualities.

REFERENCES

Aarik, J., Mandar, H., Kirm, M., Pung, L. 2004. Optical Characterization of HfO_2 Thin Films Grown by Atomic Layer Deposition. *Thin Solid Films* 466: 41-47.

Alers, G. B., Werder, D. J., Chabal, Y. 1998. Intermixing at the tantalum oxide/silicon interface in gate dielectric structures. *Applied Physics Letters* 73: 1517.

Aspnes, D. E., Studna, A. A. 1983. Dielectric functions and optical parameters of Si, Ge, GaP, GaAs, GaSb, InP, InAs, and InSb from 1.5 to 6.0 Ev. *Physical Review B* 27: 985–1009.

Aspnes, D. E., 1973. Third-derivative modulation spectroscopy with low-field electroreflectance. *Surface Science* 37: 418–442.

Andre, J. M., Filatova, E. O., Renault, O., Damlencourt, J. F., Martin, F., Jonnard, P. 2006. Characterization of a $HfO_2/SiO_2/Si$ system by X-ray reflection and X-ray emission spectroscopies. *Surface and Interface analysis* 38: 777-780.

Atanassova, E. 1999. *Micoelectronics Reliability* 39:1185.

Aygun, G., Turan, R. 2008. Electrical and dielectrical properties of tantalum oxide films grown by Nd:YAG laser assisted oxidation. *Thin Solid Films* 517: 994-999.

Aygun, G., Yildiz, I. 2009. Interfacial and structural properties of sputtered HfO_2 layers. *Journal of Applied Physics* 106: 014312-1-7.

Aygun, G. 2005. Growth and Characterization of Thin SiO_2 and Ta_2O_5 Dielectric Layers by Nd:YAG Laser Oxidation. Ph.D.'s Thesis. Middle East Techniquel University.

Aygun, G., Atanassova, E., Alacakir, A., Ozyuzer, L., Turan, R. 2004. Oxidation of Si surface by a pulsed Nd :YAG laser. *J. Phys. D: Appl. Phys.* 37:1569–75.

Azzam, R. M. A., Bashara, N. M. 1977. Ellipsometry and Polarized Light. North-Holland, Amsterdam.

Barth, K.L., Böhme, D., Kamarás, K., Keilmann, F., Cardona, M. 1993. Far-IR spectroscopic ellipsometer. *Thin Solid Films* 234: 314-317.

Bremer, J., Hunderi, O., Faping, K., Skauli, T., Wold, E. 1992. *Applied Optics* 31: 471.

Buiu, O., Davey, W., Lu, Y., Mitrovic, I. Z., Hall, S. 2008. Ellipsometric Analyses of Mixed Metal Oxides Thin Films. *Thin Solid Film.*

Buiu, O., Lu, Y., Mitrovic, I. Z., Hall, S., Chalker, P., Potter, R. J. 2006. Spectroellipsometric assessment of HfO_2 thin films. *Thin Solid Films* 515: 623-626.

Chaneliere, C., Autran, J. L., Devine, R. A. B., Balland, B. 1998. Tantalum pentoxide (Ta_2O_5) thin films for advanced dielectric applications. *Materials Science and Engineering R* 22: 269-322.

Cosnier, V., Olivier, M., Theret, G., Andre, B. 2001. HfO_2– SiO_2 interface in PVD coatings. *J. Vac. Sci. Technol. A* 19: 2267.

Deal, B. E. 1980. Standardized terminology for oxide charges associated with thermally oxidized silicon. *IEEE Trans. Electron Devices ED* 27: 606.

Dogan, I., Yildiz, I., Turan, R. 2009. PL and XPS depth profiling of Si/Al_2O_3 co-sputtered films and evidence of the formation of silicon nanocrystals. *Physica E* 41: 976–981.

Drude, P. 1890. Ann. d. Phys. 39:481.

Duenas, S., Castan, H., Garcıa, H., Gomez, A., Bailon, L., Toledano-Luque, M., Martil I., Gonzalez-Dıaz, G. 2007. Electrical properties of high-pressure reactive sputtered thin hafnium oxide high-*k* gate dielectrics. *Semicond. Sci. Technol.* 22: 1344–1351.

Duncan, Walter M., Henck, Steven A., Loewenstein, Lee M. 1992. Spectral ellipsometry for in-situ real-time measurement and control. Central Research Laboratories and semiconductor process and design center final report.

Feng, Li-ping., Liu, Zheng-tang., Shen, Ya-ming. 2009. Compositional, structural and electronic characteristics of HfO_2 and HfSiO dielectrics prepared by radio frequency magnetron sputtering. *Vacuum* 83: 902-905.

Fowler, R., Nordheim, L. 1928. Electron emission in intense electric fields. *Proceeding Royal Society A* 119: 173-181.

Frank, Martin M., Sayan, Safak., Dörmann, Sabine., Emge, Thomas J.,Wielunski, Leszek S., Garfunkel, Eric., Chabal, Yves J. 2004. Hafnium oxide gate dielectrics grown from an alkoxide precursor: structure and defects. *Materials Science and Engineering B* 109: 6-10.

Fujiwara, Hiroyuki. 2007. Spectroscopic Ellipsometry Principles and Applications. National Institute of Advanced Industrial Science and Technology, Ibaraki, Japan.

Giustino, F., Umari, P., Pasquarello, A. 2004. Dielectric effect of a thin SiO_2 interlayer at the interface between silicon and high-k oxides. *Microelectronic Engineering* 72: 299-303.

Gong, Y., Li, A., Qian, Xu., Zhao, C., Wu, Di. 2009. Interfacial structure and electrical properties of ultrathin HfO_2 dielectric films on Si substrates by surface sol-gel method. *Journal of Applied Physics* 42: 1-5.

Green, M. L., Gusev, E. P., Degraeve, R., Garfunkel, E. L. 2001. Ultrathin (<4 nm) SiO_2 and Si–O–N gate dielectric layers for silicon microelectronics: Understanding the processing, structure, and physical and electrical limits. *J. Appl. Phys.* 90: 2057.

Gruzalski, G.R., Zehner, D. M. 1990. Charge-distribution changes accompanying the formation and changes in the composition of HfC_x and TaC_x. *Physical Review B* 42: 2768-2777.

He, G., Fang, Q., Liu, M., Zhu, L.Q., Zhang, L.D. 2004. The structural and interfacial properties of HfO_2/Si by the plasma oxidation of sputtered metallic Hf thin films. *Journal of Crystal Growth* 268: 155-162.

Hecht, Eugene. 2002. Optics. Publisher: Addison Wesley 4 th edition.

Hori, N., Suzuki, K., Saitoh, T. 1991. Measurements of Optical Properties for Thin Amorphous Silicon Films Using Spectroscopic Ellipsometry. *IEEE Xplore* 1338-1341.

Houssa, M., Pantisano, L., Ragnarsson, L. A., Degraeve, R., Schram, T., Pourtois, G., De Gendt, S., Groeseneken, G., Heyns M.M. 2006. Electrical properties of high-k gate dielectrics: Challenges, current issues, and possible solutions. *Materials Science and Engineering R* 51: 37–85.

Hubbard, K. J., Schlom, D. G. 1996. Thermodynamic stability of binary oxides in contact with silicon. *Journal of Materials Research Society* 11: 2757-2776.

Ikeda, Hiroya., Goto, Satoru., Honda, Kazutaka., Sakashita, Mitsuo., Sakai, Akira., Zaima, Shigeaki., Yasuda, Yukio. 2002. Structural and Electrical Characteristics of HfO_2 Films Fabricated by Pulsed Laser Deposition. *Japanese Journal of Applied Physics* 41: 2476-2479.

Johs, Blaine., Hale, Jeff., Hilfike, James. 1997. Real-time process control with in situ spectroscopic ellipsometer. *Elsevier Science Ltd.* 10: 1290-97.

Kang, Hyunseok., Kim, Seokhoon., Kim, Jinwoo., Choi, Jihoon., Jeon, Hyeongtag. 2005. Characteristics of the HfO_2 Thin Films Grown by Remote Plasma Atomic Layer Deposition Method on the Plasma Oxidized Si Substrate. *The Electrochemical Society* 1: 459-464.

Khomenkova, L., Dufour, C., Coulon, P-E., Bonafos, C., Gourbilleau., F. 2010. High-k Hf-based layers grown by RF magnetron sputtering. *Nanotechnology* doi:10.1088/0957-4484/21/9/095704.

Khoshman, Jebreel M., Kordesch, Martin E. 2006. Optical properties of a-HfO_2 thin films. Surface & Coatings Technology 201: 3530–3535.

Krug, C., da Rosa, E. B. O., de Almeida, R. M. C., Morais, J., Baumvol, I. J. R., Salgado, T. D. M., Stedile, F. C. 2000-01. Atomic Transport and Chemical Stability During Annealing of Ultrathin Al_2O_3 Films on Si. *Physical Review Letters* 85: 4120 and 86: 4713.

Kuklia, Kaupo., Aarik, Jaan., Uustarec, Teet., Lud, Jun., Ritalab, Mikko., Aidlac, Aleks., Punga, Lembit., Hrstae, Anders., Leskelb, Markku., Kikasc, Arvo., Sammelselg, Vino. 2005. Engineering structure and properties of hafnium oxide films by atomic layer deposition temperature. *Thin Solid Films* 479: 1– 11.

Lee, P. F., Dai, J. Y., Chan, H. L. W., Choy, C. L. 2004. Two-step interfacial reaction of HfO_2 high-k gate dielectric thin films on Si. *Ceramics International* 30: 1267-1270.

Mahan, John E. 2000. Physical Vapor Deposition of Thin Films. United States of America: John Wiley and Sons.

Manchanda, L., Morris, M.D., Green, M.L., van Dover, R. B., Klemens, F., Sorsch, T. W., Silverman, P.J., Wilk, G., Busch, B., Aravamudhan, S. 2001. Multi-component high-k gate dielectrics for the silicon industry. *Microelectronic Engineering* 59: 351–359.

Martınez, F. L., Toledano-Luque, M., Gand´ıa, J. J., Carabe, J.,Bohne, W., Röhrich, J., Strub, E., Martil, I. 2007. Optical properties and structure of HfO_2 thin films grown by high pressure reactive sputtering. *Journal of Applied Physics* 40: 5256–5265.

Maunoury, C., Dabertrand, K., Martinez, E., Saadoune, M., Lafond, D., Pierre, F., Renault, O., Lhostis, S., Bailey, P., Noakes, T. C. Q., Jalabert, D. 2007. Chemical interface analysis of as grown HfO_2 ultrathin films on SiO_2. *J. Appl. Phys.* 101**:** 034112.

McKee, R. A., Walker, F. J., Chisholm, M. F. 1998. Crystalline Oxides on Silicon: The First Five Monolayers. *Physical Review Letter*, 81: 3014.

Mori, Takanori., Fujiwara, Makoto., Manory, Rafael R., Shimizu, Ippei., Tanaka, Takeo., Miyake, Shoji. 2003. HfO_2 thin films prepared by ion beam assisted deposition. *Surface and Coatings Technology* 169-170: 528-531.

Nam, Seok-Woo., Yoo, Jung-Ho., Nam, Suheun., Choi, Hyo-Jick. Lee, Dongwon., Ko, Dae-Hong., Moon, Joo Ho., Ku, Ja-Hum., Choi, Siyoung. 2002. Influence of annealing condition on the properties of sputtered hafnium oxide. *Journal of Non-Crystalline Solids.* 303: 139-143.

Neumayer, D. A., Cartier, E. 2001. Materials characterization of ZrO_2– SiO_2 and HfO_2– SiO_2 binary oxides deposited by chemical solution deposition. *Journal of Applied Physics* 90: 1801-1808.

Nicollian, E. H., Brews, J. R. 2003. MOS (Metal Oxide Semiconductor) Physics and Technology. United States of America: John Wiley and Sons.

Ng, K.L., Zhan, Nian., Kok, C.W., Poon, M.C., Wong, Hei. 2003. Electrical characterization of the hafnium oxide prepared by direct sputtering of Hf in oxygen with rapid thermal annealing. *Microelectronics Reliability* 43:1289–1293.

Park, B. K., Park, J., Cho, M., Hwan, C. S., Oh, K., Han, Y., Yang, D. Y. 2002. Interfacial reaction between chemically vapor-deposited HfO_2 thin films and a HF-cleaned Si substrate during film growth and postannealing. *Applied Physics Letters* 80: 2368.

Patterson, A. L. 1939. The Scherrer Formula for X-Ray Particle Size Determination. *Physical Review* 56:978-982.

Pereira, L., Barquinha, P., Fortunato, E., Martins, R. 2005. Influence of the oxygen/argon ratio on the properties of sputtered hafnium oxide. *Materials Science and Engineering* 118: 210–213.

Pereira, L., Marques, A., Águas, H., Nedev, N., Georgiev, S., Fortunato, E., Martins. R. 2004. Performances of hafnium oxide produced by radio frequency sputtering for gate dielectric application. *Materials Science and Engineering B* 109: 89–93.

Rangarajan, Vishwanathan., Bhandari, Harish., Klein, Tonya M. 2002. Comparison of hafnium silicate thin films on silicon (1 0 0) deposited using thermal and plasma enhanced metal organic chemical vapor deposition. *Thin Solid Films* 419: 1–4.

Robertson, J., Peacock, P. W. 2004. Atomic structure, band offsets, growth and defects at high-k oxide: Si interfaces. *Science Direct* 72: 112-120.

Robertson, J. 2000. Band offsets of wide-band-gap oxides and implications for future electronic devices. *American vacuum society* 18: 1785-1791.

Rothen, Alexandre., 1945. The ellipsometer, an apparatus to measure thicknesses of thin surface films. *Review of Scientific Instruments.*16: 26-30.

Roy, Kaushık., Mukhopadhyay, Saibal., Mahmoodi-Meimand., Hamid. 2003. Leakage Current Mechanisms and Leakage Reduction Techniques in Deep-Submicrometer CMOS Circuits. *Proceedings of the IEEE* 91: 305-327.

Röseler, A. 1990. Infrared Spectroscopic Ellipsometry. Akademie Verlag,. Berlin.

Sayan, S., Aravamudhan, S., Busch, B. W., Schulte, W. H., Cosandey, F., Wilk, G. D., Gustafsson, T., Garfunkel, E. 2001. Chemical vapor deposition of HfO_2 films on Si.100. *American Vacuum Society* 20: 507-512.

Seshan, Krishna. 2002. Handbook of Thin Film Deposition Processes and Technologies. Second edition, Noyes Publications.

Schubert, M. Infrared Ellipsometry on Semiconductor Layer Structures: Phonons, Plasmons, and Polaritons. 2004. Springer, Heidelberg.

Schuegraf, K., Hu, C. 1994. Hole injection SiO_2 breakdown model for very low voltage lifetime extrapolation. *IEEE Trans. Electron Devices* 41: 761–767.

Siervo, De., Flüchter, C. R., Weier, D., Schürmann, M., Dreiner, S., Westphal, C., Carazzolle, M. F., Pancotti, A., Landers, R., Kleiman, G. G. 2006. Hafnium silicide formation on Si(100) upon annealing. *Physical Review B* 74: 075319.

Singh, Jasprit. 2001. Semiconductor Devices Basic Principles. United States of America: John Wiley and Sons.

Sharlandjiev, Peter., Stoilov, Georgi. 2008. Modeling Optical Response of Thin Films: Choice of the refractive Index Dispersion Law. *Information Technologies and Knowledge* 2:157-159.

Sokolov, A. A., Filatova, E. O., Afanasev, V. V., Taracheva, E. Yu, Brzhezinskaya, M. M., Ovchinnikov, A. A. 2009. Interface analysis of HfO_2 films on (100) Si using X-Ray Photoelectron Spectroscopy. *J.Phys. D: Appl. Phys*. 42:1-6.

Stuart, R. V. 1982. Vacuum Technology, Thin Films, and Sputtering. Academic Press.

Suzer, S., Sayan, S., Garfunkel, E., Hussain, Z., Hamdan, N. M. 2002. Soft x-ray photoemission studies of Hf oxidation. *American vacuum society* 21:106-109.

Sze, S. M. 1981. Physics of Semiconductor Devices. United States of America: John Wiley and Sons.

Tan, Ruiqin., Azuma, Yasushi., Kojima, Isao. 2005. X-Ray photoelectron spectroscopic analysis of HfO_2/Hf/SiO_2/Si structure Applied Surface Science 241:135-140.

Tang, J., Kai, M., Kobayashi, Y., Endo, S., Shimomura, O., Kikegawa, T., Ashida, T. 1998. Geophy. Monogr. 101:401.

Taylor, C. J., Gilmer, D. C., Colombo, D. G., Wilk, G. D., Campbell, S. A., Roberts, J., Gladfelter, W. L. 1999. Does chemistry really matter in the chemical vapor deposition of titanium dioxide? Precursor and kinetic effects on the microstructure of polycrystalline films. *Journal of the American Chemical Society* 121: 5220.

Teren, Andrew R., Thomas, Reji., He, Jiaqing., Ehrhart, Peter. 2005. Comparison of precursors for pulsed metal–organic chemical vapor deposition of HfO_2 high-K dielectric thin films. *Thin Solid Films* 478: 206-217.

Toledano-Luque, M., Martinez, F.L., San Andres, E., del Prado, A., Martil, I., Gonzalez-Diaz, G., Bohne, W., Rohrich, J., Strub, E. 2008. Physical properties of high pressure reactively sputtered hafnium oxide. *Vacuum* 82:1391–1394.

Toledano-Luque, M., San Andrés, E., del Prado, A., Mártil, I., Lucía, M. L., González-Díaz , G. 2007. High-pressure reactively sputtered HfO_2: Composition, morphology, and optical properties. *Journal of Applied Physics* 102: 044106-1.

Tompkins, Harland G., Irene, Eugene A. 2004. Handbook Of Ellipsometry. Springer.

Tyagi, M. S. 1991. Introduction to Semiconductor Materials and Devices. United States of America: John Wiley and Sons.

Wang, Hao., Wang, Y., Feng, J., Ye, C., Wang, B.Y., Wang, H.B., Li, Q., Jiang, Y., Huang, A.P., Xiao, Z.S. 2008. Structure and electrical properties of HfO2 high-k films prepared by pulsed laser deposition on Si (100). *Applied Physics A* 93:681-684.

Wang, Zhan Jie., Kumagai, Toshihide., Kokawa, Hiroyuki., Tsuaur, Jiunnjye., Ichiki, Masaaki., Maeda, Ryutaro. 2005. Crystalline phases, microstructures and electrical properties of hafnium oxide films deposited by sol–gel method. *Journal of Crystal Growth* 281: 452–457.

Wilk, G. D., Wallace, R. M., Anthony, J. M. 2001. High-k gate dielectrics: Current status and materials properties considerations. Journal of Applied Physics 89:5243-5273.

Wilk, G. D., Wallace, R. M. 1999. Electrical properties of hafnium silicate gate dielectrics deposited directly on silicon. *Appl. Phys. Lett.* 74: 2854.

Yakovkina, L. V., Kichai, V. N., Smirnova, T.P., Kaichev, V.V., Shubin, Yu. V., Morozova, K. V., Igumenov, I. K. 2005. Preparation and Properties of Thin HfO_2 Films. *Inorganic Materials.* 41:1300-1304.

Yamamoto, K., Hayashi, S., Niwa, M., Asai, M., Horii, S., Miya, H. 2003. Electrical and physical properties of HfO_2 films prepared by remote plasma oxidation of Hf metal. *Appl. Phys. Lett.* 83: 2229.

Zeghbroeck, B. Van. 2004. Principles of Semiconductor Devices, Electronic Book.